TAMPERE UNIVERSITY OF TECHNOLOGY
Department of Electrical Energy Engineering

ILKKA RYTÖLUOTO

APPLICATION OF POLYPROPYLENE NANOCOMPOSITES IN METALLIZED FILM CAPACITORS UNDER DC VOLTAGE

Master of Science Thesis

Examiners: Assoc. Prof. Kari Kannus, Dr.Tech. Kari Lahti
The examiners and the topic were approved in the Faculty of Computing and Electrical Engineering Council meeting on 5.10.2011

ABSTRACT

TAMPERE UNIVERSITY OF TECHNOLOGY
Master's Degree in Electrical Power Engineering
RYTÖLUOTO, ILKKA: Application of polypropylene nanocomposites in metallized film capacitors under DC voltage
Master of Science Thesis, 90 pages, 1 Appendix page
November, 2011
Major: Electrical Power Engineering
Examiner: Associate Professor Kari Kannus, Dr.Tech. Kari Lahti
Keywords: Polymer, nanocomposite, metallized film capacitor, dielectric strength, self-healing

At the present, electrical insulation is widely based on synthetic polymers which have largely superseded traditional insulation materials such as paper and ceramics. Polymer composite materials incorporating various amounts of inorganic filler particles are often used to improve the properties and to reduce the cost of the composite. During the last years, a considerable interest has risen towards dielectric polymer nanocomposites which incorporate low mass amounts of inorganic filler particles with one or more dimension in the nanometric scale. Due to the large interfacial area between the nanoparticles and the surrounding polymer matrix, improved material properties may be achieved. Regarding to dielectric properties, improvements in e.g. dielectric strength and permittivity as well as reduction of dielectric losses may be achieved, all of which would be desirable for capacitor applications.

In the NANOPOWER –project (Novel Polymer Nanocomposites for Power Capacitors), funded mainly by the Finnish funding agency for technology and innovation (TEKES), the application possibilities of novel dielectric polymer nanocomposites in power capacitors are studied. This thesis was done as a part of the NANOPOWER-project with the focus on metallized film capacitors which incorporate thin electrodes directly evaporated on dielectric polymer film instead of separate sheets of aluminium foil traditionally used in film capacitors. Although metallized film capacitors already enable high energy density and high reliability, demands for even higher energy density, better reliability and longer life-time exist. It may be possible to fulfil these demands by utilizing nanodielectric films and thus, metallized film capacitor technology offers an interesting platform for further research and development.

The main objective of this thesis is to study the application possibilities of polypropylene nanocomposites in metallized film capacitors. The subject is approached by performing an extensive literature research on polymers, dielectric polymer nanocomposites and metallized film capacitors. In the empirical part, a measurement system which could be used in the future to conduct various DC tests on single metallized nanocomposite film samples is planned, constructed and tested. The studied electrical properties included dielectric strength, maximum permissible electric field stress and self-healing capability of the film. In addition, the dependency of these properties on external pressure was studied with the measurement setup.

TIIVISTELMÄ

TAMPEREEN TEKNILLINEN YLIOPISTO
Sähkötekniikan koulutusohjelma
RYTÖLUOTO, ILKKA: Polypropeeni-nanokomposiittien soveltaminen metalloiduissa ohutkalvokondensaattoreissa tasajännitteellä
Diplomityö, 90 sivua, 1 liitesivu
Marraskuu, 2011
Pääaine: Sähkövoimatekniikka
Tarkastajat: Dosentti Kari Kannus, TkT Kari Lahti
Avainsanat: Polymeeri, nanokomposiitti, metalloitu ohutkalvokondensaattori, läpilyöntilujuus, itseparantuvuus

Nykypäivänä synteettiset polymeeripohjaiset sähköeristemateriaalit ovat syrjäyttäneet perinteiset paperi- ja keraamieristeet lähes kokonaan. Puhtaiden polymeerien sijaan käytetään kuitenkin usein polymeerikomposiitteja, joihin on seostettu eri määriä epäorgaanisia täyteaineita, joiden avulla voidaan parantaa polymeerikomposiitin ominaisuuksia sekä laskea sen tuotantokustannuksia. Viime vuosien aikana nanokomposiittipolymeerien soveltamista sähköisenä eristeenä on tutkittu merkittävästi. Käyttämällä pieniä määriä täyteaineita, joiden partikkelikoko on nanometriluokkaa, saavutetaan nanopartikkelien ja sitä ympäröivän polymeerimatriisin välille erittäin suuri vuorovaikutusalue, johon pohjautuen nanokomposiittimateriaaleilla voidaan saavuttaa parempia eristeominaisuuksia, kuten suurempi läpilyöntilujuus, permittiviteetti sekä pienemmät dielektriset häviöt.

TEKES:n pääosin rahoittamassa NANOPOWER-projektissa (Novel Polymer Nanocomposites for Power Capacitors) tutkitaan nanokomposiittipolymeerien soveltamista kondensaattoreissa. Tämä diplomityö tehtiin osana NANOPOWER-projektia keskittyen metalloituihin ohutkalvokondensaattoreihin, joissa elektrodit on höyrystetty suoraan ohuen eristekalvon pinnalle. Tällöin käämityllä rakenteella saavutetaan suuri energiatiheys ja käyttövarmuus perinteisiin, erillisiä folioelektrodeja käyttäviin ohutkalvokondensaattoreihin verrattuna. Uusien sovelluskohteiden myötä kondensaattoreiden energiatiheyttä, käyttövarmuutta ja elinikää täytyy kuitenkin kyetä nostamaan entisestään. On mahdollista, että näitä ominaisuuksia voidaan parantaa nanokomposiittipolymeerejä käyttämällä, ja tämän vuoksi metalloidut ohutkalvokondensaattorit ovatkin erittäin mielenkiintoinen tutkimus- ja kehityskohde.

Tämän diplomityön päätavoitteena oli tutkia polypropeenipohjaisten nanokomposiittien soveltamista metalloiduissa ohutkalvokondensaattoreissa tasajännitteellä. Työn yhtenä osatavoitteena oli tehdä kattava kirjallisuustutkimus polymeereistä, nanokomposiittipolymeereistä sekä metalloiduista ohutkalvokondensaattoreista. Työn käytännön osuudessa suunniteltiin, rakennettiin ja testattiin mittausjärjestelmä, jonka avulla voidaan tulevaisuudessa suorittaa sähköisiä mittauksia nanokomposiittikalvoille. Tutkittavia sähköisiä suureita olivat läpilyöntilujuus, sähkökentän voimakkuuden maksimi sekä eristekalvon itseparantuvuus. Lisäksi tutkittiin näiden suureiden riippuvuutta ulkoisesta paineesta.

PREFACE

This Master of Science Thesis was done for the Department of Electrical Energy Engineering at Tampere University of Technology as a part of the NANOPOWER-project. The focus of the thesis was on the application possibilities of polypropylene nanocomposites in metallized film capacitors under DC voltage.

First of all, I want to thank Assoc. Prof. Kari Kannus for the extremely interesting thesis subject and for all his guidance and feedback during the writing process. The option to continue working on the project as a researcher after finishing this thesis is also deeply appreciated. Thereafter, I want to address my gratitude especially to Dr. Tech. Kari Lahti and M.Sc Hannes Ranta for the absolutely indispensable help with all the matters regarding to the theoretical background and the measurements of this thesis. I also want to thank Lab.Tech. Pentti Kivinen and Lab.Tech. Pekka Nousiainen for building the test capacitor and the bolt-adjustable clamping device, all the parties within the NANOPOWER –project and all the people at the Department of Electrical Energy Engineering for providing an enjoyable working atmosphere. Finally, I want to thank my parents and my sister for the love and support they gave me during the thesis process.

Tampere, November 17, 2011.

Ilkka Rytöluoto

TABLE OF CONTENTS

ABBREVIATIONS AND NOTATION

NOTATION

A	Electrode area
Å	Ångström, equal to 10^{-10} m
C	Capacitance
C_0	Vacuum capacitance per electrode unit area, coupling capacitor
C_a	Capacitance in the equivalent circuit for dielectric material
C_{DUT}	Capacitance of the device under test (test capacitor)
$\overline{\boldsymbol{D}}$	Flux of dielectric displacement
d	Electrode distance
d_A, d_B	Thicknesses of material volumes A and B
$\overline{\boldsymbol{E}}$	Electric field
$\overline{\boldsymbol{E'}}$	Electric field due to all dipoles inside a sphere S
$\overline{\boldsymbol{E_d}}$	Depolarizing electric field
$\overline{\boldsymbol{E_m}}$	Molecular field
$\overline{\boldsymbol{E_s}}$	Electric field due to polarization charge on the surface of a sphere S
$\overline{\boldsymbol{E_x}}$	Primary electric field from the electrodes
$E_{discharge}$	Discharge energy in one self-healing event
E_{max}	Maximum permissible electric field stress
e_i	Electric charge of a charge carrier type i
f	Frequency
i_c	Charging current
k	Constant
M_i, m_m	Molecular weight of a molecule of type i
$\overline{M_N}$	Number-average molecular weight
$\overline{M_r}$	Relative molecular mass
$\overline{M_W}$	Weight-average molecular weight
M_W	Molar mass of dielectric material
m_{12_C}	Molar mass of a ^{12}C carbon-isotope
N	Number of molecules per unit volume
N_A	Avogadro's number
n_i	Number of molecules of type i, Concentration of a charge carrier type i
P	Additional charge stored per electrode unit area due to polarization of dielectric
P_d	Dielectric loss power
$\overline{\boldsymbol{P}}$	Polarization
$\Delta\overline{\boldsymbol{p}}$	Electrical dipole moment
$\overline{\boldsymbol{p}}_{\boldsymbol{m}}$	Dipole moment of a single molecule

$p_{coulombic}$	Pressure generated by electrostatic force
$p_{external}$	Externally applied pressure
p_{tot}	Total pressure in the dielectric film
Q	Charge per electrode unit area
Q_c	Capacitive reactive power
q	Element charge
R_a	Resistance in the equivalent circuit for dielectric material
R_M	Measurement resistor
R_P	Parallel resistance
R_S	Series resistance, sheet resistance
$R_{discharge}$	Discharge resistor
$\bar{\boldsymbol{r}}$	Distance vector
T_g	Glass transition temperature
T_m	Crystalline melting point
U	Voltage
Δv	Volume element
W	Energy
w_i	Mass of a molecule of type i
w	Energy density
X_c	Capacitive reactance

α	Molecular polarizability, Weibull scale parameter
$\alpha(P)$	A function which relates the interlayer pressure of a capacitor to the clearing energy
β	Weibull shape parameter
$\bar{\varepsilon}$	Complex relative permittivity
ε'	Real part of complex permittivity
ε''	Imaginary part of complex permittivity, dielectric loss factor
ε_0	Permittivity of free space, equal to $8.85 \times 10^{-12}\mathrm{Fm}^{-1}$
ε_∞	Instantaneous relative permittivity
ε_A, ε_B	Relative permittivities of material volumes A and B
ε_r	Dielectric constant, relative permittivity
ε_s	Static relative permittivity
$\overline{\varepsilon(\omega)}$	Frequency dependent complex relative permittivity (defined by Debye equation)
φ	Rotation angle of polymer segments (conformation)
μ_i	Mobility of a charge carrier type i
ω	Angular frequency
ρ	Density, resistivity
σ	Conductivity

σ_i	Conductivity of a charge carrier type i
τ	Dielectric relaxation time
χ	Electric susceptibility
$\tan\delta$	Dissipation factor (for dielectric material and capacitor)

ABBREVIATIONS

AC	Alternating current
Al_2O_3	Aluminium oxide
BOPP	Biaxially oriented polypropylene
CNT	Carbon nanotube
DC	Direct current
DFT	Density functional theory
DP	Degree of polymerization
EP	Epoxy resin
ESL	Equivalent series inductance
ESR	Equivalent series resistance
EVA	Ethylene vinyl acetate
FEM	Finite element method
HOMO	Highest occupied molecular orbital
HVDC	High-voltage direct current
HVPS	High-votlage power source
iPP	Isotactic polypropylene
LIMM	Laser-intensity-modulated method
LIPP	Laser-induced-pressure-pulse
LS	Layered silicate
LUMO	Lowest unoccupied molecular orbital
MgO	Magnesia
MW	Molecular weight
NANOPOWER	Novel Polymer Nanocomposites for Power Capacitors - project
PA	Polyamide
PD	Partial discharge
PEA	Pulsed-electro-acoustic
PE	Polyethylene
PET	Polyethylene terephthalate
PP	Polypropylene
PVD	Physical vapour deposition
PWP	Pressure wave propagation
QDC	Quasi-DC conduction mechanism
SG	Spark gap
SiO_2	Silicon dioxide, silica

sq	Square
SR	Silicon rubber
TiO_2	Titania
TSM	Thermal step method
TUT	Tampere University of Technology
ZnO	Zinc oxide

1 INTRODUCTION

Electrical insulation materials are used for isolation of two parts at different electric potentials and thus, electrical insulation forms an essential part of any piece of electrical equipment. At the present, electrical insulation is often based on synthetic polymer materials which have largely superseded traditional insulation materials such as paper and ceramics. Apart from their superior insulation properties, polymeric insulation materials have typically excellent mechanical, thermal and erosion properties. Furthermore, due to their good moulding properties, dielectric polymer materials are widely used in various high voltage apparatus such as power transformers, insulators, capacitors, reactors, surge arresters, current and voltage sensors, bushings, power cables and terminations. [1,2,3]

Although polymers may be utilized as in their pure form, polymer composite materials incorporating various amounts of inorganic filler particles are often used to improve some properties of the composite material in comparison to the base polymer and to reduce the material cost. Polymer composite materials consisting of large mass amounts (50-60 wt-%) of micron-sized inorganic filler particles have been used for decades as with microcomposites, improvements in e.g. mechanical, thermal and erosion properties may be achieved. However, dielectric properties of microcomposites are seldom improved and former attempts to utilize microcomposite dielectrics in e.g. capacitors have failed. In general, the problem with microcomposites is that the enhancement of one property typically leads to the deterioration of another. [2,4]

However, during the last years, a considerable interest has risen towards dielectric polymer nanocomposites which incorporate low mass amounts of inorganic filler particles with one or more dimension in the nanometric scale. Various studies suggest that by introducing small amounts (0.1-10 wt-%) of inorganic nanoparticles, dielectric properties of the composite material may be improved without deteriorating other material properties. The properties of polymer nanocomposites are essentially based on the large interfacial area between the nanoparticles and the surrounding polymer matrix. Due to the large surface-to-volume ratio of nanoparticles, the interfacial area dominates the material volume and thus, the properties of the interfacial area are reflected to the bulk properties of the composite. Hence, by altering how the nanoparticles interact with the polymer chains on the interfacial area, it may be possible to tailor the properties of the whole nanocomposite. Regarding to dielectric properties, improvements in e.g. dielectric strength and permittivity as well as reduction of dielectric losses may be achieved, all of which would be desirable for capacitor applications. [4,5]

In the NANOPOWER –project (Novel Polymer Nanocomposites for Power Capacitors), funded mainly by the Finnish funding agency for technology and innovation (TEKES), the application possibilities of novel dielectric polymer nanocomposites in power capacitors are studied. The main objective of the project is to produce pilot scale nanocomposite films which enable further manufacturing of prototype film capacitors with highly tailored electrical, mechanical and thermal properties. The aim is to develop more cost-effective, energy-effective and more environment-friendly capacitors for electricity transmission and distribution networks (especially for HVDC-systems) and for various other applications such as hybrid and electric vehicles, for which a high energy density is a prerequisite. [3]

This thesis was done as a part of the NANOPOWER-project with the focus on metallized film capacitors which incorporate thin electrodes directly evaporated on dielectric polymer film instead of separate sheets of aluminium foil traditionally used in film capacitors. Essentially, metallized film capacitors comprise of two sheets of metallized films wound cylindrically in order to minimize the size of the capacitor element. In addition to increased energy density due to extremely small thickness of metallized electrodes, metallized film capacitors have a unique self-healing mechanism; during a local breakdown in the dielectric film, the dissipated energy vaporizes the metallization surrounding the breakdown channel which completely isolates the breakdown area from the rest of the electrode. Therefore, thousands of self-healing breakdowns may take place in the dielectric film without compromising the reliability of the capacitor element, whereas in a traditional film capacitor comprising of foil electrodes, only one breakdown is needed for a permanent fault to occur. [6,7,8]

Despite the fact that metallized film capacitors already enable high energy density and high reliability, demands for even higher energy density, better reliability and longer life-time exist. It may be possible to fulfil these demands by utilizing nanodielectric films and thus, metallized film capacitor technology offers an extremely interesting platform for further research and development. The main subject of this thesis is to study the application possibilities of polypropylene nanocomposites in metallized film capacitors and the main objectives of the thesis were defined as:

- To form an overall picture of the research subject by performing an extensive literature research on polymers, dielectric polymer nanocomposites and metallized film capacitors. The purpose of the study is to serve as a basis for the empirical part of this thesis and for future work.
- To plan, construct and test a measurement system which could be used in the future to conduct various DC tests on single metallized nanocomposite film samples.

The theoretical part of this thesis is divided in three chapters. Properties of polymers with a special attention to the properties related to capacitor applications are discussed in depth in Chapter 2. In the beginning, structural, chemical and thermal properties of

polymers are introduced. Thereafter, dielectric properties of polymers such as polarization, permittivity and dielectric strength are discussed in depth. In addition, conduction mechanisms and space charge phenomenon in polymers will be treated in order to understand the breakdown mechanisms associated with solid dielectrics. Lastly, the main properties of polypropylene will be introduced, as it is one of the main polymeric materials for capacitor applications and also relevant for the practical part of this thesis. Chapter 2 also serves as a basis for further discussion about dielectric polymer nanocomposites in Chapter 3 – after introducing the basics of dielectric nanocomposites and their processing, the chapter will focus on dielectric properties of nanocomposite polymers. Models for the interfacial region between the polymer matrix and the filler particles are used to explain the altered properties of nanodielectrics. In Chapter 4, the structure and the operation of metallized film capacitors as well as the self-healing mechanism will be discussed comprehensively. Thereafter, various failure mechanisms and limitations specific for metallized film capacitors are discussed. Finally, alternative capacitor design principles to overcome some of these problems are introduced.

Based on the facts discussed in the theoretical part of this thesis, a test capacitor structure and a measurement system for conducting electrical tests on single metallized dielectric films was planned, constructed and tested. The specifications of the test capacitor structure and the measurement system are given in Chapter 5. The studied electrical properties included dielectric strength, maximum permissible electric field stress and self-healing capability of the film. In addition, the dependency of these properties on external pressure was studied with the measurement setup. The results of the tests are presented and evaluated in Chapter 6. The chapter is concluded with prospects for improvements and future work.

2 POLYMERS

2.1 Basic concepts and definitions

A *polymer* is defined as a large, chain-like molecule which consists of large amount of small repeating chemical units chemically bonded to each other. The basic building block of a polymer is called a *monomer*, which, by definition, means any molecule that can be converted to a polymer by combining it with other molecules of the same or different type in a process called *polymerization*. As an example, an illustration of polymerization of styrene monomers into polystyrene is presented in Figure 2.1. It is important to notice that although the monomer on the left and the *repeating unit* of the resulting polymer on the right (the chemical unit inside the square brackets) consist of identical atoms, the chemical structure of the repeating unit differs slightly from that of the basic monomer unit. This is due to the fact that polymerization usually requires the rearrangement of electrons in order to obtain appropriate chemical bonds to form the chain structure. [9]

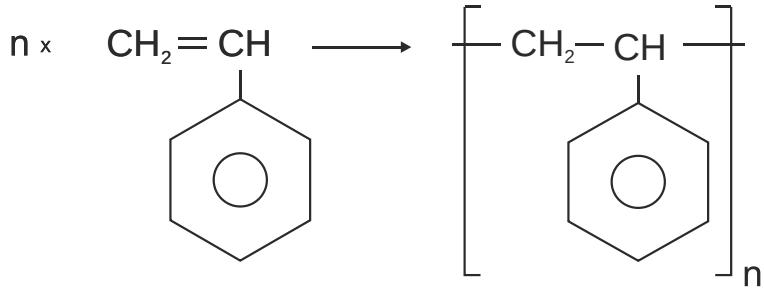

Figure 2.1. Polymerization of a styrene monomer (left) into polystyrene (right). [9]

The *degree of polymerization* (DP), which is denoted by the subscript *n* in Figure 2.1, defines the length of the polymer chain. The number of repeating units in a polymer chain varies but in a typical commercial grade polymer material a single polymer molecule consists of at least hundreds or thousands of repeating units. A high degree of polymerization is preferable, as it improves the thermal and mechanical properties of a polymer. However, polymers with short chain length also exist and they are generally referred to as *oligomers*. [9,10]

In addition to the degree of polymerization, the size of a polymer can also be quantified by defining the *molecular weight* (MW) of the polymer molecule. For a single polymer molecule, this is simply MW(polymer) = DP*MW(monomer). However, when a sample of polymer material is concerned, a distribution of various molecular weights exists, as the sample consists of massive amount of polymer molecules with

varying chain lengths and molecular weights. Therefore, the *average molecular weight* of a polymer sample can be defined. Two of the most common average molecular weight types are the *number-average molecular weight* $\overline{M_N}$ and the *weight-average molecular weight* $\overline{M_W}$, which are given by the Equations (2-1) and (2-2), respectively, and illustrated in Figure 2.2.

$$\overline{M_N} = \frac{\sum n_i M_i}{\sum n_i}, \tag{2-1}$$

$$\overline{M_W} = \frac{\sum w_i M_i}{\sum w_i} = \frac{\sum n_i M_i^2}{\sum n_i M_i}, \tag{2-2}$$

In the equations n_i is the number of molecules of molecular weight M_i and w_i is the mass (g) of material with molar mass of M_i. [11]

In addition to aforementioned definitions, the prevailing practice in SI-unit system (International System of Units) is to quantify the molecular weight as a *relative molecular mass* $\overline{M_r}$ which is defined as:

$$\overline{M_r} = \frac{12 m_m}{m_{12_C}}, \tag{2-3}$$

where m_m is the molar mass of the molecule considered and m_{12_C} is the molar mass of a ^{12}C carbon-isotope. [10]

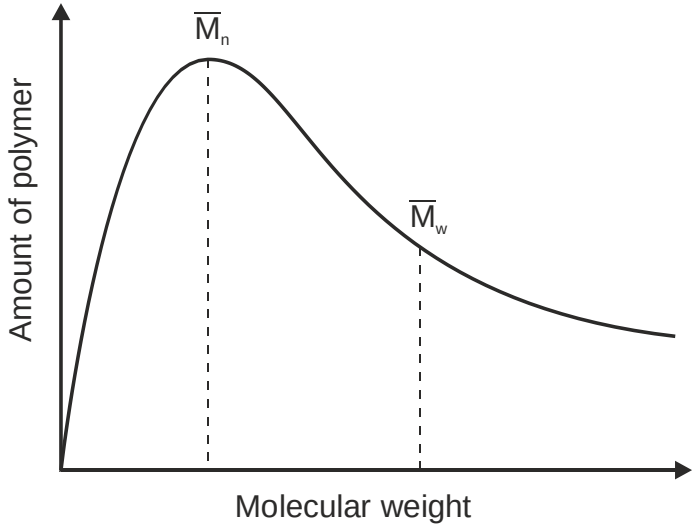

Figure 2.2. The number-average molecular weight $\overline{M_N}$ and weight-average molecular weight $\overline{M_W}$. [9]

2.2 Polymer structure

2.2.1 Polymer classification

There are numerous ways to classify polymers. For example, the classification can be based on the origin of the polymer, polymer structure, crystallinity, polymerization process and thermal properties. The most common ways to classify polymers are presented in the following.

With respect to the origin, polymers can be classified into three groups; *natural polymers (biopolymers), semi-synthetic polymers* and *synthetic polymers*. Examples of naturally occurring polymers are polymers such as polysaccharide, starch and cellulose. Semi-synthetic polymers can be manufactured from natural polymers by using chemical treatments. In contrast with natural and semi-synthetic polymers, synthetic polymers are purely man-made and consist of small monomer units manufactured by chemical industry. The group of synthetic polymers is vast and can be divided further into sub-groups such as plastics, elastomers, fibers and so on. Most common examples of synthetic polymers are polymers such as polyethylene and polypropylene. The origin-based classification can be further extended in accordance to the carbon-content of the polymer (*organic* and *inorganic polymers*). [10,9]

The classification according to the polymer structure is based on how the repeating units in the polymer chain are connected to each other. The interlinking capability of a molecule can be examined by the concept of *functionality* of a molecule. Functionality is defined as a number of sites in the molecule where a chemical bond with another molecule can be formed. Therefore, a molecule can be categorized as *monofunctional*, *bifunctional* or *polyfunctional* depending on the number of interlinking-capable sites the molecule has. Monofunctional molecules can only form oligomers with DP of two (*dimer*) as after interlinking of two molecules there are no more functional sites available for further polymerization. However, in case of bifunctional monomers, the polymerization process can proceed further and a *linear polymer* is formed. Linear sequence is an inevitable result of bifunctionality. Following the same logic, polyfunctional molecules are able to form *branched* or *crosslinked polymers*. In branched structure, branch-like chains are grown from the backbone of the polymer chain. Crosslinked structure is similar to branched structure but in this case the side chains form chemical bonds with other polymer molecules. Figure 2.3 illustrates these three polymer structures. [9]

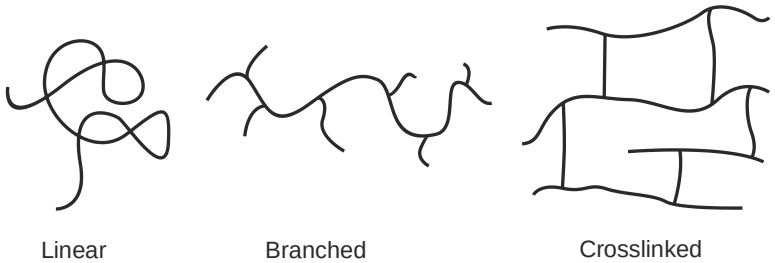

Figure 2.3. Linear, branched and crosslinked polymer structure. [9]

Polymers can also be classified based on their chemical composition. Polymers which consist of only one type of repeating unit are defined as *homopolymers*. In addition, it is also possible to manufacture *copolymers* which are composed of two or more types of repeating units. The classification of copolymers can be further extended by specifying how the repeating units are arranged in the polymer chain. If a two-component copolymer with repeating units A and B is considered, the following arrangements can be defined [9]:

- *Random copolymer*: The repeating units are randomly arranged in the polymer chain.

  -A-A-B-A-B-B-A-B-A-

- *Alternating copolymer*: The repeating units are arranged in an ordered fashion.

  -A-B-A-B-A-B-A-B-A-

- *Block copolymer*: The repeating units are arranged in blocks which may vary in length.

  -AAAA-BBBBBB-AAA-BBBB-AAAA-

- *Graft polymer*: Blocks of one type of repeating unit are grafted into chain formed by another type of repeating unit.

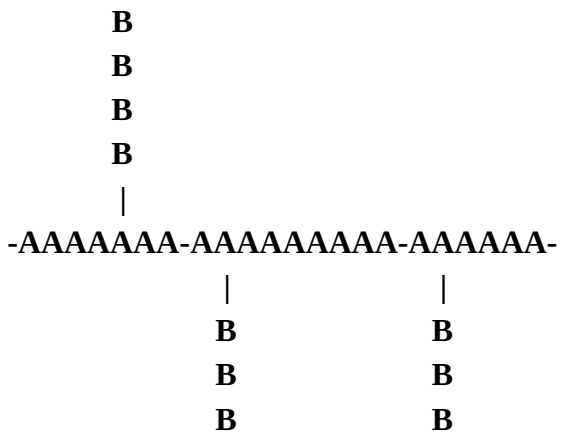

Based on the moulding properties, polymers can also be grouped in *thermoplastics*, *thermosets* and *elastomers*. Thermoplastics consist of long, non-crosslinked polymer chains. When thermoplastics are heated, the molecule-interlinking chemical bonds in the polymer chains weaken and during cooling, the bonds are restored. Thus, it is possible to reshape thermoplastics by exposing the material to increased temperature and pressure. In contrast with thermoplastics, thermosets consist of long, crosslinked polymer chains. As it is not possible to break the crosslinks between polymer molecules by heating, thermosets cannot be reshaped after the material has cooled down at the end

of the polymerization process. Therefore, thermosets have to be moulded into desired shape during polymerization. Elastomers, which are flexible, rubber-like materials, represent an intermediate form between thermoplastics and thermosets. [10]

2.2.2 Polarity and chemical bonding

When the electrical, structural and chemical properties of polymers are discussed, the concept of *polarity* is essential. Polarity refers to the separation of electric charge within a molecule. If the positive and negative charges are separated within a molecule, the molecule has a permanent dipole moment and it is said to be *polar*. Molecules can also be only *weakly polar* or *non-polar* depending on the distribution of electrons within the atoms in the molecule. For a polyatomic molecule, the polarity can be defined as a vector sum of all the dipole moments of the groups within the molecule. Therefore, the polarity of a polymer can be defined as a vector sum of all the dipole moments of the monomers it consists of. [9]

As the chemical, electrical and mechanical properties of polymers are directly related to the chemical bonds acting within and between the monomer units, the chemical bond types will be discussed briefly. Depending on whether the valence electrons are involved in the formation of the bonds or not, the chemical bonds can be divided into *primary bonds* and *secondary bonds*, as shown in Table 2.1 [9]:

Table 2.1. Chemical bond types.

Primary bonds	Secondary bonds
Ionic bond	Dipole bond
Covalent bond	Hydrogen bond
Metallic bond	Induction forces
	Van der Waals forces

Primary bonds, which are intra-molecular forces, are strong due to the involvement of valence electrons. *Ionic bonds* are formed when ions with opposite polarities are attracted to each other resulting in a stable unit. Atoms within a molecule may become cations or anions by losing or gaining valence electrons, respectively. For polymers, ionic bonding may be possible if the repeating units consist of carboxyl acid groups. *Covalent bonds* are extremely strong chemical bonds based on the sharing of valence electrons between the neighbouring atoms in a molecule. As a result, the covalently bonded atoms attain completed outer shells. For polymers, covalent bonding is the predominant bond type. *Metallic bond*, which is an intermediate between ionic and covalent bonding, is only characteristic for metals, and thus it is not relevant for polymers. [10,12]

Secondary bonds are weak inter-molecular forces which generally exist between molecules with either permanently or momentarily separated charges. *Dipole bonds* are formed between molecules with permanent dipoles. *Hydrogen bonds* are formed between positively charged hydrogen atoms and small electronegative atoms. Polar

molecules are also capable to polarize adjacent molecules via *induction force*s which results in weak bonding. *Van der Waals forces* are instantaneous, intra-molecular forces based on the movement of the electrons around the atom core. [9]

2.2.3 Configuration and conformation

Polymers with equal chemical compositions may differ from each other geometrically. To distinguish between different geometrical arrangements, the concepts of *configuration* and *conformation* can be used. Generally, polymers with equal chemical compositions but different geometrical arrangements are referred to as *isomers*.

The configuration of a polymer chain refers to the arrangement of repeating units fixed by primary valence electrons. The configuration can only be altered by breaking or reforming the chemical bonds between the molecules in the polymer chain. If the repeating units in the polymer chain are arranged and oriented in an orderly fashion and the chemical bonds between the repeating units are uniform, the polymer is said to be structurally regular.

One important aspect of the configuration is the *stereoregularity*, which describes the spatial arrangement of a polymer. Some polymers have a series of asymmetric substituent groups connected to the polymer backbone. The arrangement of adjacent substituent groups in the chain changes the stereoregularity of the polymer and is defined as *tacticity*. As an example, in polypropylene, the substituent group $–CH_3$ (methyl) of each monomer unit can be arranged in three different ways. Therefore, *isotactic, syndiotactic* and *atactic* forms of polypropylene can be defined, and they are illustrated in Figure 2.4. In an isotactic arrangement, all the substituent groups are located at the same side of the polymer backbone. In a syndiotactic arrangement, the locations of the substitute groups alternate around the polymer backbone as shown in the Figure 2.4b. In an atactic arrangement, the substitute groups are arranged randomly. Tacticity affects many of the polymer properties such as the crystallinity. Isotactic polypropylene (iPP) has high crystallinity due to its structural regularity whereas atactic polypropylene stays amorphous, as it is impossible for the irregular chains to form crystallites. [9,13,10,14]

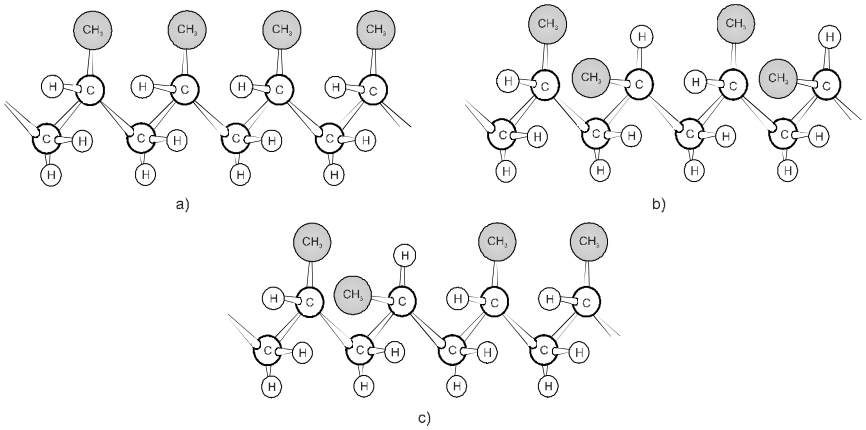

Figure 2.4. Isotactic (a), syndiotactic (b) and atactic (c) forms of polypropylene. [13]

As opposed to configuration, which refers to the arrangement of the repeating units in a polymer chain, conformation refers to an arrangement established by rotation of the polymer chain segments about primary valence bonds. The number of possible rotational states (conformations) depends on various factors such as dimensions, crystallinity and the state (solid, molten, solution) of the polymer. As an example, various conformational states of *n*-butane are shown in Figure 2.5a. Conformational states lead to variations in overall size and shape of the polymer chain. The relative orientation of the adjacent methyl groups highly affects the stability of the conformation. In *trans*-conformation (Figure 2.5b), where the methyl groups are aligned opposite each other, the potential energy between the substituent groups is smallest, and the conformation is the most stable. On the contrary, the *fully eclipsed* conformation is the most unstable. *Gauche*- and *eclipsed*- conformations are intermediate forms between trans- and fully eclipsed- conformations. For polypropylene, trans-conformations of repeating units of propylene result in isotactic arrangement shown in Figure 2.4a. Conversely, sequence of trans- and gauche- conformations in syndiotactic polypropylene result in a helical chain structure of as shown in Figure 2.4b. [9,15]

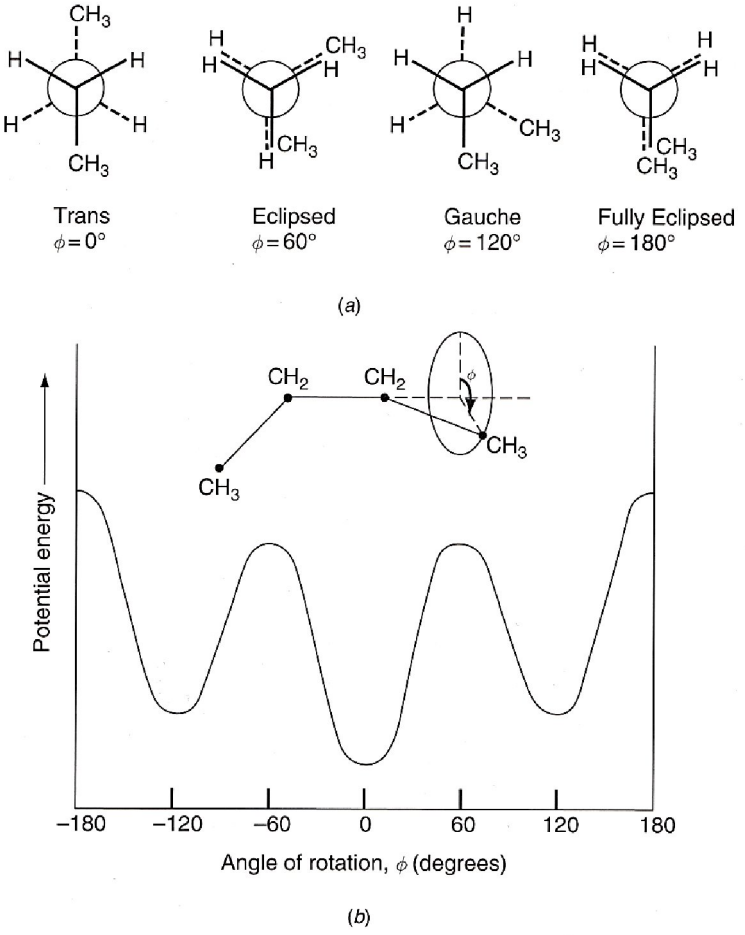

Figure 2.5. Various conformational states of n-butane (a) and the corresponding potential energy as a function of rotation angle φ in degrees (b). [15]

2.3 Polymer morphology

2.3.1 Crystalline and amorphous structure

When polymers are cooled from the molten state or concentrated from a solution, the polymer chains tend to form regular formations by packing closely to each other. These regions with long-range, three-dimensional and ordered arrangement are called *crystallites*. In contrast with the crystalline regions, in the *amorphous* regions the polymer chains are arranged and tangled with each other randomly. Due to the fact that the chain lengths, configurations and conformations of the polymer chains vary, it is impossible for the polymer chains to obtain a perfect arrangement. Therefore, polymers can never be 100 % crystalline and thus they are said to be semi-crystalline. The ratio of the crystalline polymer volume to the total volume is defined as *the degree of crystallinity*. [9]

In order to study the polymer morphology, i.e. the overall structure of a polymer system, models for the crystalline and amorphous regions have been developed. According to the earliest model, *the fringed micelle* –model, the polymer chains form crystallites of about 100 Å long as illustrated in Figure 2.6. The polymer chains pass through multiple crystallites and the regions between the crystallites are amorphous. [11]

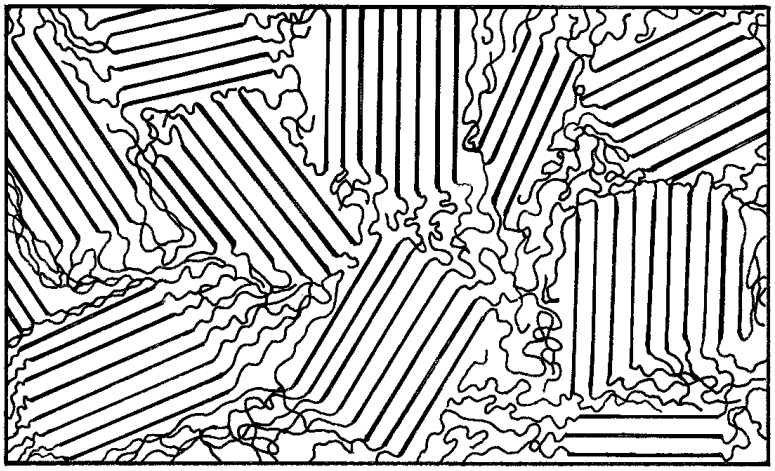

Figure 2.6. The fringed micelle –model of the crystalline structure of polymers. [9]

The fringed micelle –model was able to explain most of the properties of stiff semi-crystalline polymers, but it is not appropriate for flexible polymers [15]. Therefore, the model has been further developed leading to the *folded-chain –model*. According to this model, the polymer chains fold repeatedly on themselves forming a three-dimensional *lamella structure*, as illustrated in Figure 2.7. As depicted in the figure, the polymer chains are folded back and forth at the fold planes. The fold period, which is the thickness of the lamella structure, is approximately 100 Å (=10 nm). Irregularities, defects and loose chains may occur in the lamella structure. [9]

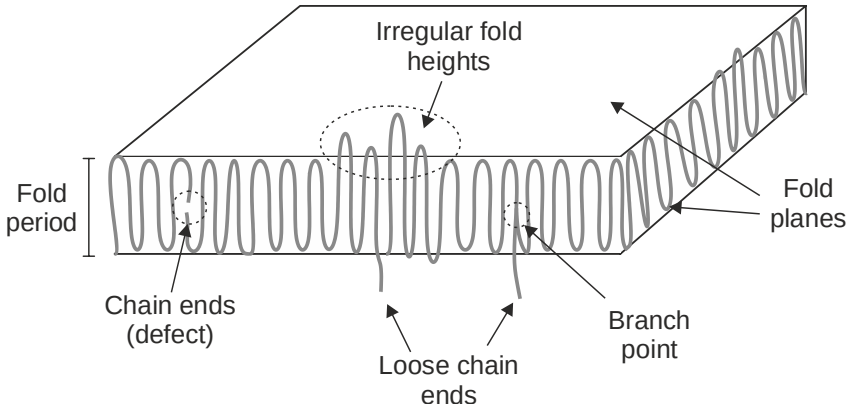

Figure 2.7. The lamella structure of a crystallite in polymer.

When polymers are cooled from molten state, during the crystallization, special structures called *spherulites* may form. Spherulites are sphere-shaped, fibre-like structures consisting of interconnected lamellae as illustrated in Figure 2.8. Spherulites grow radially from the growth-center at constant rate until the edge regions of adjacent spherulites reach each other. The growth-center may be a single crystallite or an impurity in the material. The size of a spherulite may range from approximately 0.1 µm up to few mm depending on e.g. the purity of the polymer. [11,9]

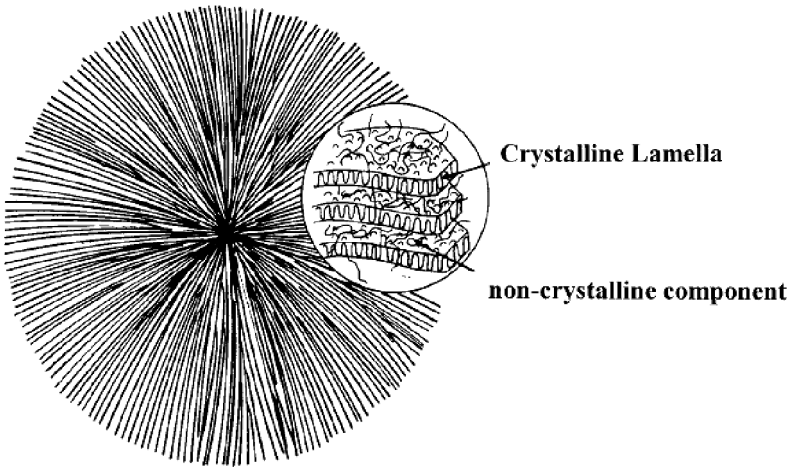

Figure 2.8. A spherulite consisting of crystalline lamellae with amorphous region between the lamellae. [14]

2.3.2 Thermal transitions

Temperature has a significant effect on the polymer morphology. As the temperature changes, polymers undergo transitions between solid, rubbery and liquid states depending on the crystallinity of the material. Therefore, thermal properties of polymers are of great importance when selecting appropriate materials for various applications.

When an amorphous polymer at a molten state is cooled down, it transforms gradually into rubbery material, because the mobility of polymer chains decreases. As the temperature is further decreased, the material eventually turns into hard, glassy and

brittle material at a material-specific temperature called the *glass transition temperature* T_g. For a semicrystalline polymer, only the amorphous regions between the crystalline regions undergo the aforementioned transition. However, when a semicrystalline polymer is heated, there is a specific temperature region where the crystallites start to melt. This temperature region is called the *crystalline melting point* T_m. Above T_m, the crystalline regions melt completely and the material turns into highly viscous fluid. The transitions between solid and liquid states for amorphous and semicrystalline polymers are illustrated in Figure 2.9. [9]

Thermal transitions also affect the specific volume of the polymer, as depicted in Figure 2.9. With decreasing temperature, the specific volume decreases, as the mobility of the polymer chains is reduced. It is also observed, that when semicrystalline polymer material is cooled from the molten state, the specific volume decreases abruptly below the T_m. This is because at this temperature region, the polymer chains begin to form crystallites which results in considerable reduction in specific volume as the polymer chains are packed close to each other. For amorphous polymers, no such abrupt change in specific volume can be observed. [12]

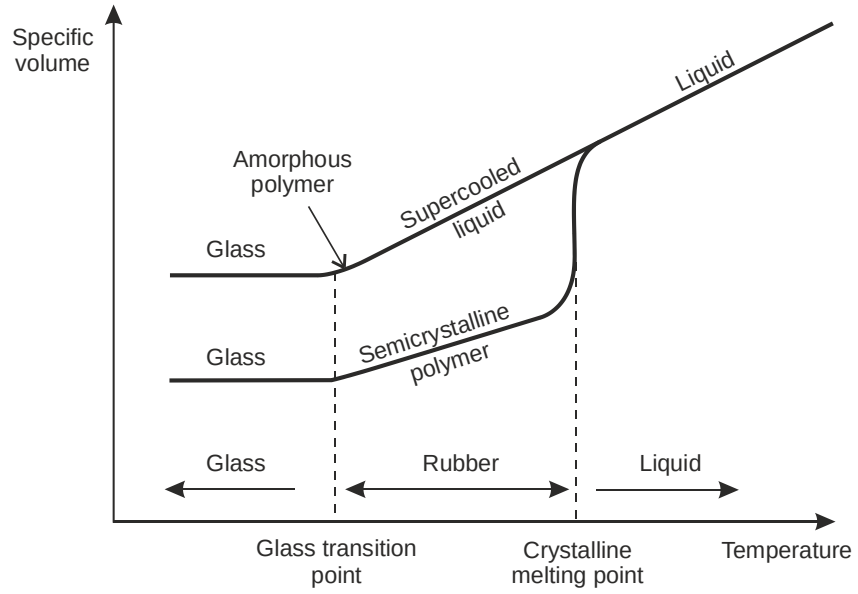

Figure 2.9. Thermal transitions and changes in specific volume for amorphous and semicrystalline polymers as a function of temperature. [12]

2.4 Electrical properties of polymers

Polymers are widely used in various applications in the field of electrical engineering, typically for insulation purposes. As the main focus of this thesis is in the application of metallized polymer films in capacitors, the dielectric properties of polymers will be discussed in depth in the following sub-chapters. In addition, conduction mechanisms, space charge phenomenon and dielectric breakdown mechanisms will be discussed in order to better understand the phenomena that may take place in capacitors.

2.4.1 Macroscopic polarization and permittivity

The dielectric properties of polymers are essentially based on the concepts of polarization and permittivity. In order to examine these in a macroscopic scale, let us consider a simple parallel-plate capacitor configuration with a vacuum between the electrodes as illustrated in Figure 2.10a.

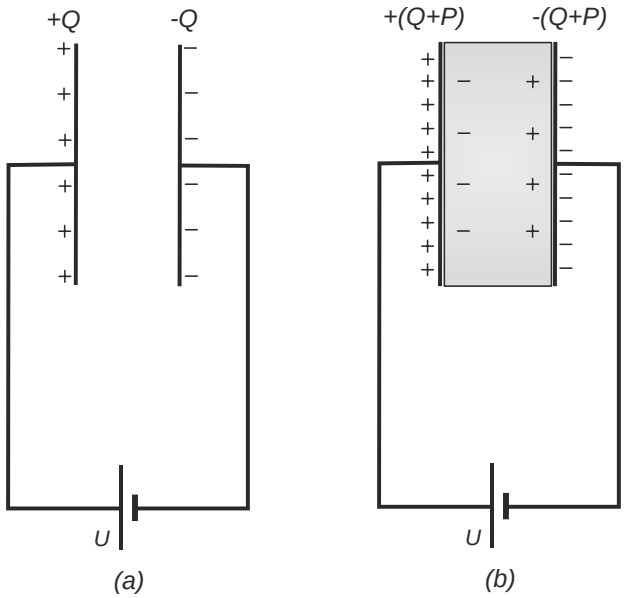

Figure 2.10. Parallel-plate electrode configuration with (a) a vacuum (b) dielectric between the electrodes.

The voltage U over the system is fixed and the distance between the electrodes is d. It is further assumed, that the electric field between the electrodes is homogeneous and isotropic, i.e. it is uniform in all directions. Therefore, the magnitude of the electric field $\bar{\boldsymbol{E}}$ is given by the equation [15]:

$$|\bar{\boldsymbol{E}}| = \frac{U}{d}. \tag{2-4}$$

According to the Coulomb's law, charges $+Q$ and $-Q$ per the electrode unit area will be stored on the electrodes and their magnitude is directly proportional to the magnitude of the electric field:

$$Q = \varepsilon_0 |\bar{\boldsymbol{E}}| \tag{2-5}$$

where the proportionality coefficient ε_0 is the *permittivity of free space* and equals to $8.85 \times 10^{-12} \mathrm{Fm}^{-1}$. [15]

For the electrode arrangement considered, the *vacuum capacitance* C_0 per unit area of the electrode can be defined as the ratio of stored charge per unit electrode area to the applied voltage [15]:

$$C_0 = \frac{Q}{U}. \tag{2-6}$$

If the same electrode configuration is now considered with insulating dielectric material inserted between the electrodes instead of a vacuum, the insulating material will be *polarized* due to the electric field, i.e. the positive and negative charges in the bulk material are separated in accordance to the direction of the electric field. If a small volume element Δv of the dielectric material is considered, the induced *dipole moment* due to the electric field is [16]:

$$\Delta \bar{\boldsymbol{p}} = \int_{\Delta v} \bar{\boldsymbol{r}} dq\ , \tag{2-7}$$

where $\bar{\boldsymbol{r}}$ is the distance vector between the separated charges $+q$ and $-q$. According to the Equation (2-7), the dipole moment depends on the size of the volume element Δv. It is therefore more convenient to define the electric dipole moment per unit volume induced by the applied electric field. This is called the *polarization* of the material, and is defined as [16]:

$$\bar{\boldsymbol{P}} = \frac{\Delta \bar{\boldsymbol{p}}}{\Delta v}. \tag{2-8}$$

Although the volume element Δv considered above is assumed to be very small, it may still contain many molecules. Therefore, it is desirable to define the electric dipole moment of a single molecule:

$$\bar{\boldsymbol{p}}_{\boldsymbol{m}} = \int_{molecule} \bar{\boldsymbol{r}} dq\ . \tag{2-9}$$

Now, as the induced dipole moment of a volume element Δv is the sum of the molecular dipole moments inside the volume, the polarization $\bar{\boldsymbol{P}}$ can be written as [16]:

$$\bar{\boldsymbol{P}} = \frac{1}{\Delta v} \sum_{m} \bar{\boldsymbol{p}}_{\boldsymbol{m}}\ . \tag{2-10}$$

The concept of polarization is illustrated in the Figure 2.11. Each volume element Δv of the polarized material consists of charges $+q$ and $-q$ and represented as a dipole $\Delta \bar{\boldsymbol{p}}$. [16] These dipoles will contribute to the overall charge distribution of the bulk material, resulting in storage of additional charges $+P$ and $-P$ on the electrodes as illustrated in Figure 2.10b. Thus, when dielectric material is inserted between the

electrodes, more charge can be stored in the electrode arrangement. The ratio of the increased capacitance to the vacuum capacitance is given by the equation [15]:

$$\varepsilon_r = \frac{C}{C_0} = \frac{Q + P}{Q}, \tag{2-11}$$

where the material-specific constant ε_r is called the *dielectric constant* or the *relative permittivity* of the material, and it is frequently independent of the applied field [16]. By combining Equations (2-5) and (2-11), the dielectric constant can be written as:

$$\varepsilon_r = \frac{\varepsilon_0 \overline{\boldsymbol{E}} + \overline{\boldsymbol{P}}}{\varepsilon_0 \overline{\boldsymbol{E}}} = 1 + \frac{\overline{\boldsymbol{P}}}{\varepsilon_0 \overline{\boldsymbol{E}}} = 1 + \chi, \tag{2-12}$$

where χ is the *electric susceptibility* of the material. Furthermore, by rearrangement of the Equation (2-12), the *flux of dielectric displacement* $\overline{\boldsymbol{D}}$ can be achieved and it can be written as [15]:

$$\overline{\boldsymbol{D}} = \varepsilon_0 \varepsilon_r \overline{\boldsymbol{E}} = \varepsilon_0 \overline{\boldsymbol{E}} + \overline{\boldsymbol{P}}. \tag{2-13}$$

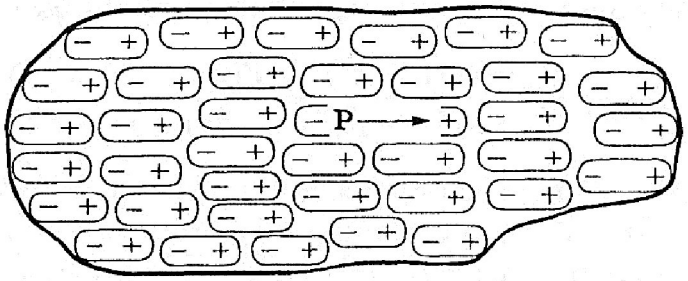

Figure 2.11. A piece of polarized material and the corresponding polarization $\overline{\boldsymbol{P}}$. Each volume element Δv is represented by a dipole moment with charges +q and –q. [16]

The Equation (2-13) for $\overline{\boldsymbol{D}}$ is a fundamental electric field equation which applies at any point inside the dielectric medium. Based on this equation, it can be defined, how an electric field is distributed in a system with different dielectric materials. For example, let us consider a series connection of dielectric materials A and B between plate electrodes as shown in Figure 2.12. The materials have thicknesses of d_A and d_B, permittivities of ε_A and ε_B and the voltage across the arrangement is U. As $\overline{\boldsymbol{D}}$ is continuous across both the materials, the ratio of electric field stresses in the materials can be written as:

$$\frac{|\overline{\boldsymbol{E}}_A|}{|\overline{\boldsymbol{E}}_B|} = \frac{\varepsilon_B}{\varepsilon_A}. \tag{2-14}$$

In other words, the electric field stress is distributed according to the material permittivities, i.e. the material with lower permittivity is subjected to higher field stress. This may be critical for dielectric materials with gas voids or impurities inside the material due to poor manufacturing process. The increased electrical stress in these areas may lead to partial discharges which may result in erosion of the dielectric. Partial discharges will be discussed more in sub-chapter 2.4.7. [1]

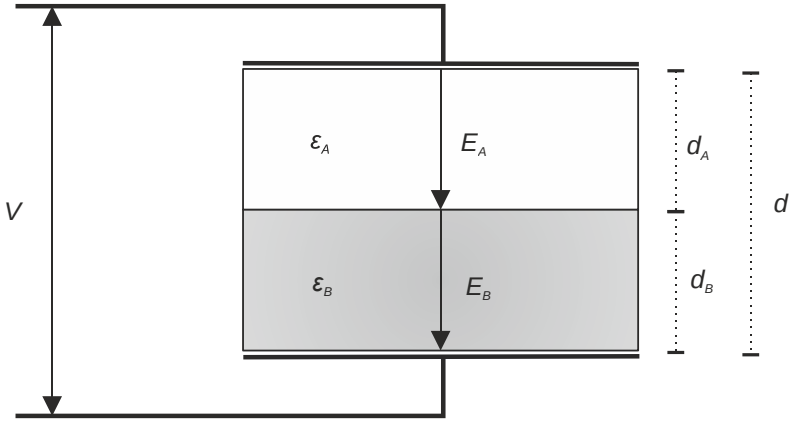

Figure 2.12. A series connection of two dielectric materials with different permittivities.

2.4.2 Molecular polarizability and permittivity

The preceding part discussed polarization and permittivity of dielectric material in a macroscopic scale. In order to better understand these phenomena in a molecular scale and to estimate permittivity of polymer materials, the local electric field which acts on a single molecule needs to be considered. This electric field is called the *molecular field* $\overline{\boldsymbol{E_m}}$ and it is produced by all the external field sources and other polarized molecules in the dielectric except for the molecule at the point under consideration.

By following the approach used by Reitz *et al*. in [16], also known as the *Lorentz cavity*, an equation for $\overline{\boldsymbol{E_m}}$ can be achieved. A parallel-plate electrode arrangement similar to the one used in the previous discussion with dielectric medium between the electrodes is considered. An imaginary sphere *S* is drawn at a point in dielectric where the molecular field is to be calculated as illustrated in Figure 2.13a. If the chosen size of the sphere is small in comparison with the size of the electrode arrangement, but large in comparison with the molecular scale, the dielectric material around this cavity can be treated as a continuum as shown in Figure 2.13b. The molecules inside the sphere are to be treated one by one. Therefore, the molecular field at a specific point inside the sphere can be written as:

$$\overline{\boldsymbol{E_m}} = \overline{\boldsymbol{E_x}} + \overline{\boldsymbol{E_d}} + \overline{\boldsymbol{E_s}} + \overline{\boldsymbol{E'}}\,, \tag{2-15}$$

where $\overline{\boldsymbol{E_x}}$ is the primary electric field from the electrodes, $\overline{\boldsymbol{E_d}}$ is the depolarizing field due to polarization charges on the outside surfaces of the dielectric (at the dielectric-

electrode interface), $\overline{\boldsymbol{E_s}}$ is the field due to polarization charge on the surface of the sphere and $\overline{\boldsymbol{E'}}$ is the field due to all the dipoles inside the sphere. After the individual electric field components of the Equation (2-15) are determined (for the details, the reader is advised to see [16]), the molecular field can be written as a function of the macroscopic electric field and the polarization:

$$\overline{\boldsymbol{E_m}} = \overline{\boldsymbol{E}} + \frac{1}{3\varepsilon_0}\overline{\boldsymbol{P}}\,. \tag{2-16}$$

Furthermore, by substituting for $\overline{\boldsymbol{P}}$ from the Equation (2-12), Equation (2-16) can be written as [15]:

$$\overline{\boldsymbol{E_m}} = \frac{(\varepsilon_r + 2)}{3}\overline{\boldsymbol{E}}\,. \tag{2-17}$$

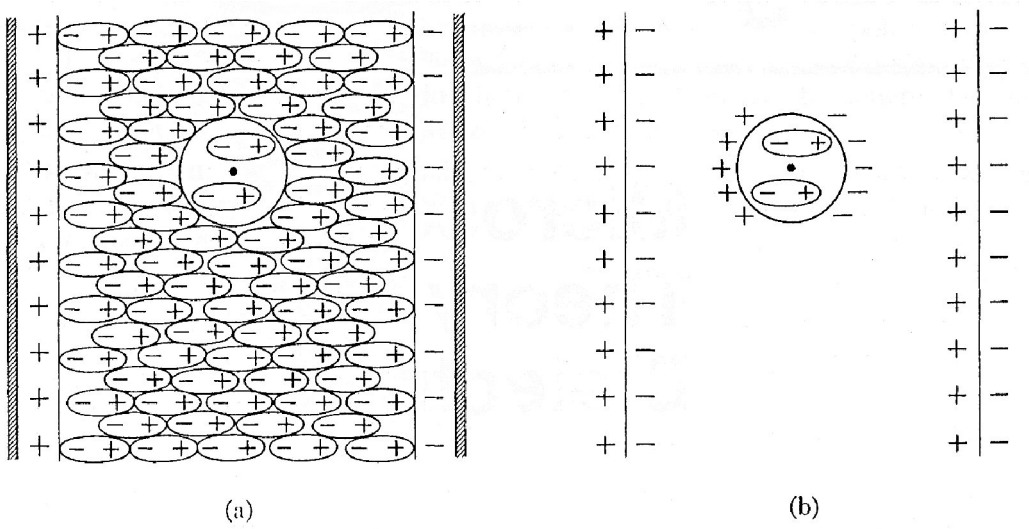

Figure 2.13. The Lorenz cavity method. [16]

As the field acting on a single molecule is now determined, the *molecular polarizability* α can be defined. Molecular polarizability is the ratio of the molecular dipole moment to the molecular electric field and it can be expressed as [16]:

$$\overline{\boldsymbol{p_m}} = \alpha\overline{\boldsymbol{E_m}}\,. \tag{2-18}$$

From macroscopic point of view, the dielectric volume contains *N* molecules per unit volume. Therefore, based on the Equation (2-18), the macroscopic polarization, which is the total dipole moment per unit volume, can be written as [15]:

$$\overline{\boldsymbol{P}} = N\alpha\overline{\boldsymbol{E_m}} = N\alpha\frac{(\varepsilon_r + 2)}{3}\overline{\boldsymbol{E}}. \tag{2-19}$$

Finally, by substituting for $\bar{\boldsymbol{P}}$ from the Equation (2-12), the *Clausius-Mosotti* relation can be acquired [15]:

$$\frac{(\varepsilon_r - 1)}{(\varepsilon_r + 2)} = \frac{N\alpha}{3\varepsilon_0}. \tag{2-20}$$

Furthermore, as the number of molecules per unit volume N inside the dielectric is not directly known, the Equation (2-20) can be expressed as:

$$\frac{(\varepsilon_r - 1)}{(\varepsilon_r + 2)}\frac{M_W}{\rho} = \frac{N_A\alpha}{3\varepsilon_0}, \tag{2-21}$$

where M_W is the molar mass of the dielectric material, ρ its density and N_A the Avogadro's number. [15]

It can be seen that Equation (2-21) relates the molecular polarizability α to the macroscopic relative permittivity ε_r. In principle, Equation (2-21) can be used to estimate the relative permittivity of a non-polar polymer, as it is possible to determine molecular polarizability of polymer molecules by using calculations based on density functional theory (DFT). [17,14]

2.4.3 Polarization mechanisms and dielectric relaxation

Polarization results from superposition of various polarization mechanisms which can be divided into [14]:

- Electronic polarization
- Atomic polarization
- Dipole polarization
- Interfacial polarization

The first three mechanisms are molecular polarization mechanisms which involve redistribution of charges which are bound in the atomic structure, whereas the fourth one is related to accumulation of charge carriers within the dielectric volume. Each mechanism has its own characteristic relaxation frequency as depicted in Figure 2.14. At higher frequencies, the slower polarization mechanisms can be disregarded, as they are too slow to have a significant contribution to the total polarization. [14,1]

When an electric field is acting on a single atom, the negatively charged electron cloud will be displaced slightly from the positive nucleus. This redistribution of positive and negative charges results in an induced dipole moment; the atom is *electronically polarized*. Electronic polarization is the fastest polarization mechanism and its characteristic resonance frequency is in the range of 10^{15} to 10^{18} Hz. [14]

As opposed to electronic polarization, *atomic polarization* results from the mutual displacement of atomic nuclei forming a molecule due to the applied electric field. These displacements may involve twisting and bending of polar groups or variations in bond length and angle between the nuclei. The characteristic resonance frequency of atomic polarization is in the range of 10^{12} to 10^{13} Hz. It is slower than electronic polarization, as the mobility of the heavy nuclei is smaller in comparison with that of the light-weight electrons. [14]

As discussed in sub-chapter 2.2.3, some molecules and polymers may possess a permanent dipole moment. When an electric field is applied, the dipole moments tend to align according to the direction of the field. *Dipole polarization* is the slowest of the molecular polarization mechanisms. As illustrated in Figure 2.14, after the threshold value of approximately 10^9 Hz, its contribution to the total molar polarization increases gradually with decreasing frequency. [14]

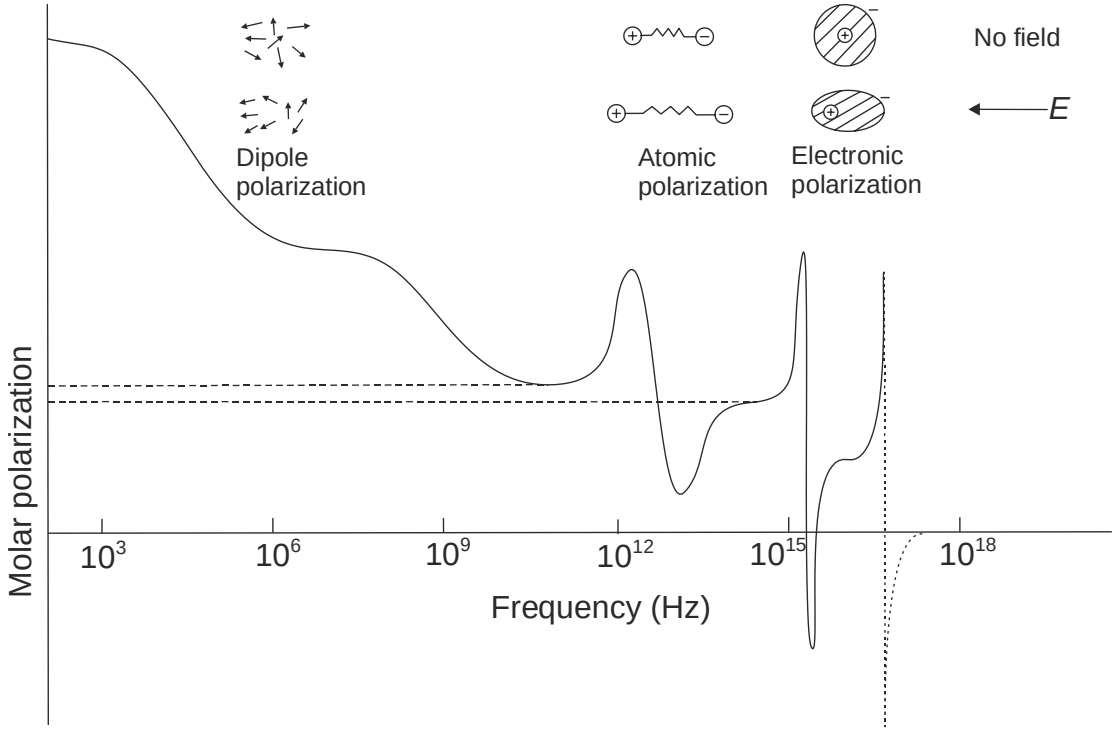

Figure 2.14. Dispersion of molar polarization mechanisms in a dielectric. [15]

Interfacial polarization refers to the accumulation of charges at the interfaces between two materials. Interfacial polarization occurs at the interfaces between crystalline and amorphous regions in polymer which may lead to deep trap sites. Voids, particles and impurities in the dielectric medium and the electrode-dielectric interfaces are also subjected to interfacial polarization. Interfacial polarization is the slowest of the polarization mechanisms and it is most significant at low frequencies. The effect of interfacial polarization at will be discussed more in sub-chapter 2.4.4 [14]

It should be noted, that when an electric field is applied to a dielectric medium, the polarization does not reach its steady state value instantaneously. Instead, it takes a finite time for the polarization to build up. Similarly, when the electric field is suddenly

removed, the dipoles in the dielectric do not revert back to random positions immediately. This decay time is called the *relaxation time* and the phenomenon in general is called the *dielectric relaxation*. Therefore, the relative permittivity of a material varies depending whether the polarization has reached its steady-state value or not. The *instantaneous relative permittivity* ε_∞ can be measured immediately after the application of the electric field. As the dipole orientation has not taken place completely, the value of ε_∞ is low. After a sufficiently long time has allowed for the dipoles to orientate, the *static relative permittivity* ε_s can be measured whose value is higher than ε_∞ due to dipole orientation and interfacial polarization. [15]

2.4.4 Complex relative permittivity and dielectric losses

As discussed in the previous sub-chapter, polarization involves movement of charge carriers which will always result in losses due to molecular friction and relaxation processes. Additionally, dielectric materials are never ideal insulators as they will always have a slight amount of conductivity which results in resistive losses. Therefore, a lossy dielectric medium can be seen as a capacitor and it can be modelled with e.g. a RC-parallel equivalent circuit as illustrated in Figure 2.15a. [1] It is important to point out that this simple model may not hold true for the whole frequency and temperature domain and typically a more sophisticated model is needed to simulate the behaviour of a dielectric more accurately. However, in terms of this thesis, the model is convenient for explaining the following phenomena. [14]

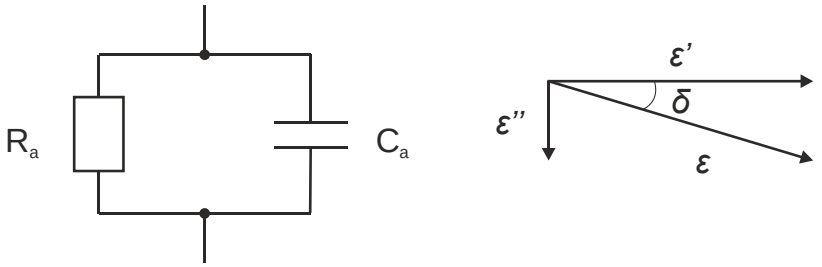

Figure 2.15. (a) A typical parallel RC circuit used to model a lossy dielectric (b) the components of complex permittivity.

As shown in Figure 2.15b, the permittivity of the material is complex, and can be written as [1]:

$$\bar{\varepsilon} = \varepsilon' - j\varepsilon'' = \varepsilon\angle - \delta \, . \tag{2-22}$$

The real part ε' of the complex permittivity and the corresponding capacitance C_a in the equivalent circuit represent the ideal insulating properties. The imaginary part ε'', or the *dielectric loss factor*, represents the losses due to polarization and conductivity, and it is

modelled as the resistance R_a in the equivalent circuit. The real and imaginary parts of the permittivity are linked together by the relation:

$$\tan\delta = \frac{\varepsilon''}{\varepsilon'} \approx \frac{\varepsilon''}{\varepsilon}, \tag{2-23}$$

where $\tan\delta$ is called the *dissipation factor*, which defines how much the dielectric differs from an ideal one. The approximation in the Equation (2-23) can be made because the conductivity of the dielectric is typically extremely low ($\varepsilon'' \ll \varepsilon'$), and thus the real part of the complex permittivity can be approximated as the total permittivity ($\varepsilon' \approx \varepsilon$). [1]

It is preferable to define expressions for the reactive power generated in the capacitor and the active power losses which occur due to polarization and conductivity of the dielectric. When sinusoidal AC voltage with angular frequency of $\omega = 2\pi f$ (where f is the frequency) is applied over the circuit, equations for the elements C_a and R_a can be obtained by defining the total admittance of the equivalent circuit and combining it with Equations (2-11) and (2-22) which results in:

$$C_a = \varepsilon_r' C_0 \approx \varepsilon_r C_0 \tag{2-24}$$

$$R_a = \frac{1}{\omega \varepsilon_r'' C_0} \approx \frac{1}{\omega \varepsilon_r \tan\delta\, C_0}. \tag{2-25}$$

Furthermore, by defining the current which flows through the equivalent circuit, expressions for the capacitive reactive power Q_c and the dielectric loss power P_d can be obtained:

$$Q_c = \omega \varepsilon_r C_0 U^2 \tag{2-26}$$

$$P_d = \omega \varepsilon_r \tan\delta\, C_0 U^2. \tag{2-27}$$

It can be seen from the above equations that the loss factor also defines the ratio of the dielectric power losses to the capacitive reactive power generated, i.e. it defines the efficiency of the capacitor. $\tan\delta$-measurements are commonly used for insulation condition monitoring in the field of high voltage engineering. [1]

It should be noted, that due to dispersion of the polarization mechanisms and the dielectric relaxation, both the permittivity and the dielectric losses are in fact frequency-dependent. It is therefore necessary to extend the preceding definition of complex permittivity to frequency domain by defining the *Debye dispersion equation* [15]:

$$\overline{\varepsilon(\omega)} = \varepsilon_\infty + \frac{\varepsilon_s + \varepsilon_\infty}{j\omega\tau}, \tag{2-28}$$

where ε_∞ and ε_s are the instantaneous and static relative permittivities, as explained in the sub-chapter 2.4.3, and the characteristic time constant τ is the *dielectric relaxation time*. The detailed derivation of Equation (2-28) is presented in reference [14]. By expressing the real and imaginary parts of Equation (2-28) separately, frequency-dependent equations for ε' and ε'' are obtained [15]:

$$\varepsilon'(\omega) = \varepsilon_\infty + \frac{\varepsilon_s - \varepsilon_\infty}{1 + \omega^2\tau^2} \tag{2-29}$$

$$\varepsilon''(\omega) = \frac{\varepsilon_s - \varepsilon_\infty}{1 + \omega^2\tau^2}\omega\tau. \tag{2-30}$$

Although the model is not accurate, the Debye equations can be used to illustrate the frequency dependency of complex permittivity. It can be seen that for low values of $\omega\tau$, the Equations (2-29) and (2-30) suggest that $\varepsilon' \to \varepsilon_s$ and ε'' is small, and for high values of $\omega\tau$, $\varepsilon' \to \varepsilon_\infty$ and ε'' is small. Therefore, for intermediate values of $\omega\tau$, the maximum of ε'' is found. This dispersion of ε' and ε'' according to the Debye equations is illustrated in Figure 2.16. [14]

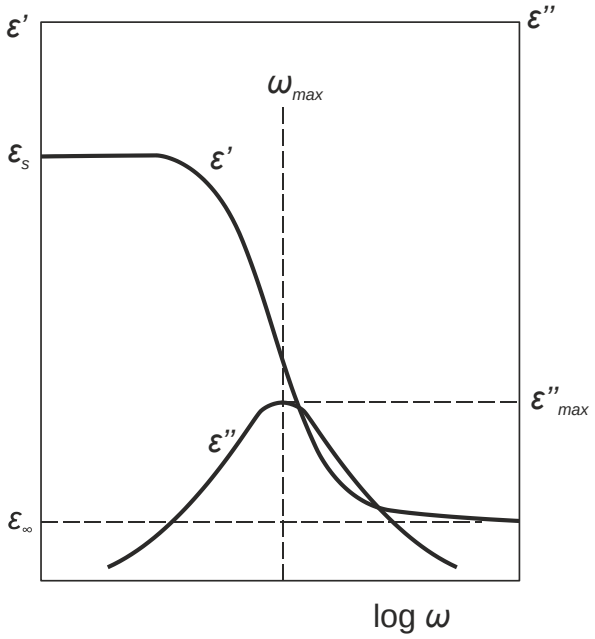

Figure 2.16. Debye dielectric dispersion curves.

The Debye equations defined above do not take interfacial polarization into account. The basic case of interfacial polarization can be modelled with the classic *Maxwell-Wagner model*, which concerns a series connection of two dielectric materials (materials A and B). If the materials have different permittivities and resistivities (i.e. $\varepsilon_A\rho_A \neq$

$\varepsilon_B \rho_B$), charge accumulation takes place on the interface between the materials. By following the derivation of Raju in [14], the dielectric loss factor can be written as:

$$\varepsilon''(\omega) = \frac{1}{\omega C_0 (R_A + R_B)} + \frac{\varepsilon_s - \varepsilon_\infty}{1 + \omega^2 \tau^2} \omega\tau, \tag{2-31}$$

where R_A and R_B are the resistances of the material volumes and C_0 is the vacuum capacitance. The first term of Equation (2-31) corresponds to interfacial polarization whereas the second term is identical to Debye equation (Equation (2-30)). It can be seen that interfacial polarization due to accumulation of charges on the interfaces inside the polymer volume has increasing contribution to dielectric losses with decreasing frequency. [14]

Lastly, it is especially interesting to notice that for DC-voltages, after the steady-state level of polarization has been reached, the dielectric losses consist only of conduction losses. This is also suggested by Equation (2-31), because when $\omega\tau \to 0$, the dielectric loss factor $\varepsilon''(\omega) \to 0$, i.e. no losses due to polarization occur. As a summary, the contribution of all the polarization mechanisms to ε' and ε'' as a function of frequency is shown schematically in Figure 2.17.

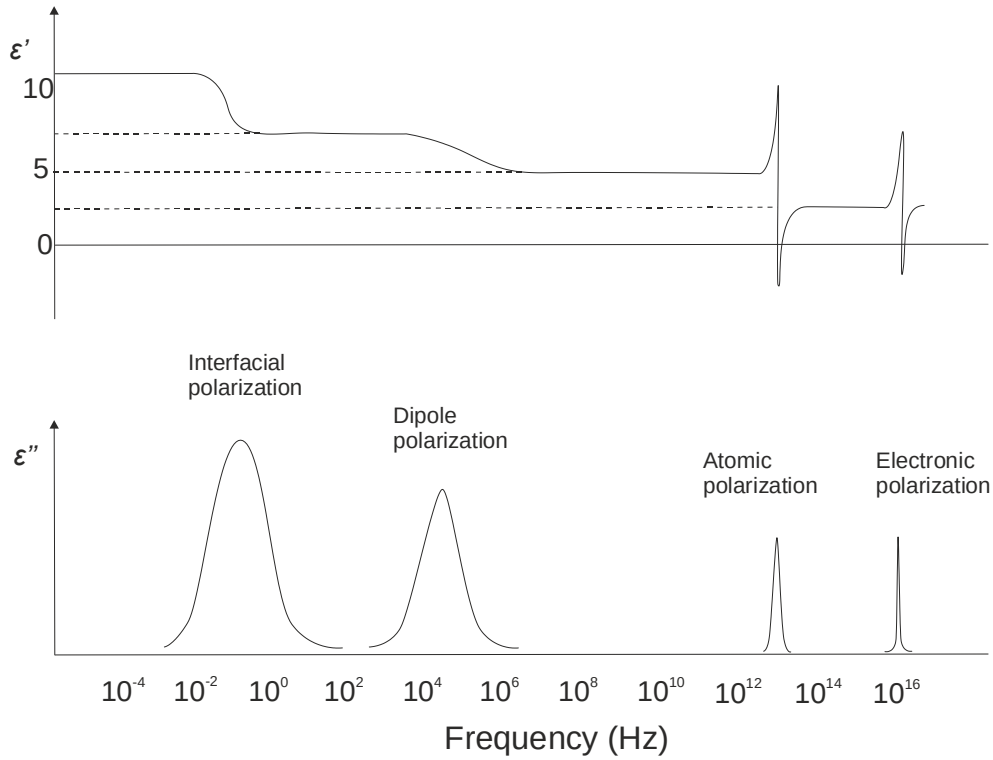

Figure 2.17. A schematical illustration of ε′ and ε″ as a function frequency with the effect of individual polarization mechanisms shown.[1]

2.4.5 Conductivity of polymers

Although the polymers that are used for insulation purposes exhibit extremely low conductivities, typically ranging from 10^{-10} to 10^{-20} $\Omega^{-1}m^{-1}$, their electrical conductivity has to be considered in order to understand the breakdown processes. Conductivity, denoted by σ, is based on drifting or diffusing of various charge carrier species such as electrons and ions as a result of applied electric field. Generally, conductivity can be expressed as:

$$\sigma = \sum_{i}^{N} \sigma_i = \sum_{i}^{N} |n_i e_i \mu_i| , \tag{2-32}$$

where σ_i, n_i, e_i and μ_i are the conductivity, concentration (m^{-3}), electric charge (C) and mobility ($m^2V^{-1}s^{-1}$) of a charge carrier of type *i*, respectively. [12]

In order to illustrate conductivity and the division of materials into insulators, semiconductors and conductors, *energy band theory* can be used. According to the Bohr's atom model, only certain discrete energy levels and the corresponding orbitals are allowed for electrons. However, when atoms are brought close to each other, for example when a molecule is formed, the electrons with the same initial energies start to interact. As a result of this so called *degeneration*, the energy states of the electrons are slightly shifted from their initial levels according to Pauli exclusion principle. As the number of interacting atoms increases, the various energy levels are so close to each other that the electrons can easily move between the energy states. Therefore, quasi-continuous *energy bands* are formed, as the discrete energy states can be considered as a continuum. The regions between the energy bands are called *gaps* (or "*forbidden zones*") as no electron can acquire energies in these regions. The formation of the energy band structure is illustrated in Figure 2.18. [12]

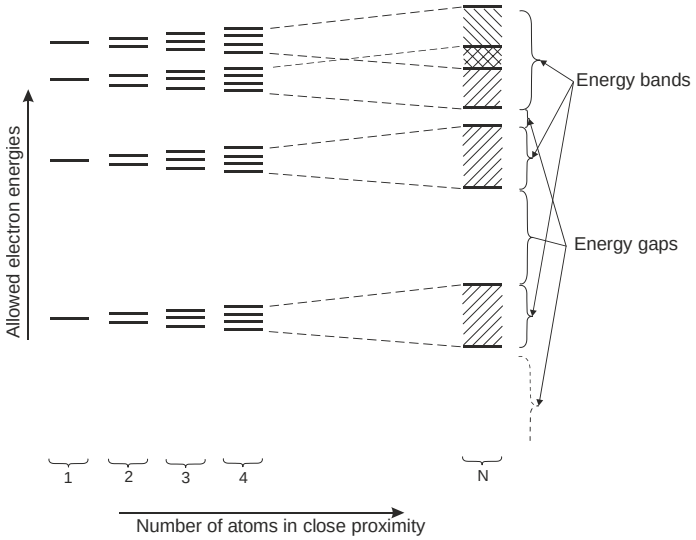

Figure 2.18. Formation of energy bands and band gaps when the amount of atoms in close proximity to each other increases. [12]

Conductivity can be examined based on the energy band theory by defining two specific energy bands, namely the *valence band* and the *conduction band*. The valence band corresponds to the highest energy band which is occupied by electrons at absolute zero temperature, i.e. it corresponds to the outermost valence electrons of an atom. Conduction band is the lowest energy band where the electrons have enough energy to separate from the nucleus and thus they can partake in the conduction process. In principle, the same energy bands can be defined for molecules, and the corresponding energy bands are HOMO (*highest occupied molecular orbital*) and LUMO (*lowest unoccupied molecular orbital*). The larger the band gap between these two bands is, the greater the amount of additional energy needed is for an electron to move to the conduction band. In general, the band gap of an insulator is more than 2 eV as opposed to gaps of 0.2 – 2 eV for semiconductors and less than 0.2 eV for conductors. The band gaps observed for polymers are typically in the range of 7 eV or more. [12,15]

Energy band theory is widely applied to covalent or ionic crystal structures such as silicon semiconductors to explain conductivity. For polymers, the application of energy band theory is possible, albeit more challenging. As opposed to simple structures like small molecules, for polymers with DP typically ranging from 10^3 to 10^5, HOMO- and LUMO bands cannot be defined very clearly. In fact, it should be considered that each monomer unit has its own energy band structure but no clear energy band structure can be defined for the whole polymer structure.

In addition, as polymers are never ideal crystalline structures, local energy states called *traps* exist in the material volume. These local energy states result from chemical and structural defects or any other irregularities in the polymer structure. If a free charge carrier enters a trap, it may need a considerable amount of energy to escape from it. The amount of energy needed is defined by *trap depth*. Therefore, trapped charges cannot partake in conduction process. In Figure 2.19, a schematical view of local trap sites in non-crystalline material is shown as a function of electron energy. Charge trapping has significant effect on space charge accumulation in polymer materials, as will be discussed in the next sub-chapter.

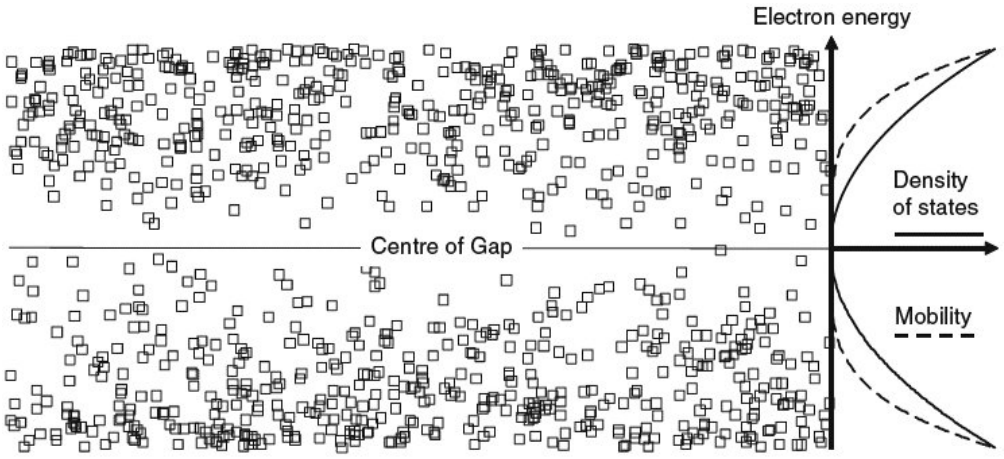

Figure 2.19. A schematical view of trap sites (marked by squares) as a function of energy. [2]

There are two major conduction mechanisms to be considered in polymers depending on the type of charge carrier involved. *Electronic conduction* utilizes negative electrons and positive holes (i.e. electron vacancies). Conduction of free electrons or holes is possible via the backbone of a polymer molecule but it is troublesome between polymer molecules. However, electrons and holes can also move between adjacent trap sites and therefore charge transfer between polymer molecules is possible. Charge carriers can move between trap sites by either gaining enough energy to overcome the potential barrier between the trap sites (i.e. hopping) or by a quantum-mechanical phenomenon called tunnelling. Tunnelling is based on the fact that the location of an electron is not well defined and is probabilistic by nature; therefore, for very narrow potential barriers, typically less than 1 nm, there is a finite possibility that the electron is actually located on the other side of the barrier. In Figure 2.19, the increasing charge carrier mobility with increasing density of trap sites is due to this mechanism. [12]

In *ionic conduction* the charge is carried by positive or negative ions. Ionic conduction can be further divided into two types of conduction according to the origin of the ions. In *intrinsic ionic conduction*, the charge carrying ions originate from dissociation of the polymer main-chain or the substituent groups. On the other hand, *extrinsic ionic conduction* is based on ions which do not originate from the polymer structure, but from impurities or additives instead.

2.4.6 Space charge

Space charge is defined as a local charge build-up inside a material volume. Space charge is typically perceived to consist of locally trapped charges inside the material volume, but more universally, space charge is formed whenever the rate of charge accumulation differs from the rate of its removal. Therefore, space charge may consist of both trapped and moving charges. The various sources of space charge are typically charges injected from the electrodes, charges drifting or diffused into the material volume or charges originating from ionic impurities within the material. Charges may be trapped in the dielectric during the fabrication process as well. In addition, charge accumulation due to interfacial polarization is also considered as space charge. The various processes are summarized in Figure 2.20, where the mechanisms responsible for space charge accumulation inside dielectric and charge behaviour at insulator-electrode interfaces are illustrated. [14,15,2]

When external electric field is applied to dielectric material with internal space charge accumulation, the local fields due to space charges distort the applied field. Whether the total field is enhanced or impaired by the space charge depends on the polarity of the space charge in comparison to the applied field. A space charge with an opposite polarity in comparison with the neighbouring electrode is called *hetero charge*. Hetero charges may be formed e.g. when a drifting charge injected at the opposite electrode is trapped near the other electrode with opposite polarity in comparison with the charge or if the electrode blocks the extraction of the charge. Hetero charges may

also be formed as a result of separation of ionic impurities within the dielectric [15]. Due to hetero charge, the local electric field at the electrode is increased and the field within the rest of the dielectric is decreased.[12]

Conversely, space charge with equal polarity to neighbouring electrode is called *homo charge*. As shown in Figure 2.20, homo charge is typically formed via charge injection at the electrodes and its formation is greatly dependent on the electrode-insulation contact, electrode material and temperature. Additionally, for DC conditions, polarity affects the formation of homo charge, as some metals may only inject charges of one polarity whereas other metals may inject charges with both polarities. As a result of homo charge, the electric field at the electrode will be reduced but the field stress at the central region of the insulation will be increased. This can be interpreted as shortening of the electrode distance. Therefore, due to higher field stress in this region, a premature breakdown may occur. [12]

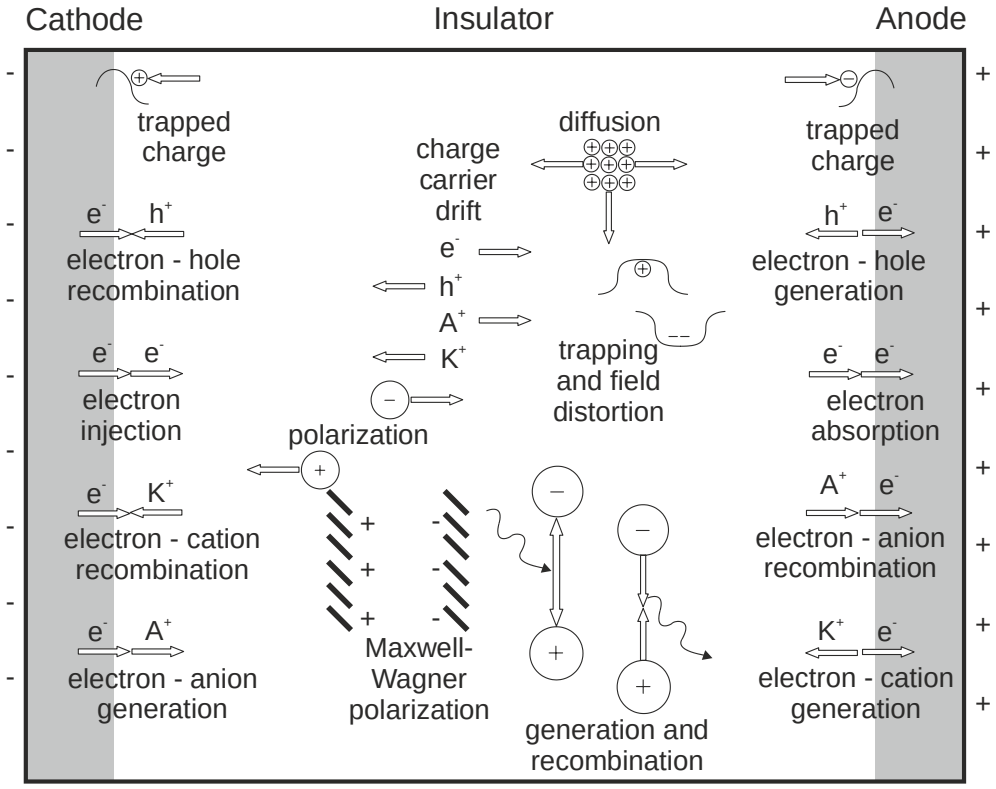

Figure 2.20. Various space charge accumulation processes and charge behaviour at insulator-electrode interfaces. [2]

The accumulation of space charge is typically emphasized under DC conditions. Under an influence of static electric field, space charges build up gradually in the dielectric. Correspondingly, as the field is removed, the charge build-up decays. These processes may occur over time periods varying from seconds up to several hours or days. As an example, in Figure 2.21, the gradual development of space charge in a polyethylene sample under DC stress of 40 kV/mm is shown. [15]

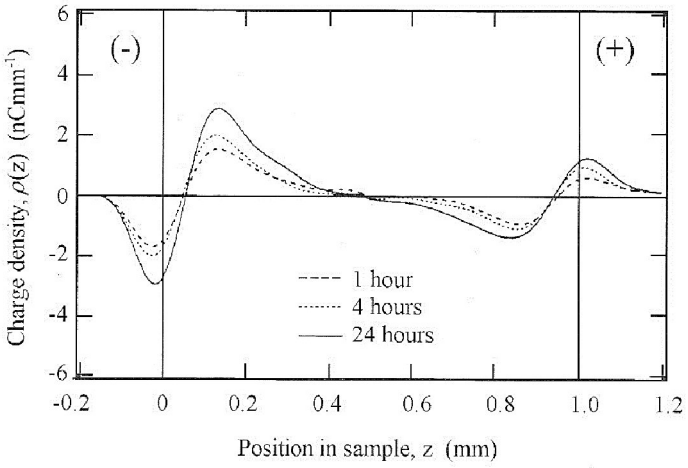

Figure 2.21. Development of space charge in a polyethylene sample under 40 kV/mm DC stress. [15]

At the present, there are various measurement techniques for determining the space charge profile inside a dielectric for both thick and thin insulation systems. The measurement techniques are non-destructive and generally these methods can be divided into two categories, namely *acoustic* and *thermal* measurement methods. The four main techniques are [2]:

1. Pressure wave propagation (PWP) or laser-induced-pressure-pulse (LIPP)
2. Pulsed-electro-acoustic (PEA)
3. Thermal step method (TSM)
4. Laser-intensity-modulated method (LIMM)

Generally, the acoustic techniques are based on the dimensional changes of the dielectric sample by a pressure wave. As the pressure wave propagates through the dielectric, it encounters and interacts with the space charges in the dielectric volume. As a result, the charges are displaced mechanically from their initial positions which induces slight changes in the local electric fields. This generates a small current *i(t)* through the dielectric which can be measured with a specific measurement circuit. In LIPP-technique (which is practically the same as PWP), the pressure wave is generated by applying a short laser pulse to the sample, whereas in PEA-method, the pressure wave is generated by a short voltage pulse. [18]

Thermal techniques utilize the thermal expansion of the dielectric induced by the application of a heat pulse. Similarly to acoustic techniques, the thermal front displaces the charges, and a small current is induced through the dielectric. The thermal pulse may be induced with e.g. laser as in LIMM-method. However, with acoustic techniques, a better spatial resolution may be achieved in comparison with the thermal methods. For example, LIPP-method may be applied to both thick (1 to ~20 mm) and thin (10-100 μm) samples, which enables the determination of the space charge profile in a thin dielectric film sample as well. [19]

2.4.7 Dielectric strength and breakdown mechanisms

Dielectric strength of an insulating material is defined as the maximum electrical stress per unit length (e.g. kV/m) the material can withstand continuously without losing its insulating properties. If this threshold is exceeded, a *breakdown* will occur resulting in a high current through the material and formation of conductive channel between the electrodes in the case of solid insulation. As opposed to gaseous and liquid dielectrics, breakdown in solid dielectrics is always destructive, as the damage is irreversible and the insulating properties are impaired permanently. Although no universal model for breakdown in solid polymers exists, there are various models for the breakdown mechanisms, and they will be introduced in the following. [12]

Electronic breakdown is generally divided into two possible breakdown mechanisms. In *intrinsic breakdown*, the energy of electrons accelerated by high electric field exceeds the amount of energy the crystalline structure of the solid dielectric can absorb. Due to this unstable state, the crystalline structure collapses and a breakdown occurs. Intrinsic breakdown strength can be seen as the ultimate breakdown strength of the material. *Avalanche breakdown* occurs when the field-accelerated electrons gain so much energy that ionization during collisions with the bound charges of the dielectric material is possible. If no considerable recombination occurs, this may lead to the multiplication of the current through the dielectric and eventually a breakdown will occur. Generally, intrinsic breakdown is not considered to be a very probable type of electric breakdown occurring in solid polymers, as it requires such high field strengths ($>10^{10}$ V/m) that the polymer would break down due to other mechanisms before such a field could be reached. [1,12]

Thermal breakdown may occur when the equilibrium between heat generation and heat removal in solid dielectric is lost. Due to increased temperature in the dielectric, conductivity increases as more charge carriers are available. This will lead to further increase in temperature and if the electric field is maintained, a thermal runaway and a breakdown will eventually occur. [1]

Electromechanical breakdown is based on physical contraction of the insulating material due to electrostatic attraction force of the electrodes when high electric field is applied. As the width of the insulation decreases the effective field strength between the electrodes is increased which leads to further increase in the attractive force. Additional softening and melting of the material may occur and if the voltage is maintained, e.g. an electronic breakdown may eventually occur. For polymeric insulations, electromechanical breakdown is commonly not considered as a probable breakdown mechanism. [1]

Breakdown based on the aforementioned mechanisms may take place considerably fast depending on the magnitude of the applied electric field and its duration. However, breakdown may also occur due to electrical degradation over a long period of time with voltages substantially below the breakdown strength. *Partial discharges* (PD) may take place in gas-filled voids inside a solid dielectric. As introduced in sub-chapter 2.4.1, the

electric field stress inside such a void is higher than in the surrounding insulation volume due to lower permittivity of the gas. A discharge inside a void may result in erosion of the void surface and after consecutive discharges an *electrical tree* may eventually grow. The growth of an electrical tree may also initiate from impurities in the polymer or from the electrodes. Electrical trees may eventually lead to total breakdown of the insulation. [1]

2.5 Polypropylene

2.5.1 Basic structure, properties and polymerization

Polypropylene (PP), which is the main polymer discussed in this thesis, is one of the most used thermoplastic polymers with numerous applications ranging from e.g. packaging to capacitor insulation. Polypropylene belongs to the group of *polyolefins* which are defined as polymers consisting of monomer units with at least one carbon-carbon double bond. As shown in Figure 2.22, during the polymerization process of polypropylene, the electrons associated with the double bond are redistributed and a linear or branched polymer chain is formed. Polypropylene has excellent mechanical, thermal and electrical properties; it is a relatively stiff polymer with a high melting point, low density, relatively good impact resistance and low dielectric losses. The most important properties of polypropylene related to capacitor applications are summarized in Table 2.2. [10,20]

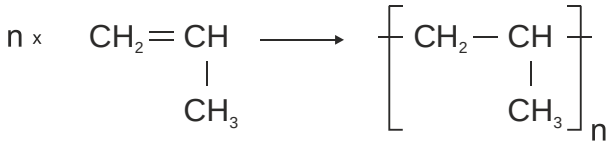

Figure 2.22. Polymerization process of polypropylene.[10]

Table 2.2. Properties of polypropylene related to capacitor applications. [20,21]

Density	0.905 g/cm^3
Melting temperature	162 °C
Glass transition temperature	-10 °C
Maximum operating temperature	105 °C
Average breakdown voltage	640 V/µm
Relative permittivity	2.25
Dissipation factor at 1 kHz	<0.02
Energy density	1-1.2 J/cm^3

The aforementioned properties of polypropylene are mainly based on the high isotactic content which is typically more than 96 % for commercial grade polypropylene. As discussed in sub-chapter 2.2.3, tacticity reflects directly to the degree of crystallization and thus to bulk properties of the polymer. Polymerization of propylene monomers into homopolymer form of polypropylene can be achieved e.g.

with *Ziegler-Natta catalysis process*. The process is stereospecific, i.e. it is possible to control the tacticity of the polypropylene. Copolymer form of polypropylene consisting of propylene monomers and small amounts of other monomers such as ethylene may also be used to improve e.g. surface properties, but copolymer forms of polypropylene are not relevant for capacitor applications. [20,22]

2.5.2 Biaxially oriented polypropylene film

If polymer material is stretched when it is molten or during cooling, the polymer chains are oriented lengthwise in the stretch direction. The crystalline regions and spherulites are also oriented and in some cases the degree of crystallinity may even slightly increase if the polymer chains are oriented in a more orderly fashion. Orientation greatly improves the dielectric strength and mechanical properties. In film capacitors, *biaxially oriented polypropylene* (BOPP) is used in the form of insulating films between the electrodes. [10,23]

The most common techniques to manufacture capacitor grade BOPP-films are *blown-film process* and *cast film process*, and they are illustrated in Figure 2.23a-b. Essentially, in the blown-film process, a polypropylene tube is formed by an annular die fed by a screw extruder. Air is then injected in the tube and the pressure inflates the tube, which enlarges the film dimensions and provides biaxial orientation of the polypropylene. The tube is then solidified by cooling which results in crystallization of the polymer. [24]

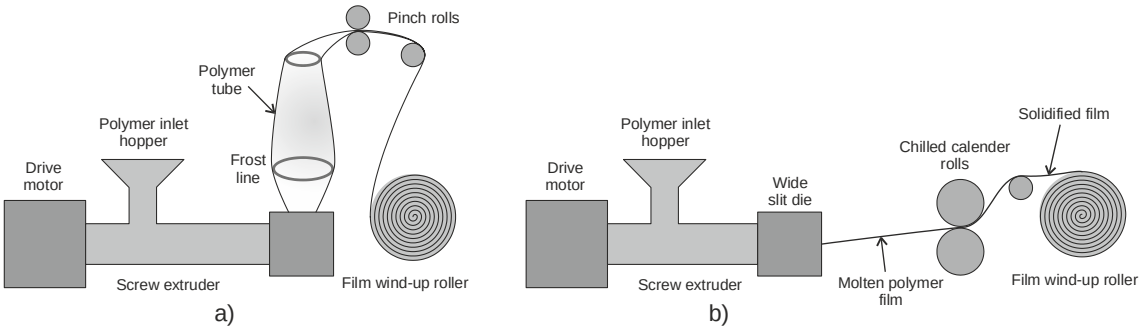

Figure 2.23. (a) Blown-film process, (b) cast film process.

In cast film process, the PP-film is produced by a thin, horizontally wide slit die. The film is drawn from the extruder by cooled calender rolls which cool down the film and initiate the crystallization. The resulting film has a very smooth surface and the size of the crystal size is smaller than with films produced with blown-film process. The film is oriented in the machine direction by the calender rolls. Biaxial orientation can be achieved by drawing the film perpendicular to the flow with tenter frames. [24]

3 DIELECTRIC POLYMER NANOCOMPOSITES

3.1 Introduction to polymer nanocomposites

Composite polymeric materials incorporating nanometric filler particles are often considered as the next generation of insulation materials as improved electrical properties may be achieved with these materials in comparison to the base polymer. The field of dielectric nanocomposites is still relatively new; the possibilities of dielectric nanocomposites were first considered theoretically by Lewis in 1994 and the first experimental work was published not until 2002. The basics of polymer nanocomposites and the mechanisms behind the altered properties are discussed in the following. [2,25]

3.1.1 Polymer composites and the importance of filler size

A polymer-based *composite material*[1] can be defined as a combination of base polymer and one or more *filler materials* such as filler particles. The base polymer serves as a matrix where the filler materials are dispersed. [5] The purpose of a composite material is to achieve enhanced properties in comparison with the constituent materials. With composite polymers, improvement in e.g. mechanical, thermal or erosion properties can be achieved. Traditionally, composite polymers with 50-60 wt-% of *micron-sized* inorganic fillers have been incorporated in various fields of engineering for many decades. However, even though some other properties may be improved by introducing microfillers, dielectric properties of microcomposites are seldom improved. For example, former attempts to improve capacitor energy density by using microcomposites have failed, as an improvement in the permittivity of a microcomposite resulted in impaired breakdown strength. More generally, the problem with microcomposites is that the enhancement of one property typically leads to the deterioration of another. [26,4]

Recently, a significant interest towards *nanocomposite dielectric materials* has risen, as with nanocomposites, it may be possible to avoid the disadvantages of microcomposites and to achieve multifunctional materials. Nanocomposites can be defined as composite materials with small amounts of inorganic fillers (0.1 – 10 wt-%) with one or more dimension less than 100 nm. By incorporating nanometric fillers, extremely large interfacial region between nanoparticles and the base polymer matrix can be achieved in comparison with microcomposites. The concept of large interfacial region is illustrated in Figure 3.1; the reduction of filler particle size from micrometric

[1] Generally, a composite material is defined as any combination of two or more materials. However, in terms of this thesis, the word “composite material” refers to a polymer/filler –composite system.

to nanometric scale results in a significant increase in the surface-to-volume ratio of a particle. The unique properties of nanocomposites are essentially based on this large interfacial region between the fillers and the base polymer, as the material properties in the interfacial region differ from those of the both constituents of the nanocomposite. In fact, as the filler size is reduced to nanometric scale, the properties of the interfacial region will dominate the material volume. Therefore, in principle, the properties of a nanocomposite material can be tailored as desired by changing the properties of the interaction zone. [2,4]

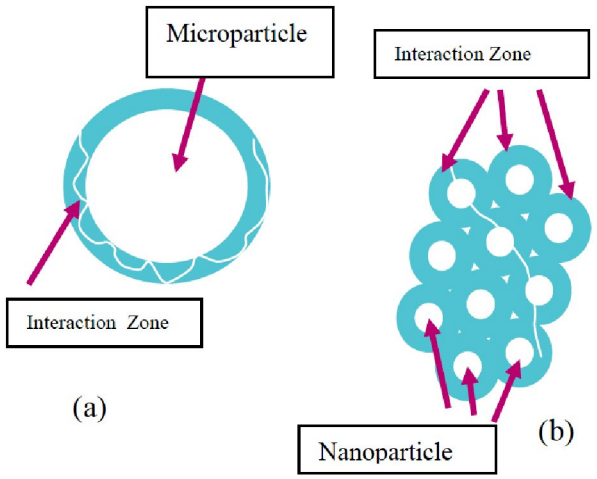

Figure 3.1. Comparison of interaction zone volume in case of microparticles (a) and nanoparticles (b). [27]

3.1.2 Processing of nanocomposites

For compounding of dielectric polymer nanocomposites, wide range of base polymers and inorganic filler particles can be used. The most common types of polymers and fillers are shown in Table 3.1 [4,2]. Silicon dioxide (SiO_2) alone or combined with metallic oxides (forming silicates) are commonly used as nanofillers in thermoplastic and thermosetting insulating polymers. Metal oxides such as titania, alumina, magnesia and zinc oxide are generally electrically insulating and thus they can be used to manufacture dielectric nanocomposites. In addition to the filler materials listed in Table 3.1, nanoclays and carbon nanotubes (CNT) may be utilized as well. [2]

Table 3.1. Typical base polymers and filler materials used for dielectric nanocomposites.

Base polymers	Nanofillers
Polyamide (PA)	Silica (SiO_2)
Polyethylene (PE)	Layered silicate (LS)
Polypropylene (PP)	Titania (TiO_2)
Ethylene vinyl acetate (EVA)	Alumina (Al_2O_3)
Epoxy resins (EP)	Magnesia (MgO)
Silicone rubbers (SR)	Zinc oxide (ZnO)

Proper *distribution* and *dispersion* of nanoparticles during manufacturing process of a nanocomposite are vitally important as otherwise the large interfacial area and the beneficial properties of nanocomposites may not be achieved. The distribution refers to the homogeneity of nanofillers through the composite and dispersion refers to the level of *agglomeration*. As nanoparticles have high surface energies, they tend to pack together, or agglomerate, which will result in smaller interfacial area between the particles and the base polymer. Agglomerates also act as impurities or defects in the material volume and they may decrease the dielectric strength. Therefore, low amounts of nanoparticles are used, as the probability for agglomeration tends to increase with nanofiller loading. Additionally, for some nanoparticles, e.g. for silica, surface treatment with coupling agents prior to compounding may be needed in order to prevent excess agglomeration. Variations of distribution and dispersion of nanoparticles are shown in Figure 3.2a-d; Figure 3.2d obviously represents the optimal case. [2,28]

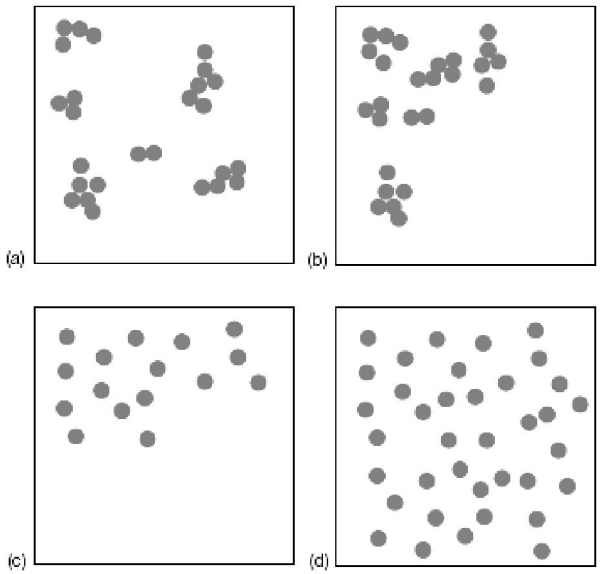

Figure 3.2. Variations of distribution and dispersion of nanoparticles. (a) good distribution but poor dispersion (b) poor distribution and dispersion (c) poor distribution but good dispersion (d) good distribution and dispersion. [28]

At the present, four different techniques for production of polymer nanocomposites are available. *In situ polymerization* is based on polymerization of monomer-nanofiller mixture. Appropriate dispersion of nanofillers in the monomer is required and therefore surface treatment of the nanoparticles is often used. In *melt blending*, the nanoparticles are compounded directly in the molten polymer during the extrusion process. In situ polymerization and melt blending processes are the most commonly used techniques. The other processing techniques include *solvent method*, in which solutions of base polymer and nanofillers are combined, and *sol-gel process*, which consists of hydrolysis of base polymer and nanofiller solutions and condensation into glass-like form. [2,28]

3.1.3 Interfacial region

As introduced in the beginning of this chapter, in a properly processed nanocomposite, the interfacial region between the filler particles and the polymer matrix will dominate the material volume which results in altered properties in comparison to the constituent materials. In Figure 3.3, an illustration of the interfacial region is shown. The polymer chains around the nanoparticle are chemically and physically bound to the particle resulting in an interfacial region with thickness varying from less than 1 nm to more than 10 nm. The nature of these bonds depends on the constituent materials and their polarity and on the surface treatment of the nanoparticles. The *bound polymer* at the interfacial layer exhibits changes in crystallinity, mobility, chain conformation, molecular weight and chain entanglement density. The region closest to the particle is more tightly bonded than the outermost regions. Due to the massive interfacial region, these altered material properties are reflected to the bulk properties of the composite.

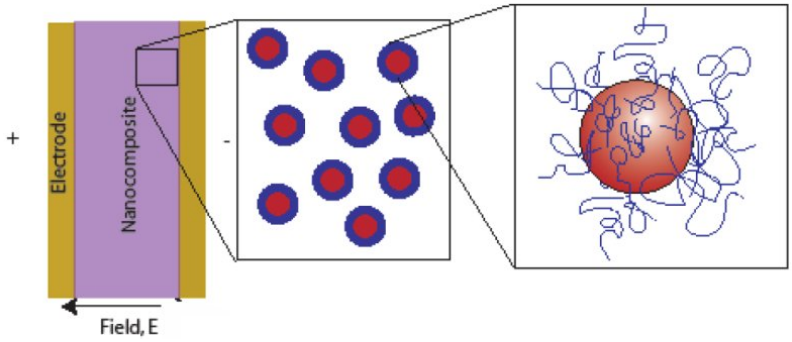

Figure 3.3. Illustration of the interfacial region between a nanoparticle and the surrounding polymer matrix. [29]

Based on the aforementioned changes in the polymer properties, a multi-core interface model for a spherical nanoparticle-polymer interface has been proposed by Tanaka *et al*. in [30]. As illustrated in Figure 3.4, the model consists of three physical layers with varying properties and an electric double layer overlapping the aforementioned layers. The first layer with thickness of approximately 1 nm corresponds to the region of tight chemical bonding between the nanoparticle surface and the surrounding polymer chains. The second layer is an interfacial region with thickness of 2-9 nm strongly bound to the first layer and the particle surface. The third layer with thickness of several tens of nm is loosely bound to the second layer. All the three layers correspond to altered polymer properties as mentioned above. Closer to the particle surface, the polymer chains are highly immobilized. [30]

The electric double layer overlapping the three physical layers corresponds to the charge behaviour of the interfacial region. If the polymer material surrounding a nanoparticle contains mobile charge carriers, the surface charge of the nanoparticle will be screened by counter-charges from the polymer as shown in Figure 3.4. The resulting electric double layer with exponentially decaying charge is similar to the Gouy-Chapman diffuse layer associated with liquid interfaces. Due to the electric double

layer, a long-distance dipole is formed, which influences greatly the dispersion of the nanoparticles and the electric properties of the nanocomposite. [2,29,30]

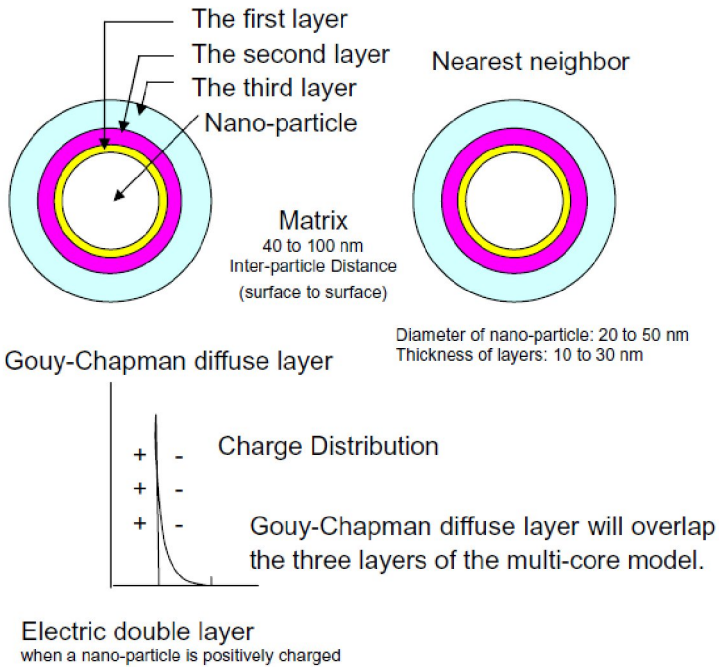

Figure 3.4. The multi-core model for a spherical interface between a nanoparticle and a polymer matrix. [30]

3.2 Electrical properties of nanocomposites

As introduced in the beginning of this chapter, with nanocomposites, improved electrical properties may be achieved in comparison to the unfilled base polymers or the corresponding microcomposites. However, the electrical properties depend largely on wide range of variables such as the constituent materials of the composite, the filler content, the properties of the interfacial region and the manufacturing process. Therefore, it is challenging to make universally applicable arguments about how exactly the electrical properties will change in nanocomposites. Nevertheless, the main electrical properties of nanocomposites which are closely related to this thesis will be discussed in the following.

3.2.1 Relative permittivity and dielectric losses

In microcomposites, it is typical that with increasing filler content, the relative permittivity and dielectric losses increase too, as the filler particles have typically higher relative permittivity than the base polymer. In addition, with increasing filler content, the degree of interfacial polarization increases which further contributes to the increase in relative permittivity and dielectric losses [31].

However, with nanocomposites, this is typically not the case. With low filler contents, nanocomposites have usually lower relative permittivities in comparison with the constituent materials. This interesting behaviour cannot originate from the

permittivities of the incorporated nanofillers, as the relative permittivities of nanofillers (ε_r = 4-12) are typically higher than those of the base polymers (ε_r = 2-4) [32]. Instead, the reduction in permittivity is seen to be connected to the restriction of polymer chain movement in the interfacial regions and reduced interfacial polarization. As the interfacial region dominates the material volume, this results in lower total polarization and lower relative permittivity. [26,31,4]

Dielectric losses of nanocomposites are generally at the same level as those of the base polymer, although reduction in $\tan\delta$ is also possible when low amount of nanofillers is used. With low filler content, the reduction in $\tan\delta$ value may be based on smaller bulk conductivity due to reduced amount and mobility of free charge carriers in the nanocomposite. However, when the filler content is increased above a certain threshold level, the $\tan\delta$ losses (and relative permittivity) begin to increase beyond those of the reference material, possibly because of the overlapping of interfacial regions and thus, higher conductivity. [4]

3.2.2 Space charge accumulation

The density of space charge and the charge decay time have been found to be lower for various nanocomposites [27,31]. Although no universal explanation for the reduction of space charge accumulation and decay time exists, the probable reason for lower space charge accumulation is the increased charge mobility due to so called *"quasi-DC" conduction mechanism* (QDC); as the filler content is increased above a specific value, the interfacial regions of the nanoparticles will start to overlap, as shown in Figure 3.5. In these *interaction zones* the local charge mobility is increased, which aids in space charge mitigation [33]. Importantly, it has been found that these regions of local conductivity do not impair the bulk resistivity of the material as long as a certain threshold value of the filler content is not exceeded [29]. Furthermore, the reduced interfacial polarization discussed earlier is directly related to the reduction of space charge as well. [26]

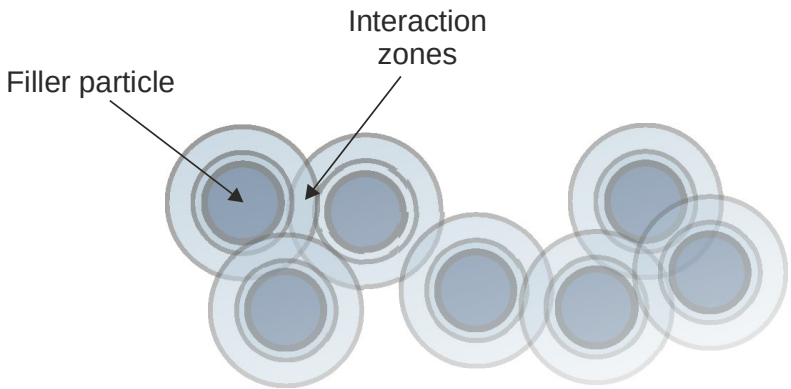

Figure 3.5. Overlapping of interfacial regions results in local regions of conductivity.

3.2.3 Dielectric strength

For insulation applications, the dielectric strength is the determinant factor and even a slight increase would be highly desirable. For example, higher dielectric strength would enable higher energy density in the case of capacitor applications and reduced insulation thickness in the case of cable insulation. Generally, the dielectric strength of nanocomposite materials appears to stay at least at the same level as the base polymer or to increase, especially under DC voltages [2,33]. For example, in a study by Takala *et al.* [32], the dielectric strength of 5 wt-% SiO_2-PP nanocomposite increased 20% and 52% for AC and DC voltages, respectively. The results also indicated that the standard deviation of the breakdown strength was smaller which suggests that the material is more homogeneous. Similar results have also been achieved with other nanocomposite materials, as reviewed by Nelson in [2].

There are various factors and mechanisms which may be responsible for the increased dielectric strength. Basically, nanoparticles can be seen to act as barriers to the flow of electric current which restricts the breakdown mechanisms discussed in sub-chapter 2.4.7. Thus, higher voltage is needed to initiate the charge carrier multiplication. Due to the massive interfacial volume fraction, the overall density and depth of trap sites in the material volume may be increased which limits the mobility and energy of free charge carriers. Generally, the reduced space charge also increases the breakdown strength, as the adverse distortion of the applied field due to the local fields is reduced. On the other hand, if free charge carriers are trapped in trap sites near the electrodes forming homo charge, the field near the electrodes is mitigated which increases the voltage required for charge injection from the electrodes especially under DC voltages [29]. Due to the aforementioned mechanisms, nanocomposites have also been found to be more resistant against treeing and partial discharges. [33]

4 METALLIZED FILM CAPACITORS

4.1 Capacitor fundamentals

Capacitors are devices used for short-term energy storage and they are applied in every field of electrical engineering ranging from small components of electronics industry to high voltage reactive power compensation units in power systems. Typical targets of application are filtering in both AC and DC systems, various devices based on power electronics (such as switched-mode power supplies), fast energy discharge applications and power factor control. Currently, depending on the technology used, four main types of capacitors exist, namely *film*, *ceramic*, *electrolytic* and *electrochemical* capacitors. [7]

The focus of this thesis is on metallized film capacitors which incorporate thin electrodes directly evaporated on dielectric film instead of separate sheets of aluminium foil traditionally used in film capacitors. At the present, metallized film technology already enables high energy density due to more compact structure and higher reliability due to unique self-healing properties of metallized films. However, demand for even higher energy densities and better reliability for capacitors exists. Nanocomposite dielectric films may be a solution to fulfil these requirements in the future.

4.1.1 Operation principle

A capacitor is basically an energy storing device consisting of two electrodes separated by insulating dielectric material. When a capacitor is charged via an external voltage source, the dielectric material between the electrodes is polarized and electric energy is stored in the system. The simplest form of capacitor is a parallel-plate capacitor configuration with dielectric material between the electrodes as shown in Figure 4.1 where A is the electrode area, d is the distance of the electrodes, ε_r is the relative permittivity of the dielectric and U is the voltage across the system. A similar arrangement was already used in sub-chapter 2.4.1 to discuss the polarization and permittivity of a dielectric. Capacitance C and stored energy W for such an arrangement can be easily written as [34]:

$$C = \frac{Q}{U} = \varepsilon_r \varepsilon_0 \frac{A}{d} \tag{4-1}$$

$$W = \frac{Q^2}{2C} = \frac{1}{2} C U^2 . \tag{4-2}$$

Furthermore, based on Equation (4-2), as the volume between the electrodes is *Ad* and voltage *U=Ed*, the energy density *w* of a capacitor can be written as [34]:

$$w = \frac{1}{2}\varepsilon_r \varepsilon_0 E^2 \ . \tag{4-3}$$

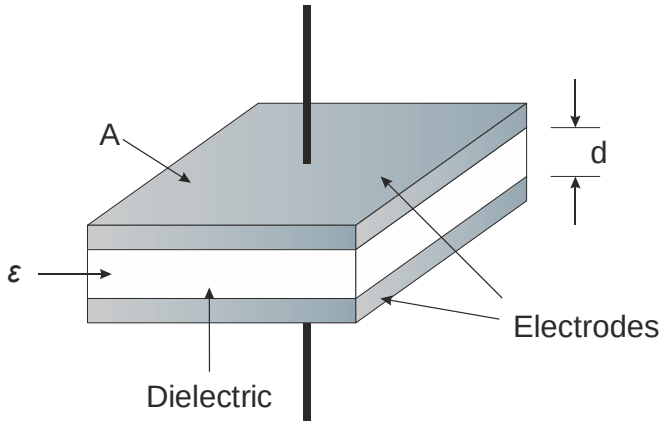

Figure 4.1. A charged parallel-plate capacitor with dielectric material between the electrodes.

The preceding fundamental equations define the general design principles for capacitors. In order to increase capacitance, large electrode area and thin insulation layers are required. In practice, this can be achieved e.g. by using thin foil electrodes layered with insulating films and winding the arrangement cylindrically to minimize the space requirements. It is also interesting that according to Equation (4-3), the energy density of a capacitor is squarely proportional to electric field magnitude; therefore, even a small increase in the maximum permissible electric field stress of the dielectric would result in a substantial increase in energy density. An increase in the relative permittivity of the dielectric would also increase both capacitance and energy density of the capacitor. This serves as a basic motivation for using nanocomposite polymer dielectrics in capacitors, as their properties may be tailored towards higher dielectric strength, lower dielectric losses and possibly higher relative permittivity.

4.1.2 Equivalent circuit and capacitor losses

A capacitor is typically modelled with an equivalent circuit model shown in Figure 4.2a. The model consists of a parallel RC connection which corresponds to a lossy dielectric, as already discussed in the sub-chapter 2.4.4. The capacitance *C* models the ideal dielectric properties and the parallel resistance R_P corresponds to losses in the dielectric. In addition, resistive and inductive losses in the other parts of a capacitor have to be considered as well. Series resistance R_S models all the resistive losses occurring in the metal parts of a capacitor such as internal wiring, terminals, electrodes and metallization. The *equivalent series inductance* (ESL) models the inductance due to the geometry of the capacitor as a single lumped series element. For AC voltages at a

specific frequency, the resistive part of the impedance of the R_P-C –parallel connection may be combined with R_S as a single series resistance called the *equivalent series resistance* (ESR), as shown in Figure 4.2b. [35,8]

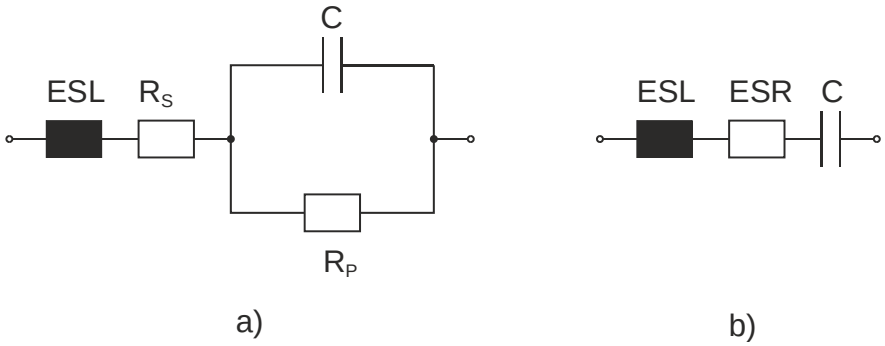

Figure 4.2. a) Typical equivalent circuit of a capacitor b) equivalent circuit with R_P and R_S combined as ESR. [8]

It should be noted that the parallel resistance R_P equals to a large amount of complex energy loss mechanisms in the dielectric and its value is not constant. In fact, R_P corresponds to all loss mechanisms such as dielectric losses due to molecular polarization and relaxation phenomena, conduction losses through the dielectric and losses due to interfacial polarization and space charge to name a few. Therefore, the value of R_P is frequency-, temperature-, voltage- and time-dependent. The losses occurring in internal wiring, terminals, electrodes etc. are quite constant as a function of temperature and frequency, although at high frequencies, losses due to skin effect become considerable. Typically, R_S is really small (<0.1 Ω) in comparison with R_P (several hundreds of gigaohms [36]). However, for high current applications, R_S may become important. [35]

By the means of the equivalent circuit shown in Figure 4.2b, the total losses occurring in a capacitor can be estimated. At frequencies well below the resonance frequency of the equivalent circuit, capacitor losses can be defined as the ratio of total ESR to capacitive reactance X_c (reactive part of the impedance of the R_P-C –parallel connection). This ratio is also defined as the dissipation factor or $\tan\delta$ of a capacitor, i.e.:

$$\tan\delta = \frac{ESR}{X_c} = ESR \cdot \omega C \,. \tag{4-4}$$

The dissipation factor of a capacitor differs slightly from the dissipation factor defined formerly for dielectric material (Equation (2-23)), as ESR now includes the effect of R_S as well. Nevertheless, as R_S is small in comparison with R_P, the aforementioned dissipation factors are practically the same thing. As already discussed in the sub-chapter 2.4.4, for DC voltages, when steady-state polarization has been reached, R_P consists only of losses due to the leakage current through the dielectric. Therefore, the total losses of a capacitor under DC conditions are purely resistive.

4.2 Structure of metallized film capacitors

As introduced in the beginning of this chapter, metallized film capacitors consist of polymeric insulation film with thin metal electrodes evaporated directly on the film. The insulating film thickness is typically 6-10 μm, and nowadays, the dominant types of polymer used are capacitor-grade biaxially oriented polypropylene (BOPP) and polyethylene terephthalate (PET). The metallized electrodes, with thickness ranging only from 20 to 100 nm, consist of zinc, aluminium or a metal alloy specifically designed to minimize the resistance and corrosion of the electrodes. Essentially, capacitor elements are made by stacking two layers of metallized film onto each other and winding them around a hollow cylindrical core. End connections are made by spraying molten metal particles at the both ends of the cylindrical element and by attaching the terminals. The basic structure of a metallized film capacitor is shown in Figure 4.3. The structure and design principles will be discussed in more depth in the following. [6,7,37]

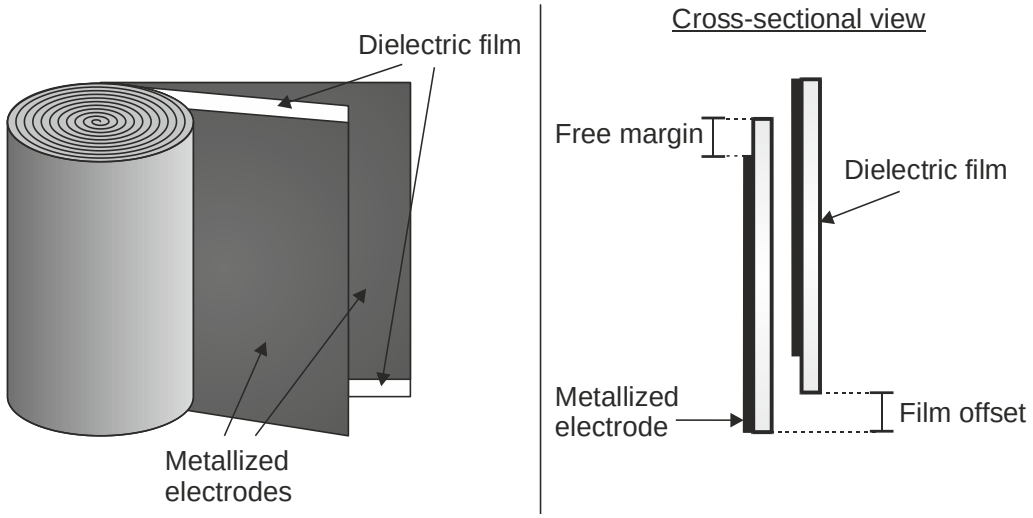

Figure 4.3. Basic structure of a metallized film capacitor. The winding principle and orientation of the metallized films is shown on the left. A cross-sectional view of one winding layer is shown on right.

4.2.1 Metallization

Before metallization, sufficient adhesion of the electrode to the film surface has to be ensured. This can be achieved by oxidizing one side of the film with *corona treatment*, which is illustrated in Figure 4.4. In this process, an insulating film is laid on earthed metal base and above the film, a wire, connected to a high voltage source, is stretched across the whole width of the film. The air around the wire is ionized and as the wire is moved across the film surface, the ions move towards earthed base resulting in an increase in the surface charge density of the film. Corona treatment is especially important in case of polypropylene films, as its surface properties are poor due to the fact that PP is only weakly polar. Generally, corona treatment is not necessary with other polymer films. [6,15]

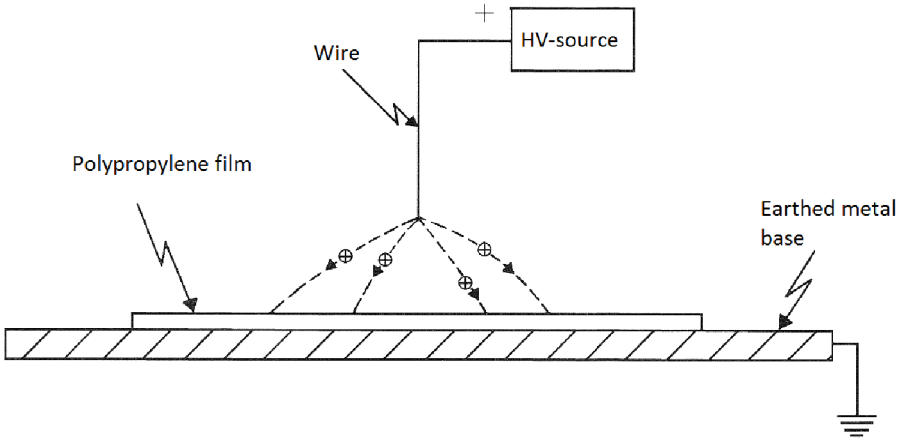

Figure 4.4. Schematical view of corona treatment of the film surface. [15]

After ensuring proper adhesion to film surface, the metallization is done by *physical vapour deposition* (PVD), in which vaporized metal is layered on the film surface under a vacuum and a very thin electrode is formed [6]. A schematical view of a metallized film is shown in Figure 4.5a. At the one edge of the film, a margin area has to be left without metallization in order to prevent flashover to the opposite electrode. The width of the margin area is typically 1.5 – 5 mm. At the opposite end where the end-connections are made, the metallization has to be thicker due to high current density. As shown in Figure 4.5b, the electrode profile may be either linearly thickening towards the end-connection region or reinforced only at the end-connection region. Generally, the resistivity[2] of a metallized electrode is 5 – 12 Ω/sq. The resistivity is decreased at the reinforced edges to 2 – 4 Ω/sq. It should be noted that the electrode resistivity is inversely proportional to the thickness of the electrode. [21,35,7,38]

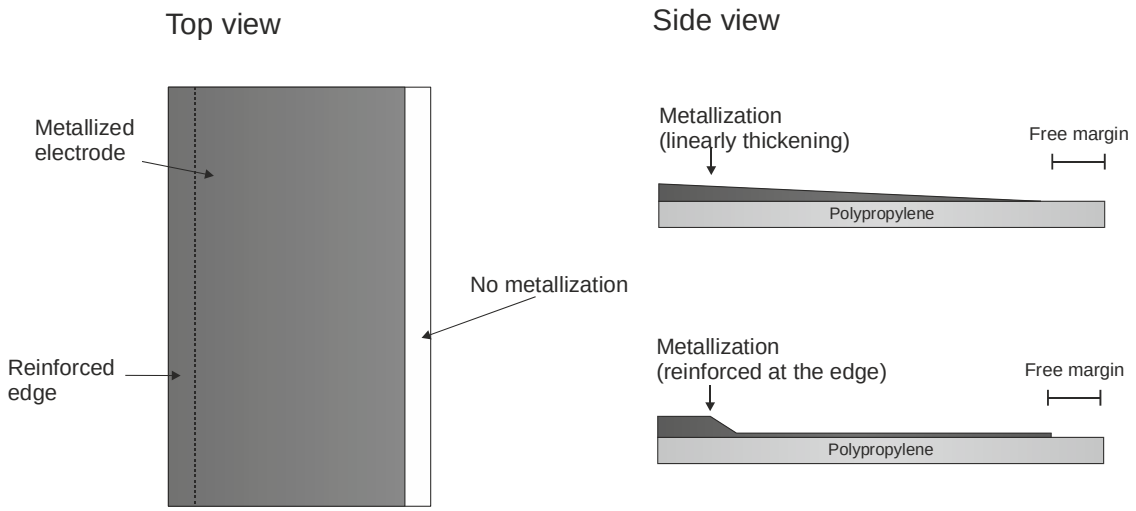

Figure 4.5. (a) Metallization principle (top view) (b) various metallization profiles (side view).

[2] The resistivity of a metallized electrode is expressed as *sheet resistance* $R_s = \rho/t$, where ρ and t are the resistivity and thickness of the electrode material, respectively. Although the resulting unit of sheet resistance is Ω, the unit Ω/sq (ohms per square) is used to avoid confusion with the bulk resistance. [**59**]

4.2.2 Capacitor winding

The capacitor winding principle and a cross-sectional view of one winding layer are illustrated in Figure 4.3. When metallized films are wound, they are oriented in a way that the margin areas are located at the opposite ends. The films are also slightly extended from the both ends of the element to expose some of the electrode area to ensure sufficient connection with the molten metal when the end-connections are made. The capacitor rolls have to be wound as tightly as possible in order to prevent formation of air voids between the layers. During the last winding rounds, a non-metallized cover film with thickness of 15-30 μm is added between the metallized films and a few additional winding turns are made. Capacitor elements are then heat-treated in order to compact the structure and minimize the air gaps. Prior to encapsulation, the element may be impregnated, although at the present, the trend is towards dry structure. [35,23,39,40]

4.2.3 End-connections

The end-connections are done by plasma spraying molten metal particles (also referred to as “schooping”) to the exposed electrode ends at the both ends of a wound capacitor element and soldering leads to end-spray. Typically, the same metal is used as in electrodes, i.e. aluminium or zinc. As the adjacent film layers are slightly shifted and margin areas are left without metallization, proper connections to both cathode and anode can be achieved without short-circuiting the electrodes. A schematical view of end-connection area of a capacitor is shown in Figure 4.6. [41]

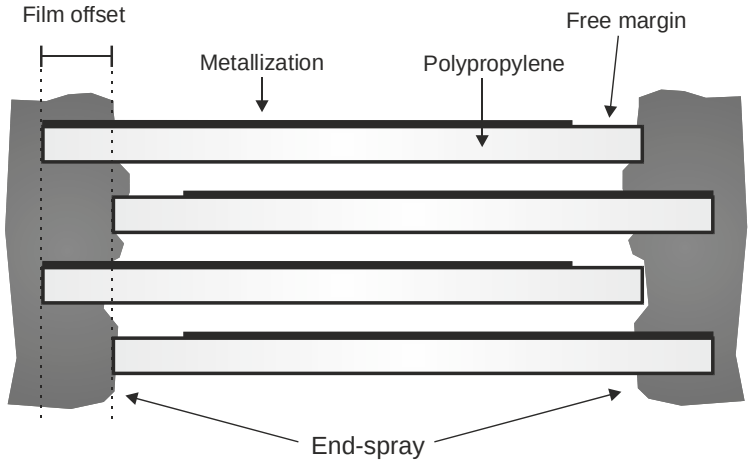

Figure 4.6. Schematical view of the end-connection area.

Due to the fact that the electrode thickness is extremely small, it is not sufficient to make the contact only via the electrode edge. Therefore, in order to transfer enough current in the capacitor, the contact has to be made partly on the electrode surface as well. The diameter of a sprayed metal particle is typically ~50 μm but as the film thickness is only 10 μm or less, the gaps between the films where the metal particles have to penetrate in are really small in comparison. As the liquid metal particles reach

the capacitor end, they splash into the small gaps and the resulting effective connection is irregular along the film edge. In addition, the metal spray does not bond metallurgically with the electrode material. Instead, shrinkage of the polymer film around the molten metal particles occurs which adheres the metal particles to the metallized electrodes to some extent. Due to aforementioned reasons, it is crucial to optimize the parameters of the metal spraying process to ensure sufficient end-connection. [41,37]

4.3 Self-healing mechanism

In a traditional film-foil capacitor, a single breakdown of the dielectric film always results in catastrophic damage to the capacitor element. Therefore, the faulted element has to be disconnected from the capacitor unit by internal fusing and the resulting loss of capacitance is considerably high. However, in case of metallized film capacitors, this can be avoided. The most significant advantage of metallized film capacitors is their unique ability to undergo *self-healing* (or *clearing*), as illustrated schematically in Figure 4.7. [37]

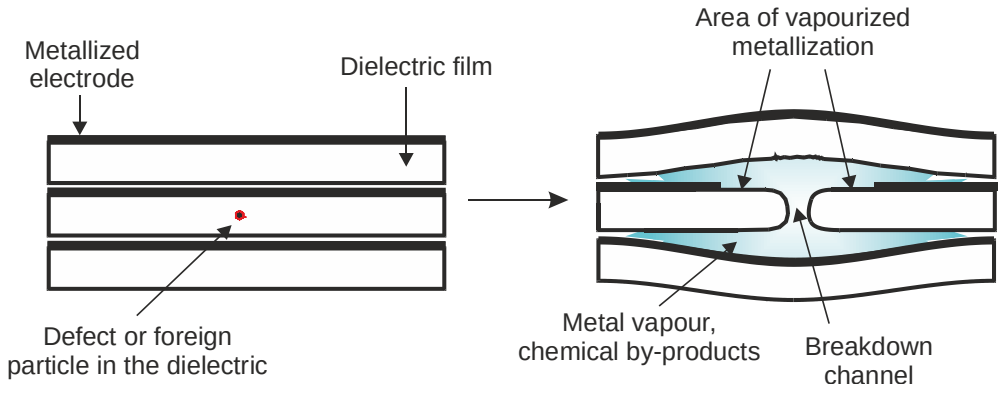

Figure 4.7. A Schematical view of a self-healing area during a breakdown. [42]

When a local breakdown occurs in the insulating film, the local temperature at the fault spot can rise to as much as 6000 K due to the breakdown arc. Consequently, the dielectric film is transformed into highly compressed plasma which pushes the dielectric layers apart and rapidly evaporates the metallization around the defect site. As the plasma expands, it cools down after a few microseconds and the arc is extinguished leaving behind small amounts of vaporized metal and chemical by-products. As a result, the area around the breakdown site is isolated, the fault is cleared and the capacitor can continue its operation. The discharge energy and time in one successful self-healing process are so small that the capacitor remains fully functional during the breakdown. After one clearing process, typically only ~5-8 mm^2 of effective electrode area is removed. Therefore, only a minor loss of capacitance occurs and in practice, a metallized film capacitor can undergo thousands of self-clearings before a noticeable loss of capacitance can be measured. In practice, after a loss of capacitance of 2-5 %, it is considered that the capacitor has reached the end of its life-time. [7,37,42,43]

4.4 Failure mechanisms in metallized film capacitors

Despite the fact that metallized capacitors are considered to be more reliable than traditional film-foil capacitors mainly due to their self-healing capability, there are various mechanisms specific for metallized capacitors which may lead to the total failure of a capacitor unit. Three of the most common failure mechanisms are discussed in the following sub-chapters.

4.4.1 Failure of self-healing mechanism

The energy discharged during one self-healing event is a function of various variables. For a self-healing event to be successful, it is necessary that the discharge energy during one clearing is not too large. If the discharge energy and the corresponding fault current are too high, the arc may not extinguish quickly enough or the resulting puncture in the dielectric may not be completely isolated. This may lead to consecutive self-healings in the adjacent layers close to the initial puncture and as more and more heat is dissipated, a large, low-resistance short circuit may develop which may lead to the complete failure of the capacitor. [23]

The dependency of self-cleared area on the discharge energy was first studied by Kammermaier and Heywang [44,45]. Based on their results, Shaw *et al.* deduced an experimental expression for the discharge energy $E_{discharge}$ during one self-healing event [23]:

$$E_{discharge} = \frac{k \cdot U^{4.7} \cdot C}{{R_S}^{1.8} \cdot \alpha(P)}, \tag{4-5}$$

where U is the applied voltage, C the capacitance, R_S is the sheet resistance of the electrode (expressed in Ω/sq) , $\alpha(P)$ is a function which relates the interlayer pressure of a wound capacitor to the clearing energy and k is an experimentally definable constant. Although Equation (4-5) only applies under a certain set of conditions (V=400-1000 V, R_S=1.4-4.5 Ω/sq), it can be used to examine the self-healing mechanism. The validity of Equation (4-5) is also supported by more sophisticated studies by Tortai *et al*. in reference [46].

According to Equation (4-5), with a good choice of operation voltage, capacitance, electrode thickness and interlayer pressure, the discharge energy and capacitance loss due to self-healing can be minimized. However, it is often not possible to alter the operation voltage, capacitance or sheet resistance to a large extent, as they are determined by the target application. Thus, the interlayer pressure will dominate the discharge energy during self-healing. Essentially, higher pressure leads to lower discharge energy, shorter discharge time and smaller discharge area [6]. However, it is hard to achieve a fixed inter-layer pressure in a wound capacitor, as the inner layers are subjected to the compressive radial force from the outer layers, which results in higher pressure in the inner layers (typically in the range of several MPa) than in the outer

layers. Due to this, self-healing events occur more frequently in the outer layers of a capacitor. [47]

In practice, an additional safety mechanism may be achieved by using segmented electrodes. An example of a segmentation pattern is shown in Figure 4.8; the electrodes comprise of segments interconnected via fuse links. Therefore, if a local breakdown with too high discharge energy takes place in any of the segments and the self-healing mechanism fails, the high current density through the fuse link will melt and vaporize it and the faulty segment will be isolated from the rest of the electrode [21,48].

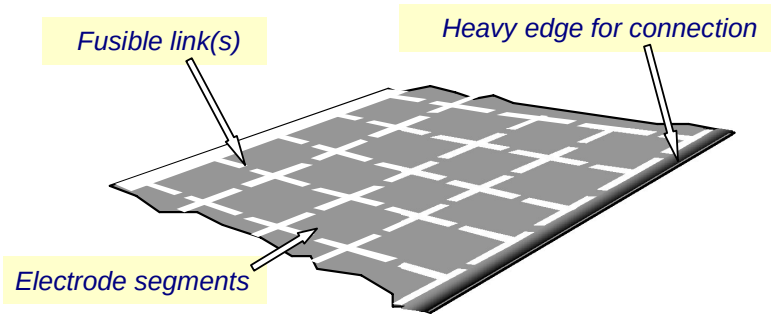

Figure 4.8. Various electrode segmentation patterns. [48]

In some cases, segmentation may not be technically and economically feasible, as in practice, the energy needed for self-healing to fail is considerably large. Greater loss of capacitance and increased costs are also the disadvantages of segmented metallization. [36]

4.4.2 Electrode corrosion

Due to the materials and extremely small thickness of the metallized electrodes, the electrodes are vulnerable to various corrosion mechanisms. Moisture is required for the corrosion mechanisms to initiate. Due to corrosion, the effective electrode area decreases gradually which leads to reduction of capacitance, longer path for charging current, higher current densities in the healthy parts of metallization, increased ESR and increased losses. Eventually, these issues may lead to the failure of a capacitor.

Atmospheric corrosion is based on the moisture originating from the surrounding environment. Although the capacitor encapsulation is tightly sealed, small amounts of moisture may penetrate inside the element axially from the end-spray regions, which may initiate the corrosion of the electrodes. Generally, the outer layers of a cylindrically wound capacitor element are more susceptible to the corrosion as it is easier for the moisture to penetrate in and accumulate on the electrodes due to the lower inter-layer pressure. As a consequence of corrosion, a gap between the end-connection and the central parts of the metallization may develop which directly results in loss of capacitance. Furthermore, as these regions are disconnected from the end-spray, more current has to flow through the healthy parts of the metallization still connected to the

end-spray. This leads to increased current densities, current path, ESR and losses. The effect of atmospheric corrosion is illustrated in Figure 4.9a. [49]

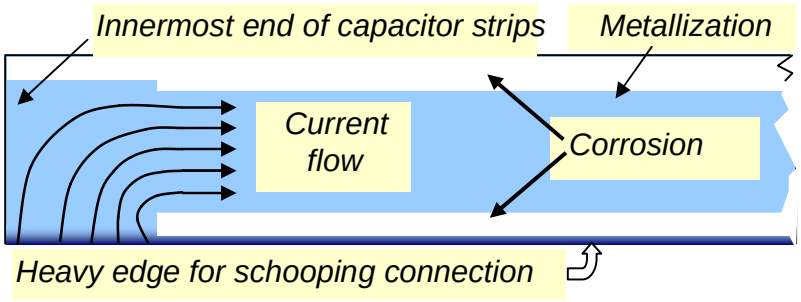

(a)

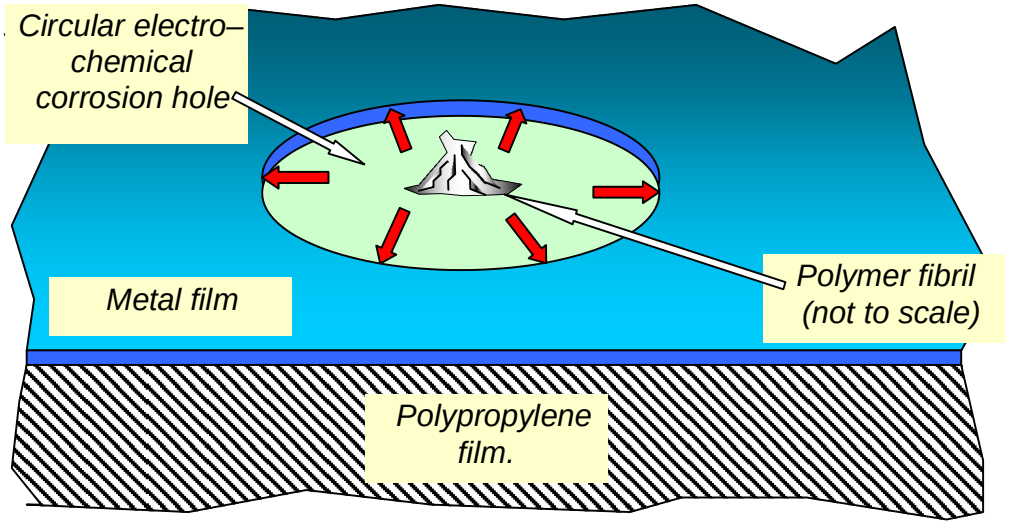

(b)

Figure 4.9. Corrosion mechanisms in metallized film capacitors. (a) corrosion of metallized electrode due to atmospheric moisture (b) electrochemical corrosion. [49]

Electrochemical corrosion is a specific corrosion mechanism taking place on metallized aluminium electrodes under AC voltage. As a result of electrochemical corrosion, parts of aluminium are converted into insulating oxide (Al_2O_3). The moisture and oxygen needed for the chemical reaction migrate from polypropylene film to the insulator-electrode interface. As the electrochemical corrosion progresses, corrosion spots develop around fibrils on the polypropylene surface or around particles and impurities in the aluminium as illustrated in Figure 4.9b. As a result, the capacitance is reduced and losses increase due to higher ESR. The corrosion process is strongly dependent on the electrode thickness, as with reducing electrode thickness the number and size of the corrosion spots increases. The surface properties of the polypropylene film, temperature, humidity and the possible impregnant used also affect the corrosion process. Electrochemical corrosion may be prevented by using aluminium-zinc alloy as the electrode material. However, zinc is more vulnerable to atmospheric corrosion and its electrical conductivity is smaller, which may limit its usability in some cases. [6,49]

4.4.3 End-spray disconnection

As discussed in sub-chapter 4.2.3, the end-connection formed by spraying molten metal particles to the exposed ends of a capacitor element is not continuous along the electrode edge. Therefore, the contact is formed via irregular spots which are subjected to high current density. This is crucial especially for high-current pulsed applications, as it has been observed that partial disconnection of the sprayed ends may occur which subjects the remaining healthy contact area to even higher current density. Eventually, this may result in the total failure of a capacitor unit. [6]

In a study by Nucci *et al*. [50], it was concluded that end-spray disconnection may be related to erosion due to electric sparks occurring in the regions where the end-spray is connected to the metallized electrode. The sparks began to occur after a certain peak value of discharge current pulses was exceeded. The occurrence of the sparks was followed by an increase in the $\tan\delta$ value of the capacitor which indicates an increase in the ESR. Nucci *et al*. also conducted tear-down analysis of some of the tested capacitor elements which showed that erosion of metallized electrode had occurred only in regions of the electrode edge where the contact with end-spray was made.

4.5 Design principles for high power density applications

For high power applications, which involve high voltages, high peak currents and/or fast discharge times, the basic structure of a metallized capacitor discussed in sub-chapter 4.2 may not be sufficient. The current-carrying capability of the capacitor is the most important construction criterion in order to manufacture reliable capacitors for pulsed power applications. Alternative capacitor design principles are illustrated in Figure 4.10 and will be discussed briefly in the following.

The *internal series connection structure* with varying number of electrode sections is illustrated in Figure 4.10a-c. The structure is based on capacitive coupling, i.e. the electrode sections which are in floating potential are connected capacitively to the overlapping electrode sections thus forming a series connection. By dividing the metallized electrodes into multiple sections, the voltage stress acting on each section is equal to U_{tot}/N, where U_{tot} is the voltage over the capacitor and N is the number of sections. As the voltage stress on each section is lower than in case of single section electrode, thinner insulation thickness can be used and a more compact structure can be achieved. However, in order to prevent flashover between adjacent electrode sections, a margin area without metallization has to be left between the electrodes. With increasing number of sections, this reduces the effective area and the energy density of the capacitor quickly. Furthermore, when clearing occurs in one electrode section, the voltage of that section is transferred to the other sections, which may lead to further clearings on other sections especially in case of a capacitor with only few electrode sections. [51]

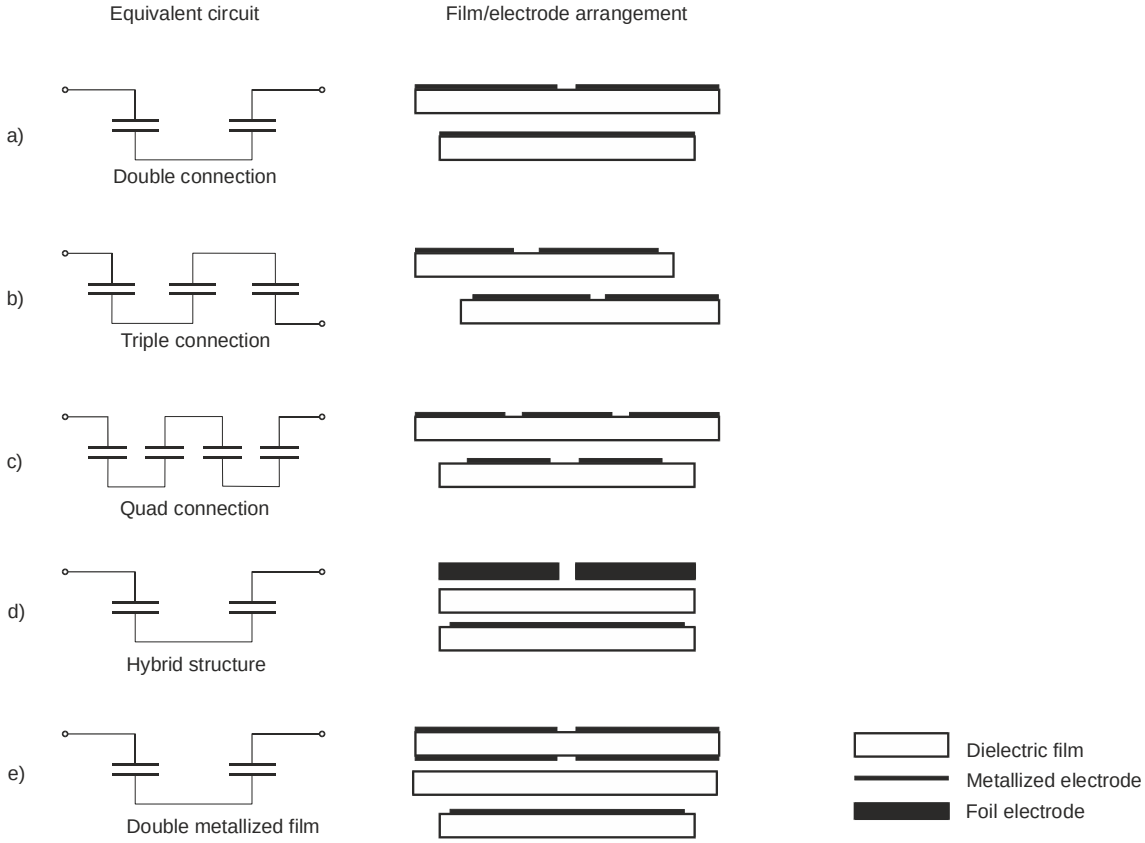

Figure 4.10. Various capacitor design principles. (a)-(c) Internal series connection (d) hybrid structure (e) double-sided metallized film.

The current-carrying capability of a metallized electrode is limited in comparison with a traditional foil electrode. Therefore, in order to sustain high currents, a *hybrid structure* may be utilized. Essentially, the hybrid structure comprises of foil electrodes, a metallized film and an insulating film, as illustrated in Figure 4.10d. Foil electrodes are used to conduct the current in the capacitor and a metallized film in floating potential is used as a carrier film. Thus, the hybrid structure combines both the self-healing capability of a metallized film and the high current-carrying capability of a foil electrode. Additionally, the end-connection quality and heat conduction capability is improved, due to larger thickness of the foil electrodes. [52]

As an alternative to foil electrodes, *double-sided metallization* can also be used to increase the current-carrying capability. As illustrated in Figure 4.10e, electrodes may be vapour deposited on both sides of an insulating film. The electrodes at the both sides of the film are then joined together as a conductor by end-spray. Thus, the current-carrying capability of the electrodes is doubled. The dielectric properties of the insulating film with double-sided metallization are irrelevant as the film is in field-free space. With double-sided metallization, high current carrying capability can be combined with self-healing. [53]

The maximum rate of rise of current is crucial for pulsed power applications and it is determined by the capacitor ESL ($dI/dt = U_0/\mathrm{ESL}$). The magnetic field outside the winding can be minimized by using coaxial structure, i.e. the input and return

connectors have to be at the same end of the capacitor element. In practice this can be done by threading the return wire from the other end of the capacitor element through the hollow cylindrical core to the same end with the input connector. Other options are to use a coaxial return conductor or to employ two coaxial windings separated with coaxial insulator, so that the current goes down one winding, transfers to the other winding and returns to the same end of the capacitor. [51]

4.6 Advantages and limitations of metallized capacitors

As a summary to this chapter, the advantages and limitations of metallized capacitors will be revised in the following.

Metallized capacitors have many advantages over traditional film-foil capacitors. Significantly higher energy density can be achieved, as metallized capacitors can be safely operated close to the average breakdown strength of the insulating film. In comparison with film-foil capacitors, energy density of metallized capacitors is also higher as the volume occupied by the electrodes is reduced. Due to self-healing mechanism, the reliability and life-time of metallized capacitors are greatly improved. Thousands of self-healing events can take place before a significant loss of capacitance can be measured whereas for film-foil capacitors, only a single breakdown of the dielectric is needed for a catastrophic failure of a capacitor element to occur. [35]

On the other hand, the extremely thin electrodes utilized in metallized capacitors limit the application possibilities. Peak power and current has to be limited in order to prevent damage to the end-connections. Due to the limitations in current, metallized capacitors are also less tolerant to external short-circuit currents. The ESR of a metallized capacitor is higher when compared with an equivalent film-foil capacitor as the resistance of a metallized electrode is higher. In addition, heat conduction capability of a metallized electrode is poor in comparison with film-foil capacitor which further limits the maximum operation current, as excess heat dissipation in the electrodes and dielectric may lead to a thermal breakdown. Thin metallized electrodes are also subjected to various corrosion mechanisms. [35]

Regardless of the limitations, due to the superior energy density, reliability and lifetime, metallized capacitor technology is widely used especially for low-voltage applications. Recently, metallized capacitor technology has also been shifted towards higher voltages. For example, the Dry-Q metallized film capacitor units by ABB can be utilized for up to 150 kV DC. [40]

5 TEST ARRANGEMENTS

5.1 Objectives of the measurement system

In the empirical part of this thesis the objective was to plan, construct and test a measurement system which could be used to conduct various DC tests on single metallized dielectric films. Originally, the measurements were intended to be conducted for both industrial-scale metallized polypropylene films and for metallized nanocomposite film samples obtained within the NANOPOWER -project. However, it was later decided to define the scope of this thesis to cover only the measurements with industrial-scale films and to serve as groundwork for future research. The decision was based on the fact that it was not reasonable to proceed with the metallization of nanocomposite film samples until the final processing recipes are determined for the material candidates to be further developed in the project.

The electrical properties to be tested have to be closely related to the phenomena taking place in metallized film capacitors. As discussed in Chapter 4, one of the most significant advantages of metallized film capacitors is their ability to self-heal. Therefore, the main properties of metallized films to be studied with the measurement system are:

- Breakdown strength
- Self-healing capability
- Maximum permissible electric field stress E_{max}

Self-healing can be utilized in order to examine the breakdown strength of a metallized film as each self-healing event represents a local breakdown at a specific voltage. Therefore, a statistical analysis of the breakdown strength may be performed by using e.g. Weibull-distribution [54]. As the voltage across the test capacitor is increased, some self-healing events corresponding to the weak parts of the polypropylene film may occur at relatively low breakdown voltages. More self-healing events will occur as the voltage is increased and as a certain material-specific threshold voltage is exceeded, the self-healing becomes continuous.

The self-healing capability refers to the ability of the dielectric film to clear well during local breakdown. As discussed in sub-chapter 4.4.1, it is important that the average required discharge energy $E_{discharge}$ for a successful self-healing is not too large, as with too high discharge energy, consecutive self-healing in adjacent capacitor layers and larger scale damage may occur. In case of nanocomposite dielectrics, it has to be ensured that the film clears well and that the required discharge energy is not too large

(which, in theory, could be due to better breakdown and treeing resistance often related to dielectric nanocomposites).

The maximum permissible electric field stress E_{max} refers to the threshold value of the electric field that can be sustained continuously over one capacitor winding layer with no or only a few self-healing events taking place in the dielectric film. When nanocomposite dielectrics are concerned, it would be preferable to determine whether the maximum operating field is higher than that of a reference film. In practice, capacitors are always operated way below the E_{max} of the dielectric in order to have a sufficient safety margin so that the reliability of the capacitor is not compromised. However, if E_{max} of the dielectric is increased in comparison to a reference, a capacitor utilizing such a dielectric may be operated with a higher nominal voltage which leads to an increase in energy density, as the operating voltage is squarely proportional to the maximum energy density of a capacitor (see Equation (4-3)).

In practice, the measurements should be made in conditions closely resembling those inside a wound capacitor element. Thus, the amount of air voids between the film layers has to be minimized. In addition, as the measurements will be made for single metallized film layers, the effect of inter-layer pressure due to cylindrical winding should be simulated artificially. Typically, the inter-layer pressure in a wound capacitor element is in the range of 1–10 MPa [47,55]. In practice, the effect of inter-layer pressure could be simulated by adding external mechanical pressure on the film layers with e.g. weights or a clamping device. Finally, the effect of temperature on the aforementioned properties should also be taken into account.

5.2 Measurement system specification

As the purpose of the measurement system is to perform electrical measurements for single metallized polypropylene films, a specific test capacitor structure and measurement circuit was constructed. Certain aspects of the measurement system and general guidelines were adopted from the test setups formerly used by various authors (references [23], [46], [56], [57] and [58]). The film arrangement, the structure of the test capacitor and the measurement circuit are discussed in the following.

5.2.1 Film arrangement

For measuring the effect of UV treatment on dielectric strength of BOPP capacitor films [56], Ho & Boggs have used a film arrangement shown schematically in Figure 5.1. A similar film arrangement was used for the test capacitor in this thesis.

As illustrated in Figure 5.1a, the test film (A=16 cm^2) is oriented so that the metallization is facing down. The metallization of the test film serves as the bottom electrode of the capacitor arrangement. Electrical contact to the test film is achieved with a strip of metallized film laid under the test film with metallization facing upwards. A windowed dielectric film is then laid on the test film. The purpose of the mask film is to prevent flashover between the electrodes and to determine the effective area of the

capacitor arrangement. In practice, a polyimide mask film with thickness of ~50 µm and with a 9 cm^2 window was used. Another metallized film is then laid over the mask film with metallization facing down. This film serves as the top electrode and is connected to high voltage source. The completed film structure is shown in Figure 5.1b.

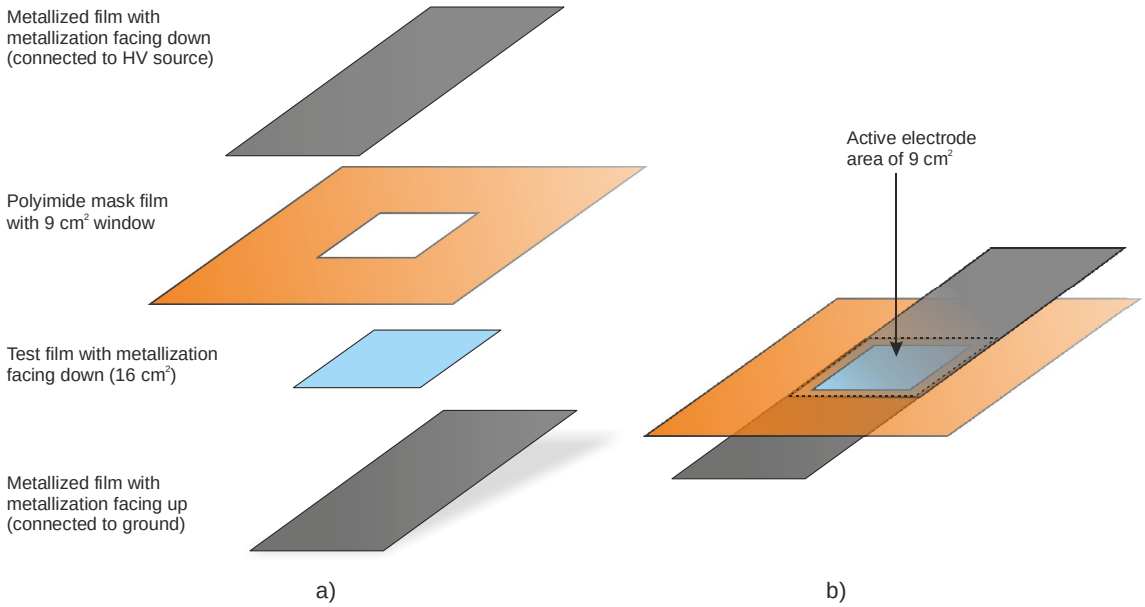

Figure 5.1. The film arrangement used for the test capacitor: (a) with layers shown individually, (b) completed film arrangement.

When DC voltage over the arrangement is increased, the layers are drawn together by electrostatic force which effectively removes air voids and creates a smooth interface between the layers [56]. The pressure generated by the electrostatic force can be expressed as:

$$p_{Coulombic} = \frac{\varepsilon_0 \varepsilon_r U^2}{2l^2}, \tag{5-1}$$

where ε_0 is the vacuum permittivity, ε_r the relative permittivity of the material, U the voltage over the arrangement and l the film thickness. As an example, with voltage gradient of 700 V/µm, the pressure on 7 µm BOPP film (ε_r = 2.3) due to electrostatic force is approximately 5 MPa. Therefore, it should be noted that in case of a single layer capacitor arrangement, the test film is exposed to a compressive force gradually increasing with voltage which may be reflected to the dielectric strength of the film material; similarly to gaseous dielectrics, with increasing pressure, the dielectric strength of solid insulation material may increase as well [55]. However, in a wound capacitor element the inter-layer pressure due to electrostatic force is considerably lower, as the electrostatic forces generated between the wound layers cancel each other except for the inner- and outermost layers and thus, the resulting compressive force is lower [59].

5.2.2 Test capacitor structure

A schematical illustration of the test capacitor is shown in Figure 5.2. The test capacitor comprises of bottom and top plates made of Bakelite (thickness 10 mm). The film arrangement described in the previous sub-chapter is sandwiched between the plates. The additional strips of metallized film which are used for making electrical contact to the test capacitor structure are extended to the opposite ends of the bottom plate. At the both ends of the bottom plate, electrode clamps comprising of two aluminium plates are used for making electrical contact to the metallized films. With clamping electrodes, the contact to the metallized films can be made on large area which ensures sufficiently low current densities through the contact areas with metallization. Furthermore, as the clamping electrode consists of top and bottom electrode plates, electrical contact can be made regardless of the film orientation.

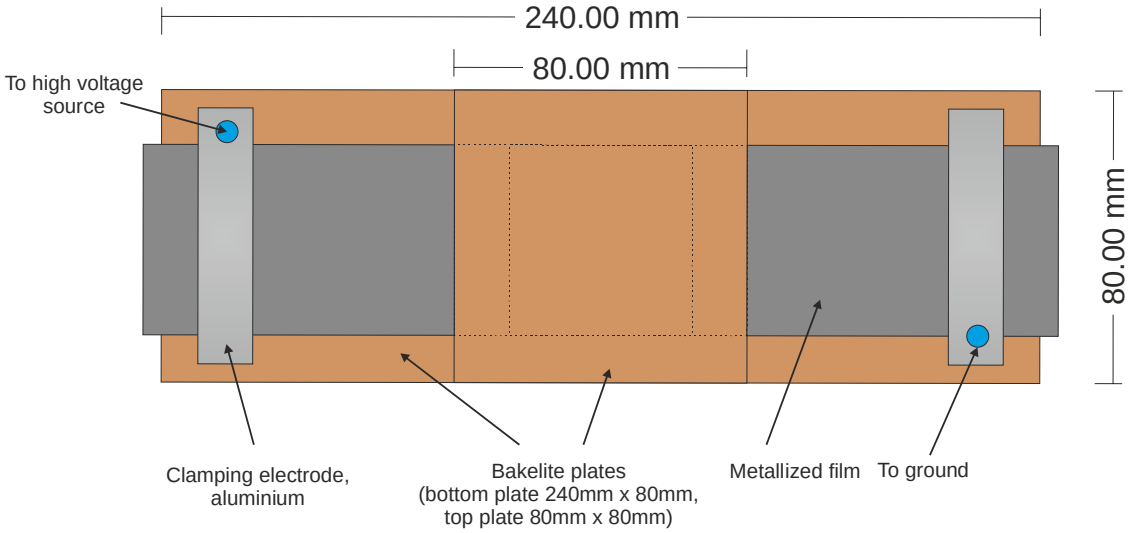

Figure 5.2. Schematical illustration of the test capacitor.

5.2.3 Application of external pressure

As the effect of inter-layer pressure had to be simulated, a bolt-adjustable clamping device was used to exert perpendicular force to the Bakelite plates and thus, pressure $p_{external}$ to the film arrangement. Therefore, in an ideal case, the total resulting pressure in the dielectric film layer is $p_{tot}=p_{Coulombic}+p_{external}$. The clamping device is illustrated in Figure 5.3.

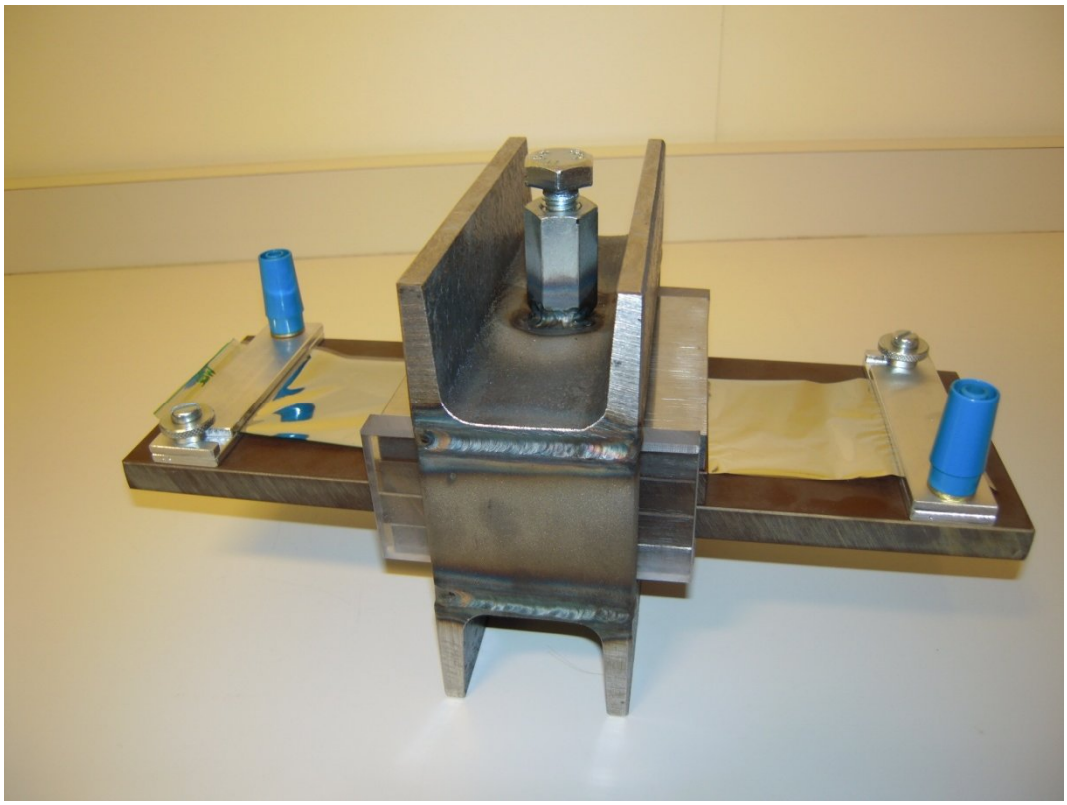

Figure 5.3. A bolt-adjustable clamping device used for applying external pressure to the test capacitor.

In practice, the pressure generated by the clamping device was measured with Fujifilm Prescale pressure sensitive film [60]. The pressure range of the Prescale film was 0.2-2.5 MPa and although not exact, an adequate approximation of the external pressure was obtained by using the pressure sensitive film. The pressure was measured by placing a 16 cm^2 piece of Prescale film under the film arrangement. An additional piece of polyimide film slightly smaller than the window area was used on top of the film arrangement in order to focus the pressure on the effective area of the test capacitor. The bolt was adjusted until inter-layer pressure of approximately 2.0 MPa was obtained in the effective area of the test capacitor. Similar pressure values have been formerly used by Shaw *et al.* for studying self-healing phenomenon (approximately 1.3 to 1.7 MPa) [23]. The tightness of the bolt was adjusted with a torque wrench in order to be able to reproduce the same inter-layer pressure value for each sample. Figure 5.4 presents the pressure distribution on the effective electrode when the torque of the bolt was adjusted to 4.0 Nm. The ambient temperature and relative humidity were 25 °C and ~40 RH%, respectively. Thus, according to the pressure chart of Prescale film (see Appendix A), the average pressure obtained with the clamping device was approximately 2.0 MPa. Multiple measurements were made to ensure the reproducibility of the aforementioned pressure.

It can be seen from Figure 5.4 that the achieved pressure distribution is not totally even. The most probable reasons for this were assumed to be the surface roughness of the additional piece of polyimide film and air bubbles or foreign particles between the

film layers. It was also later noticed that with externally applied pressure, the above mentioned film arrangement induced electric field distortions which caused problems with the measurements. This will be further discussed in Chapter 6.

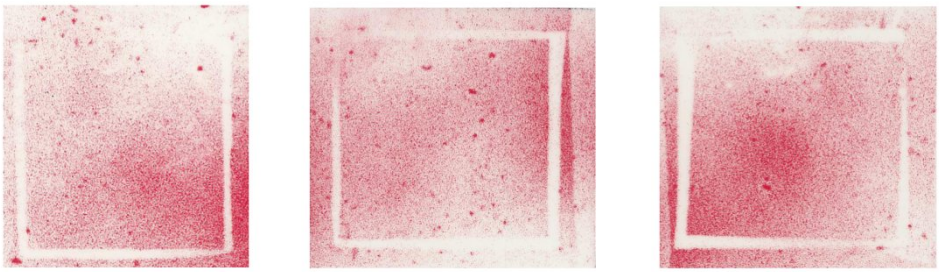

Figure 5.4. Pressure distribution on the effective test capacitor area (4.0 Nm bolt-torque).

5.2.4 Measurement circuit and data acquisition

The measurement circuit used for the tests is presented schematically in Figure 5.5. Some resemblance with a typical partial discharge measurement system can be noticed [1], and in fact, some of the circuit elements, measurement techniques and general principles are directly adopted from PD-measurement systems formerly used in TUT.

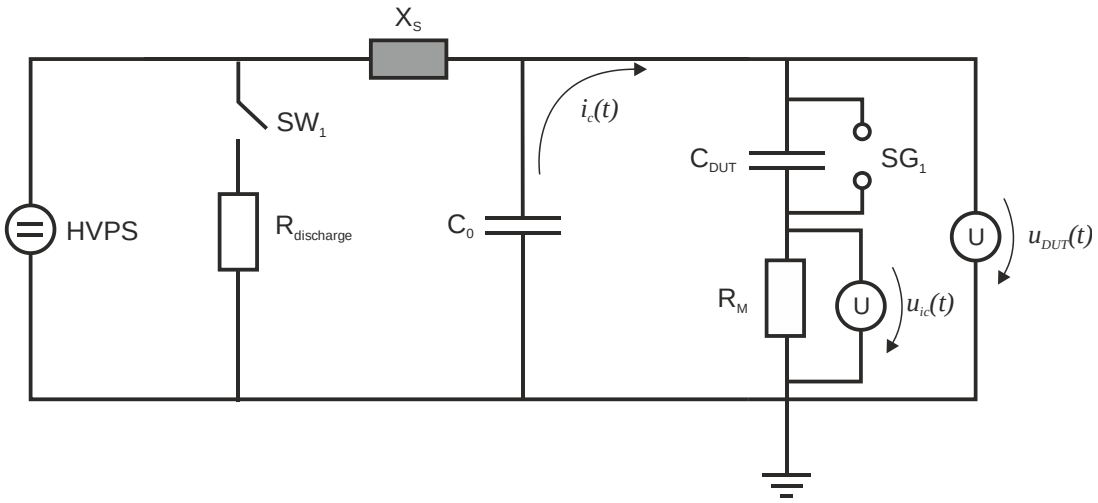

Figure 5.5. Measurement circuit.

A Spellmann SL 1200 DC power source (with nominal power of P_n=1200 W) was used as the high voltage power source (HVPS). The test capacitor described earlier corresponds to the capacitance C_{DUT}. Parallel to the test capacitor, a 4 nF coupling capacitor C_0 is used (Hipotronics PSF100-4, U_N=100 kV AC, discharge free at rated voltage). The coupling capacitor holds the voltage across C_{DUT} steady and it may also be considered to simulate the "healthy part" of a capacitor element.

When a breakdown takes place in C_{DUT}, the discharged energy is replaced by C_0. During a breakdown event, C_{DUT} is short-circuited (corresponding to the spark gap SG_1) and the charging current pulse $i_c(t)$ from C_0 can be measured with a measurement

resistor (R_M =4.983 Ω) as a voltage signal $u_{ic}(t)$. The voltage across the test capacitor $u_{DUT}(t)$ is measured with a voltage probe (Tektronics P6015A, attenuation factor of 1000). The Hipotronics coupling capacitor also comprises of a built-in series coil X_s which isolates the high-frequency charging current to flow only from the coupling capacitor to the test capacitor during self-healing. At the end of each measurement, capacitive elements may be discharged via a resistor $R_{discharge}$ by closing the switch *SW1*. A photograph of the measurement system is presented in Figure 5.6.

The test capacitor voltage and the charging current signals were routed via a National Instruments PCI-6221 data acquisition card to a computer running LabVIEW-software. This allowed logging of the test capacitor voltage and charging current during each test with a moderate sample rate (50 - 100 S/s). In order to obtain more accurate data during self-healing, the charging current and the test capacitor voltage were recorded during each self-healing event by using a Lecroy LT624M oscilloscope triggered to the charging current signal.

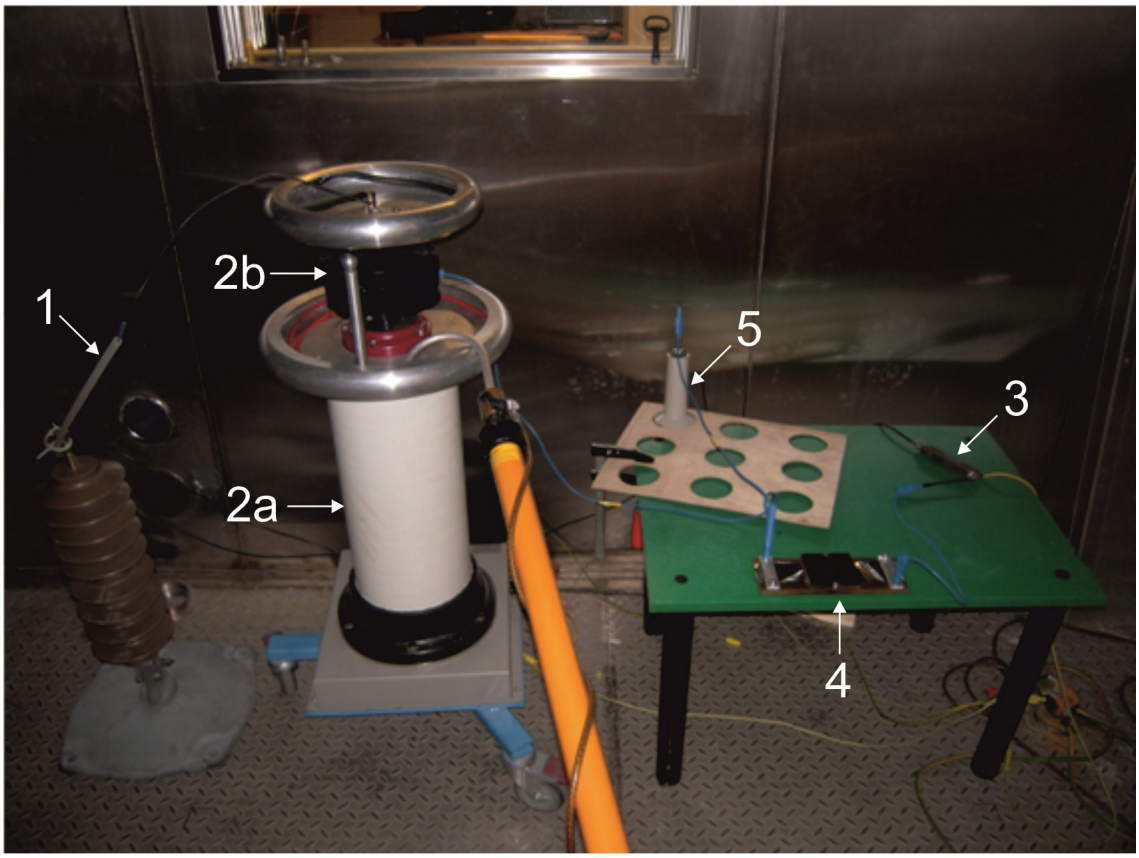

Figure 5.6. The measurement system: 1. Supply lead from HVPS, 2.a coupling capacitor, 2.b series coil, 3. measurement resistor, 4. test capacitor, 5. high-voltage probe.

5.2.5 Test film specifications

The metallized polypropylene film which was used for the measurements was manufactured by Tervakoski Films Group and the film was received from Alstom Grid Oy. The film, Tervakoski Film PZY, is single-sided metallized polypropylene film with linearly thickening metallization. The metallization material is zinc. The main properties of the film are listed in Table 5.1. Thus, based on Equation (4-1), the capacitance of the test capacitor with a 9 cm^2 effective area was approximately 2.50 nF.

Table 5.1. Properties of Tervakoski Film PZY.

Tervakoski Film PZY		
Film dimensions	Film thickness	7.0 μm
	Film width	105.0 mm
	Free margin	2.5 mm
Metallization	Resistivity	
	- at contact edge:	2.0-4.0 Ω/sq
	- close to free margin:	14-28 Ω/sq
Dielectric properties	Dielectric constant (at 25 °C, 50 Hz - 1 MHz)	2.2
	Dissipation factor	$\leq 3 \times 10^{-4}$
	Film resistivity	$> 1 \times 10^{15}$ Ωm

6 RESULTS AND EVALUATION

6.1 Breakdown strength analysis

6.1.1 Breakdown strength with no external pressure

The first set of measurements was conducted for 10 metallized polypropylene film samples with no externally applied pressure. The film arrangement described in the previous chapter was assembled carefully and air bubbles between the films were removed by flattening out the films. For each measurement, a new pair of metallized films was used for making electrical contact to the test film. Based on Equation (4-1), the capacitance of the test capacitor was calculated to be 2.50 nF ($\varepsilon_r = 2.2$).

The voltage across the test capacitor was increased steadily with a ramp speed of 30 V/s and the test capacitor voltage was recorded with data acquisition rate of 50 S/s. The maximum voltage level of the ramp was set to 5600 V which equals to electric field stress of 800 V/µm across the dielectric. The voltage was quickly ramped down if a permanent breakdown occurred or when the limiting voltage level was reached. As an example of the typical behavior of the test capacitor voltage during a measurement, the measured voltage of sample no. 8 is presented in Figure 6.1. As seen in the figure, the self-healing events with zero external pressure can be clearly distinguished as a sudden voltage drops. Typically, a few single self-healing events took place at lower voltages and as the voltage gradient of approximately 700 V/µm was reached, the self-healing became more or less continuous.

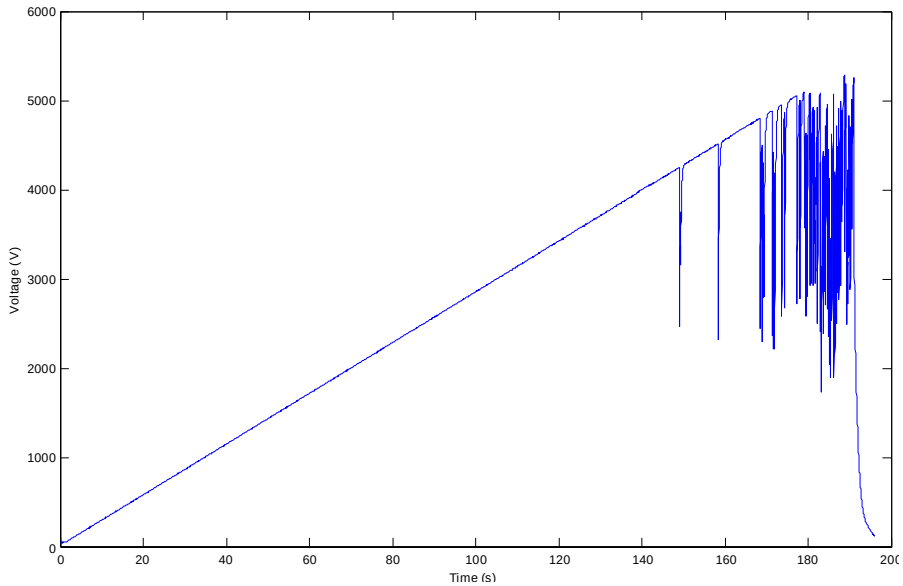

Figure 6.1. Typical behaviour of the test capacitor voltage as a function of time.

During the measurements it was noticed that especially at higher field stresses, multiple self-healing events may take place during a short period of time very rapidly. This is probably due to dissipated heat and expansion of the hot vaporized plasma during self-healing which may lead to consequential thermal breakdowns close to the initial breakdown location. An example of such a sequential event is presented in Figure 6.2. It can be clearly seen that the test capacitor voltage does not fully recover between the clearings and that such a sequence of events may be considered as a continuum.

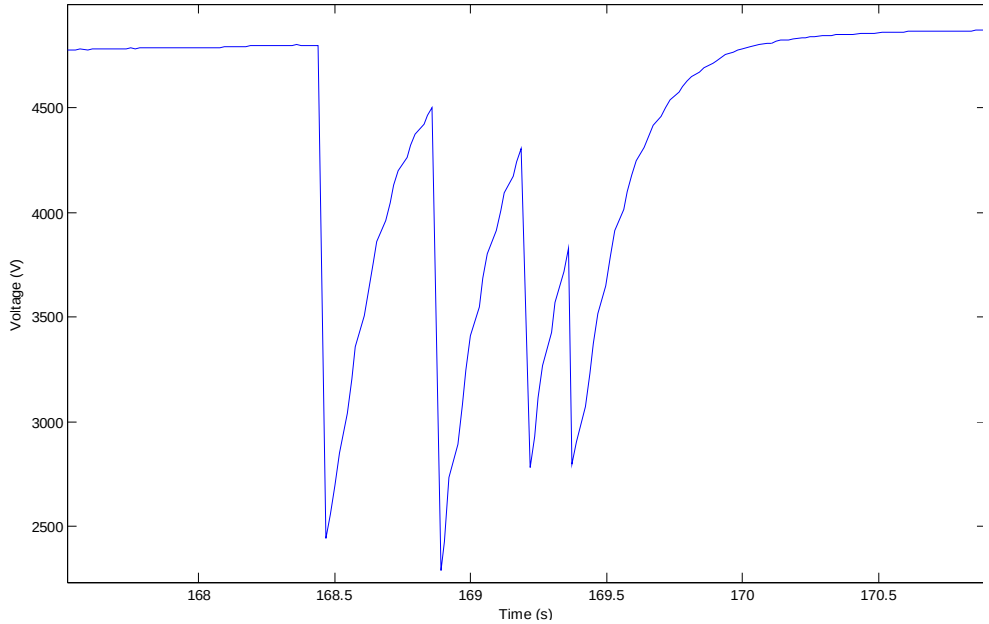

Figure 6.2. Consequential self-healing events over a short period of time.

The breakdown strength analysis of samples 1-10 was done by examining the test capacitor voltage data in Matlab. The data is presented in Table 6.1. Only the clearly distinguishable self-healing events, for which the test capacitor voltage recovered fully, were taken into account. This was done in order to obtain the breakdown values which more clearly represent the intrinsic breakdown strength of the polypropylene film. It is interesting to notice that for all the samples except for sample no. 6, the self-healing mechanism was always successful even up to the limiting value of 5600 V of the voltage ramp.

Possible reasons for the permanent breakdown of sample no. 6 could be a defect in the polypropylene, although a more probable reason is the local electric field distortion due to the edges of the polyimide mask film or foreign particles such as dust between the film layers. It was also noticed between the measurements that black residual matter accumulated on the window edges of the polyimide mask film as depicted in Figure 6.3. The residual matter was assumed to be vaporized zinc and other chemical by-products originating from self-healing. Similar observations have also been made in the reference [55]. The increase in local pressure during self-healing seems to be in fact so considerable, that the plasma is capable to propagate between the film layers. The residual matter was removed by cleaning the polyimide mask film with acetone,

although it was not possible to remove the entire residue. Especially during later measurements with externally applied pressure, it was noticed that the breakdowns often took place close to the edges of the mask film with the residual matter. This is assumed to be caused by the local distortion of the electric field at these areas.

Table 6.1. Breakdown voltage data of samples 1-10 (no external pressure).

Sample number	1	2	3	4	5	6*	7	8	9	10
Breakdown voltages (V)	4585	4560	4255	4798	4538	4432	4383	4429	4933	3668
	4719	4726	4460	4881	4786	4519	4428	4893	4829	4623
	4975	4774	4673	4948	4837	4551	4786	5056	4909	4696
	4984	4818	4668	5053	4880		4840	5073	4989	4902
	4987	4854	4708	5101	4871		4888	5067	4968	4915
	4960	4838	4994	5084	4958		4960	5078	5006	4952
	5101	4874	5060	5074	4968		4939	5099	5072	4995
	5244	4966	4879	4966	4956		4991	5160	5021	5068
	5314	4987	5116	5076	5015		5026	5182	5043	5043
	5402	5009	5408	4917	5017		4922	5182	5062	
	5378	4924	5408	4992	5100		4971	5043	5040	
		4989		5286	5034		4961	5319	5251	
		5065		5194	5070		4911		5289	
		5067			4900		5058		5344	
		5080			4907		5045		5398	
		5144			4955		5103		5346	
		5146			5178		5172		5113	
					5239		5205			
					5290		5239			
					5400		5243			
					5346		5209			
							5337			
							5374			
Average breakdown voltage (V)	5059	4931	4875	5028	5012	4501	5000	5048	5095	4762
Standard deviation (V)	250	153	349	126	196	50	239	211	164	412
Total number of breakdown values	11	17	11	13	21	3	23	12	17	9

*) Sample 6 suffered a permanent breakdown at 4551 V

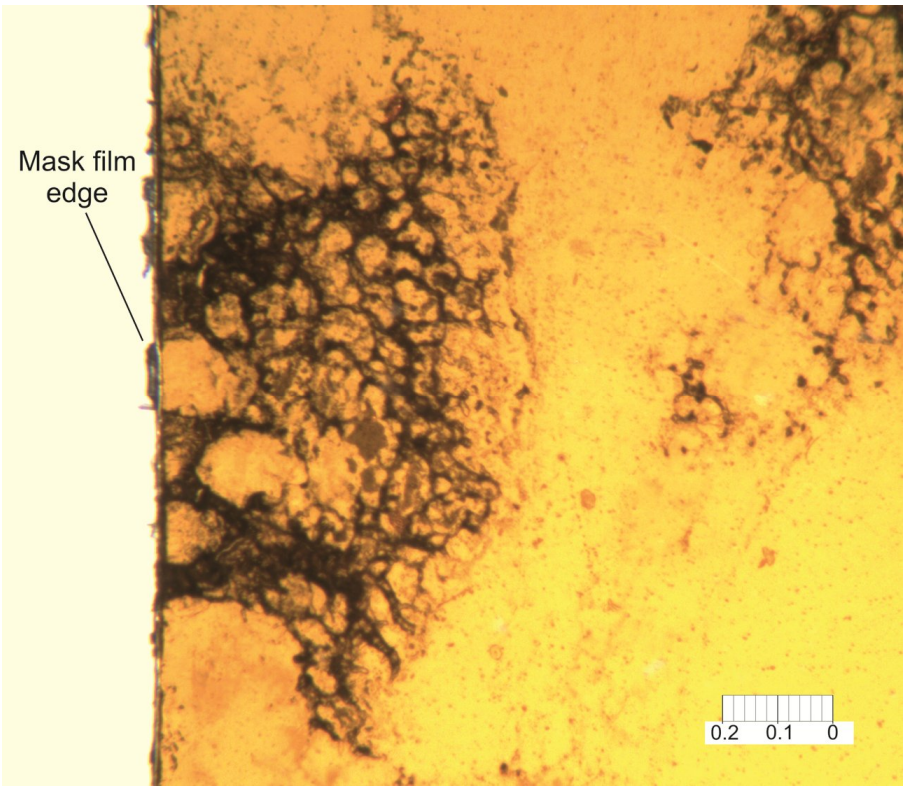

Figure 6.3. Microscope image of a mask film edge after measurements showing black residue. Scale bar is in millimeters.

The breakdown data presented in Table 6.1 was further analyzed by performing Weibull-analysis according to the IEEE 930 standard [54]. The breakdown voltage values were first transformed to breakdown field values before the analysis. The Weibull parameters are presented in Table 6.2 and the Weibull plot of the data with 95 % confidence bounds is presented in Figure 6.4. The scale parameter of ~727 V/µm, which corresponds to 63.2 % breakdown probability in Weibull-distribution, is in good agreement with the intrinsic breakdown strength value of 700 V/µm often cited for polypropylene films (see e.g. [56]). In addition, according to the IEEE 930 standard, the correlation coefficient should be equal or greater than ~0.97 for a good fit in two-parameter Weibull-distribution; this criterion is clearly met. Furthermore, if the worst breakdown strength value of 3668 V is omitted from the analysis, the correlation coefficient is 0.988, i.e. the breakdown voltage data fits well in Weibull-distribution. This is of course understandable, as the intrinsic breakdown voltage of polypropylene is widely known to follow the Weibull-distribution [12].

Table 6.2. Weibull parameters of the breakdown voltage data of samples 1-10.

Number of break-down values	Correlation coeffi-cient	Scale parameter α (V/µm)	Shape parameter β
137	0.978	727.673	24.021

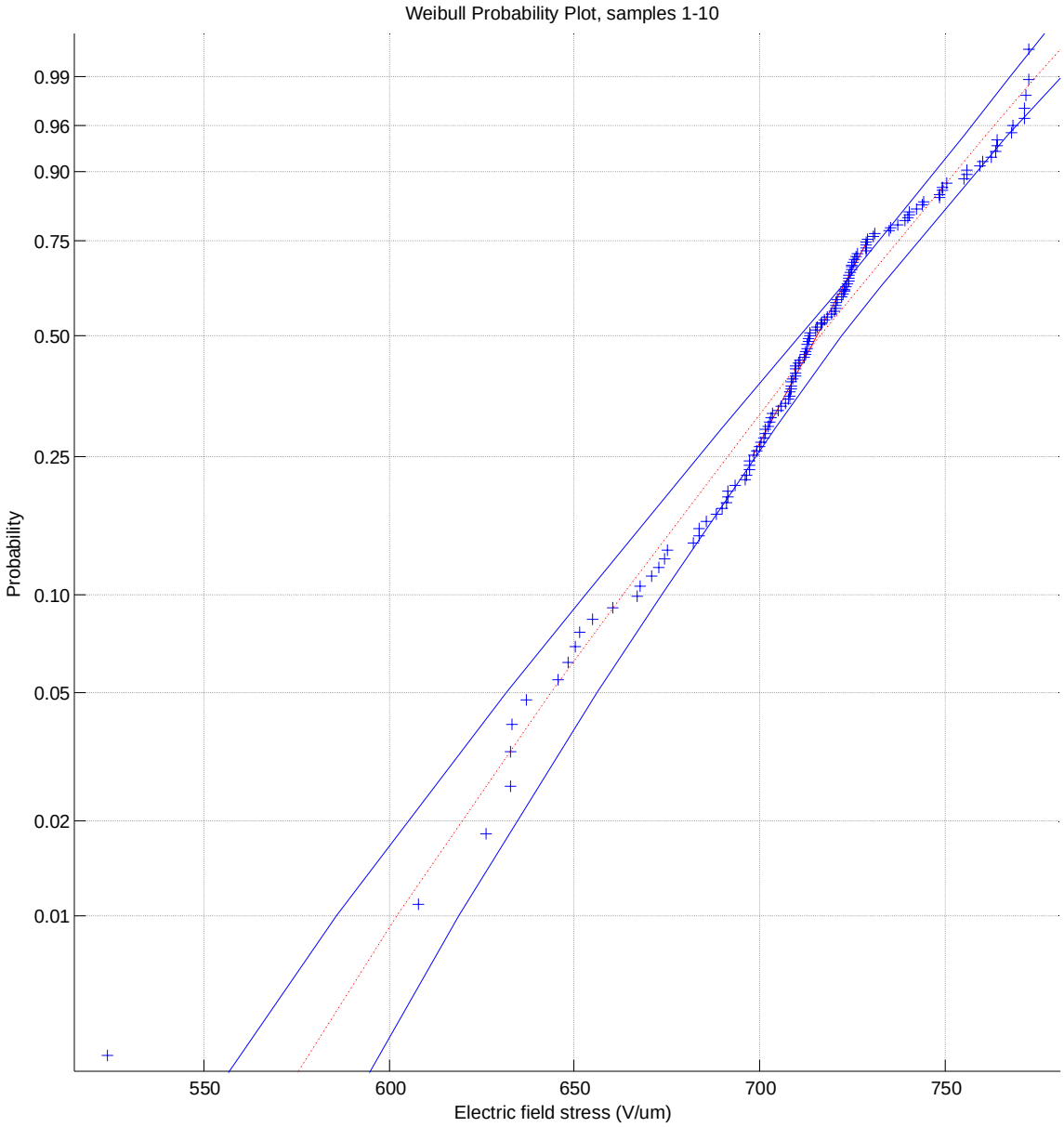

Figure 6.4. Weibull-probability plot of the breakdown data of samples 1-10 with 95 % confidence bounds.

The maximum permissible electric field stress E_{max} can be approximated from the Weibull plot presented in Figure 6.5. The results suggest that with E_{max}=600 V/µm, the failure probability of Tervakoski PZY-film would be approximately 1 %. However, it should be noted that as the breakdown values are obtained from short-term measurements, the results should be interpreted carefully, although a comparison between various dielectric materials can be made based on short-term measurements too. Nevertheless, long-term measurements with constant voltage stress are certainly needed in the future.

6.1.2 Breakdown strength with external pressure

After the initial tests with zero external pressure, a new set of measurements was performed with externally applied pressure by using the bolt-adjustable clamping device. As described in sub-chapter 5.2.3, an additional piece of polyimide film slightly smaller than the window area was used between the film arrangement and the top Bakelite plate in order to exert the pressure on the effective area of the test capacitor. For the measurements with externally applied pressure, the limiting value of voltage ramp was set to 5950 V (which is equal to electric field of 850 V/µm through the dielectric).

During the measurements it was noticed that the external pressure had a significant effect on the electrical properties of the polypropylene film. During a typical self-healing event, the peak current and the voltage drop were significantly lower, which suggest that the average energy discharged during a self-healing was greatly reduced. In addition, the average duration of the clearing events was much shorter in comparison to the clearing events at zero external pressure. In fact, some of the clearing events were so fast and low in energy that it was challenging to trace the exact breakdown voltages from the measurement data after the test.

However, as opposed to initial expectations, the application of external pressure had a negative effect on the dielectric strength of the polypropylene film. In general, low-energy self-healing events began to take place at relatively low field stresses, and as the voltage was increased enough, the self-healing mechanism often failed which resulted in a permanent breakdown of the test sample. It was soon concluded, that a rather obvious explanation for the impaired dielectric strength was the structure of the test capacitor itself; the edges of the mask film window and the additional piece of polyimide film which was used to focus the pressure on the right area were clearly distorting the electric field distribution. Thus, due to local increase in the electric field, a breakdown of the polypropylene film may occur prematurely. In addition, it was noticed that the permanent breakdowns often occurred on the low-pressure area between the additional piece of polyimide film and the window edge (see Figure 5.4). At a later stage, it was attempted to compensate the electric field distortion by using a mask film with a circular window. This seemed to reduce the amount of self-healing events at lower voltages to some extent, although it did not remove the initial problem with the field distortion due to the additional piece of polyimide film.

At first, five film samples were tested with ~2.0 MPa of external pressure using the square-windowed mask film. Similarly to samples 1-10, the breakdown voltages were traced from the measurement data. However, as the external pressure greatly reduced the duration and amplitude of a clearing event, it was challenging to trace all the breakdown voltages from the measurement data. Thus, some of the lower-energy clearing events were definitely missed, although the amount of breakdown voltages obtained is still statistically adequate. The breakdown data of the samples 11-15 is presented in Table 6.3. It is also notable, that with externally applied pressure, the self-

healing mechanism eventually failed at higher voltages (as denoted by the red cells in Table 6.3).

Table 6.3. Breakdown voltage data of samples 11-15.

Sample number	11	12	13	15	16
Breakdown voltages (V)	1764	1022	565	1282	1079
	2364	1659	719	2587	2027
	2527	1739	1037	2865	2333
	2998	2033	1525	2928	2643
	3060	2446	1616	2972	2732
	3232	2878	1671	3443	2828
	3663	3041	1770	3488	2846
	3865	3293	1930	3641	2899
	4097	3408	1982	3726	3190
	4196	3532	2094	3797	3319
	4330	3627	2311	3798	3534
	4451	3720	2409	3958	3663
	4487	3955	2431	3990	3732
	4511	4051	2490	4040	3781
	4547	4108	2528	4097	3892
	4732	4194	2637	4125	3920
	4779	4263	2750	4165	4155
	4832	4287	2865	4256	4231
	4861	4317	3080	4327	4228
	4923	4363	3200	4355	4286
	4988	4485	3289	4363	4703
	5067		3350	4358	4852
	5146			4449	4915
	5221			4512	4926
	5319				4982
	5413				5046
	4560				5086
					5182
					5237
					5411
					5752
					5778
Average breakdown voltage (V)	4220	3353	2193	3730	3975
Standard deviation (V)	975	1027	791	754	1159
Total number of break-down values	27	21	22	24	32

Red cell = permanent breakdown

It can be clearly seen from Table 6.3 that the application of external pressure greatly increased the deviation of the breakdown voltages, especially when compared to samples 1-10 with no external pressure (see Table 6.1). The breakdown voltage data of samples 11-15 was further analyzed with Weibull analysis and the corresponding parameters and the Weibull-plot are presented in Table 6.4 and Figure 6.6, respectively. Obviously, the premature breakdowns of the polypropylene film at low voltages resulted in a poor Weibull-shape parameter and a lower scale parameter. Therefore, when a linear x-axis is used, the Weibull plot (Figure 6.6) shows a downward curve at lower voltages.

Table 6.4. Weibull parameters of the breakdown voltage data of samples 11-15.

Number of break-down values	Correlation coefficient	Scale parameter α (V/μm)	Shape parameter β
126	0.989	573.554	2.985

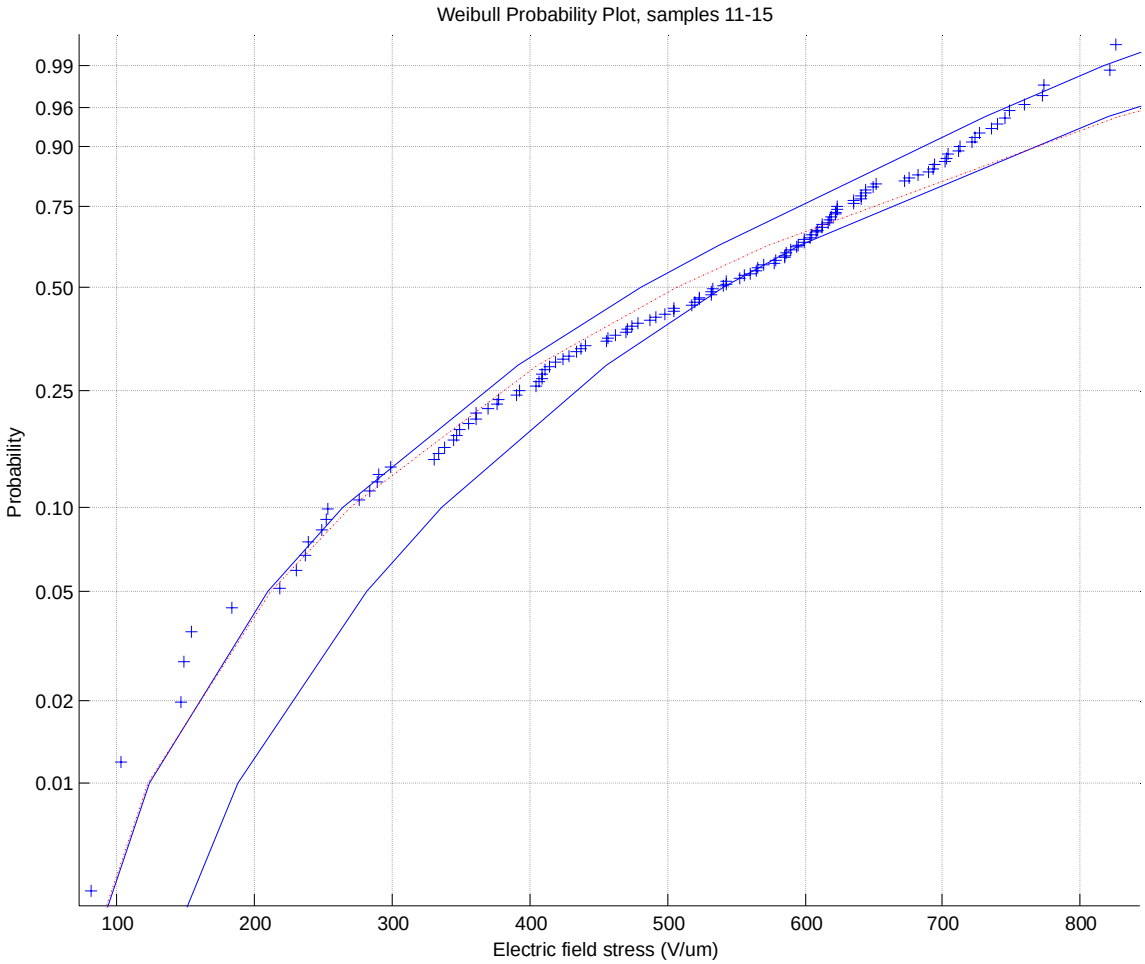

Figure 6.6. Weibull-probability plot of the breakdown data of samples 11-15 with 95 % confidence bounds.

Thereafter, additional measurements were made using a polyimide mask film with circular window (radius 1.25 cm). With circular-windowed mask film, the capacitance of the effective area of the test capacitor was 1.37 nF. For these measurements, it was decided that a slightly higher external pressure should be used in order to examine if the increase in pressure had a positive effect on the dielectric strength of the film. Three measurements were made with the bolt-torque of the clamping device adjusted to 6.0 Nm (samples 16-18) and three more measurements with torque of 8.0 Nm (samples 19-21). The aforementioned torque values were approximated to result in external pressure ranging between 2.5 to 3.5 MPa, although the pressure range of the Prescale film was not sufficient. Various pressure distributions with bolt-torques ranging from 4.0 to 8.0 Nm are presented in Figure 6.7.

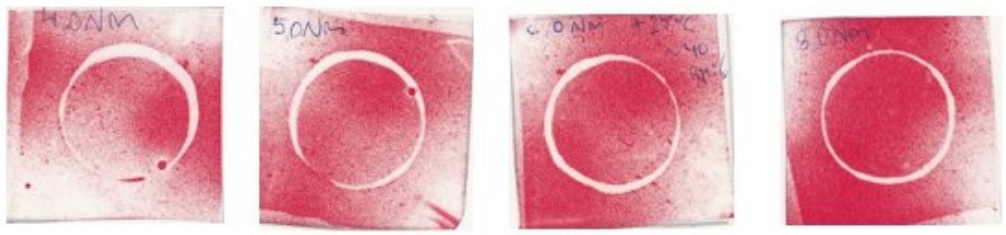

Figure 6.7. Pressure distributions when using mask film with circular window. (a) 4.0 Nm torque, (b) 5.0 Nm torque, (c) 6.0 Nm torque (d) 8.0 Nm torque.

The breakdown data of samples 16-21 is presented in Table 6.5 and the corresponding Weibull-parameters in Table 6.6. Weibull plots of samples 16-18 (6.0 Nm torque) and samples 19-21 (8.0 Nm torque) are presented in Figure 6.8 and Figure 6.9, respectively. As can be seen, only a slight improvement in the Weibull-shape parameter was achieved but the results are still scattered.

Therefore, it should be concluded that the film arrangement used in the measurement system of this thesis is not very suitable for examining the effect of external pressure on the breakdown strength of metallized dielectric film. This is presumably due to electric field distortion caused by the windowed mask film and the additional piece of polyimide film. A more appropriate way to exert pressure on the dielectric film is needed in the future in order to properly examine the pressure dependency of the dielectric strength of nanocomposite films. Possible solutions and future work will be discussed in the sub-chapter 6.3.

However, it should be noted that the film arrangement used in this thesis proved to be functional for measuring the breakdown strength of metallized dielectric film with no externally applied pressure. Especially in case of small sample areas, the film arrangement comprising of a windowed mask film is a sensible way to test the breakdown strength of dielectric film.

Table 6.5. Breakdown voltage data of samples 16-21 (polyimide mask film with circular window, increased pressure).

Sample number	16	17	18	19	20	21
Bolt-torque of the clamping device (Nm)	6.0	6.0	6.0	8.0	8.0	8.0
Breakdown voltages (V)	1094	1888	1569	3294	1321	918
	1797	2084	2816	4071	1935	1147
	2174	2280	2910	4705	2277	1691
	2219	2368	3186	4918	2856	1925
	2541	3324	3237		2978	2034
	2511	3522	3703		3020	2102
	2695	3487	3727		3223	2210
	2892	3889	3771		3318	2216
	3095	3987	3816		3465	2421
	3153	4140	3940		3555	2539
	3430	4555	3992		3728	2650
	3810	4840	4002		3792	2897
	3955	4882	4079		3942	2915
	4089	4944	4136		3991	3130
	4263	5034	4175		4015	3630
	4360	5215	4376		4183	3726
	4393	5366	4441		4211	3810
	4557	5407	4483		4367	3883
	4786		4520		4511	4123
	4886		5015		4708	4139
	5028				4814	4207
	5135				4860	4332
	5520				5108	4371
	5560				5158	4410
	5612					4400
						4443
						4538
						4854
						4873
						5126
						5166
						5508
Average breakdown voltage (V)	3742	3956	3795	4247	3722	3448
Standard deviation (V)	1276	1183	764	730	989	1254
Total number of break-down values	25	18	20	4	24	32

Red cell = permanent breakdown

Table 6.6. Weibull parameters of the breakdown voltage data of samples 16-21

	Number of breakdown values	Correlation coefficient	Scale parameter α (V/µm)	Shape parameter β
Samples 16-18 (6.0 Nm)	63	0.994	606.478	3.684
Samples 19-21 (8.0 Nm)	60	0.988	578.060	3.233

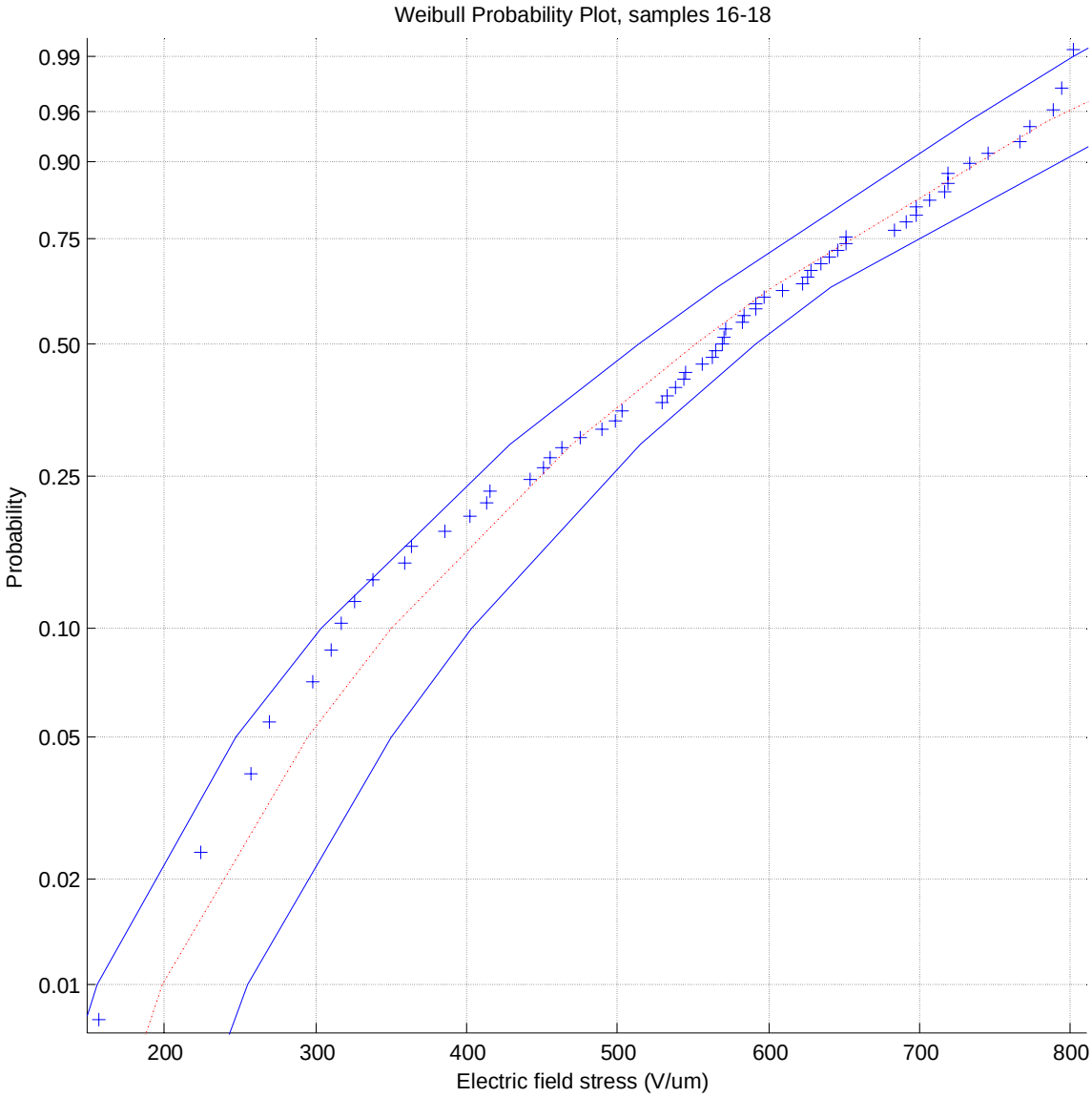

Figure 6.8. Weibull-probability plot of the breakdown data of samples 16-18 with 95 % confidence bounds.

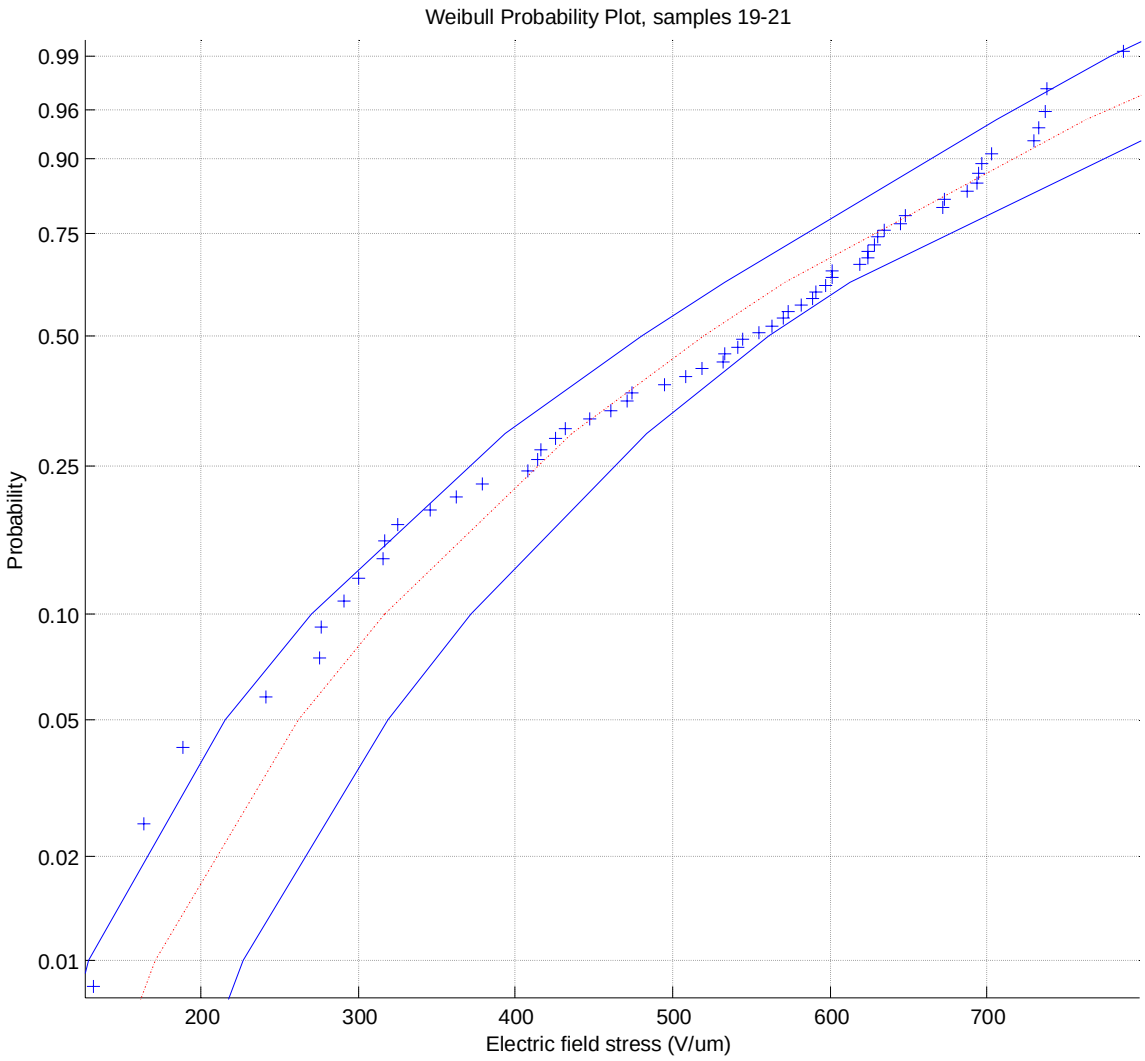

Figure 6.9. Weibull-probability plot of the breakdown data of samples 19-21 with 95 % confidence bounds.

6.2 Self-healing capability

6.2.1 Self-healing with no external pressure

Visual and microscopic examination

During a local breakdown in the dielectric film, a low-impedance conductive channel is formed through the dielectric and as a result, a portion of the energy stored in the capacitor is discharged. As a result, the metallization around the breakdown spot is vaporized which effectively isolates the breakdown site.

As an example of the clearing spots at zero external pressure, pictures of sample films 7 and 10 are presented Figure 6.10. As described in Chapter 4, the clearing spots were characterized by a small, pinhole-like breakdown channel through the polypropylene surrounded by an area of vaporized metallization of approximately 5-8 mm^2. By comparing the average size of the clearing areas of both samples, the difference between low- and high-energy clearings can be clearly seen; the clearings

that have taken place in sample 10 have been more intense which has resulted in a greater area of vaporized metallization. In fact, upon closer examination of sample 10 with a microscope, it was noticed that the larger clearing spots contained multiple breakdown channels, i.e. it is probable, that the energy discharged during the initial breakdown and the expansion of the plasma has lead to consequential (thermal) breakdowns close to the initial clearing spot. A microscope picture of a typical clearing spot is depicted in Figure 6.11 which clearly shows the breakdown channel in the middle surrounded by the area of vaporized metallization. Lastly, it is also notable that the energy discharged during self-healing also damaged the metallization of the adjacent film layers used in the test capacitor.

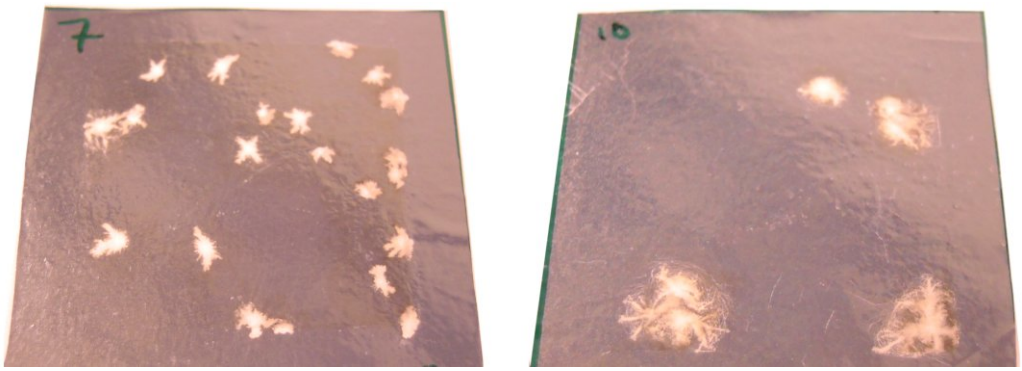

Figure 6.10. A Clearing spots at zero external pressure as seen from the metallized side.

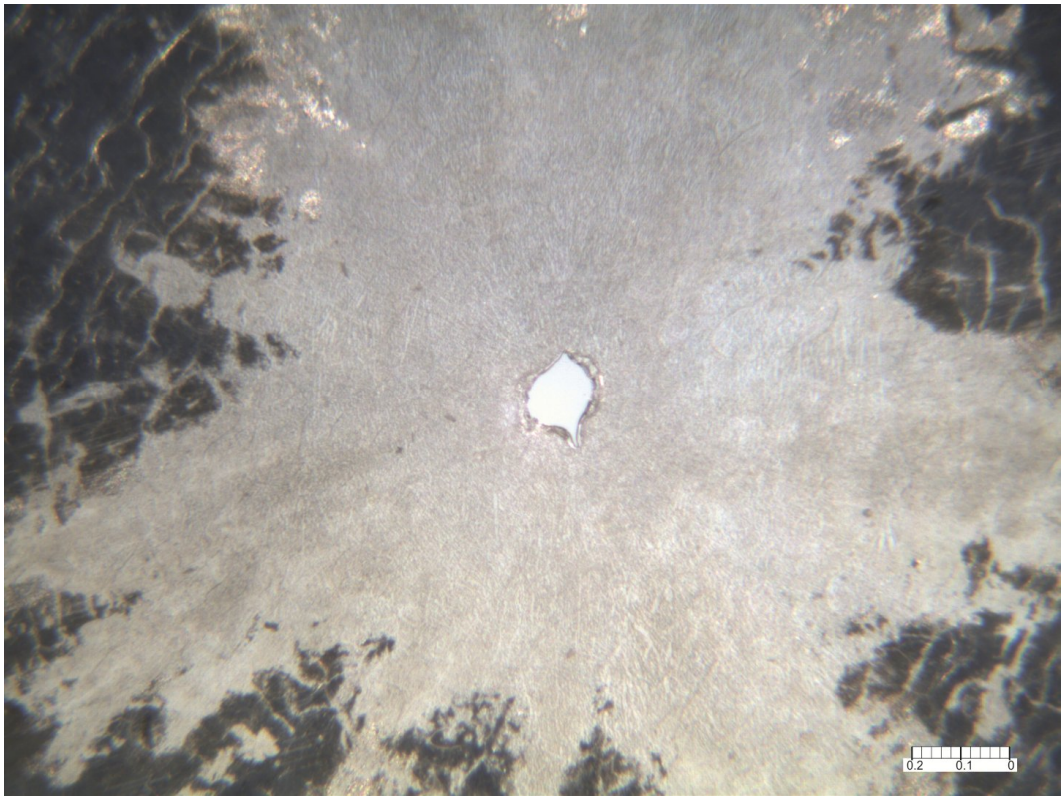

Figure 6.11. A microscope picture of a self-healed breakdown at zero external pressure. The scale bar is in millimeters.

Discharge energy analysis

In general, the self-healing mechanism in zero external pressure was effective even up to the limiting value of the voltage ramp. Typically, the self-healing process may be characterized by the momentary, pulse-like current flowing through the breakdown channel. For each sample film, the current pulse and the voltage drop during each distinguished self-healing event were recorded for further analysis. As an example, a plot of a typical current pulse during self-healing in zero external pressure is presented in Figure 6.12. The current pulses were characterized by a very fast initial current peak after which the current returned to zero through small damped oscillations. The calculated average time to peak value was 30.7 ns and the average pulse duration was 341.9 ns. These observations are in a good agreement with similar studies made with metallized polypropylene films (see e.g. reference [58]).

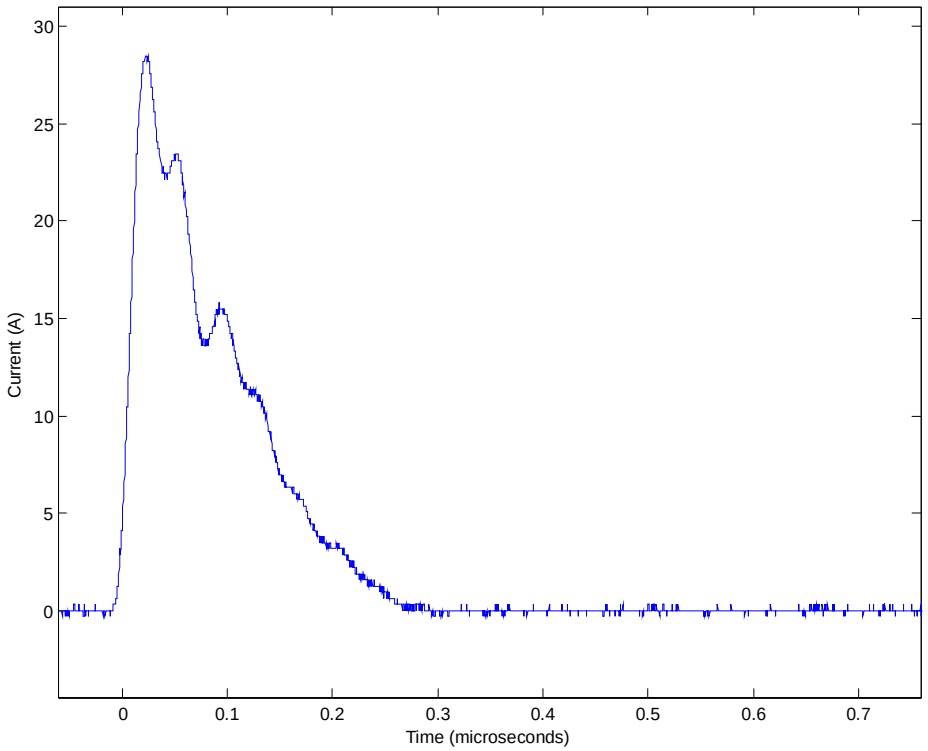

Figure 6.12. A typical current pulse during self-healing in zero external pressure (sample 1, self-healing occurred at 4895 V).

The discharge energies of the recorded self-healing events were calculated with Matlab and the results are presented in Table 6.7. In the table, the average and maximum peak current during self-healing of each sample film are also shown. The discharge energies were calculated by forming the momentary electric power $P(t)=u(t)i(t)$ and by integrating it over the whole pulse duration. Shaw *et al.* have conducted discharge energy analysis for metallized polypropylene films under various inter-layer pressures and they obtained an average discharge energy of 275 mJ with zero external pressure [23]. Although the average value of 50.16 mJ obtained in the

measurements of this thesis is several times smaller, this is probably due to the differences in the thickness of the polypropylene film and the metallization resistivity. In addition, the current-feeding capability of the external circuit during a self-healing breakdown is reflected to the time needed for the metallization to vaporize and thus to isolate the breakdown site.

Table 6.7. Self-healing analysis of samples 1-10.

Sample number	Number of self-healing events recorded	Avg. peak current (A)	Max. peak current (A)	Avg. clearing energy (mJ)
1	24	23.01	40.19	50.7
2	54	25.79	40.19	52.3
3	17	12.97	30.38	42.7
4	50	18.42	39.55	50.5
5	28	16.83	29.43	55.4
6	5	17.66	25.31	40.4
7	27	19.63	33.86	53.1
8	13	21.76	29.74	56.3
9	31	20.87	35.44	55.0
10	11	13.35	23.42	45.3
Average:	*26*	*19.03*	*32.75*	*50.16*

It should also be noted that the deviation in the clearing energies of Table 6.7 is partly caused by the linearly thickening metallization profile of the Tervakoski PZY-film, as according to Equation (4-5) the discharge energy is inversely proportional to the resistivity of the metallization. For the sake of result analysis this is not necessarily a negative aspect though, as the results shown in Table 6.7 better correspond to an actual capacitor element. However, for future studies with metallized nanocomposite films, the metallization thickness should be constant in order to study the self-healing mechanism more accurately.

6.2.2 Self-healing with externally applied pressure

The application of external pressure on the test capacitor had a significant effect on the self-healing of the metallized polypropylene film. In comparison to self-healing with no externally applied pressure, the duration of a typical clearing event, the average discharge energy and the size of a typical clearing area were generally much smaller. Due to external pressure, the expansion of the plasma during self-healing was clearly hindered and thus the time and energy needed for the electrode to vaporize was smaller. On the other hand, consecutive self-healing events at higher voltages often lead to the failure of the self-healing mechanism and a permanent breakdown. These observations are consistent with the general principles and the references presented in Chapter 4.

Visual and microscopic examination

The application of external pressure on the test capacitor clearly reduces the average size of the clearing areas. Pictures of film samples under approximately 2.0 MPa and 3.5 MPa of pressure are depicted in Figure 6.13. Especially when compared to average clearing area when no pressure is applied (see Figure 6.10), the difference is notable. As the external pressure hinders the expansion of the plasma during self-healing, the dissipated heat during a self-healing event is concentrated on a smaller area. Due to this, lower amount of energy is needed for the metallization to vaporize and thus, the clearing area is reduced. A microscope picture of a typical clearing spot at 2.0 MPa of pressure is shown in Figure 6.14. A typical size of a clearing spot with externally applied pressure was approximated to be approximately 0.5 mm^2 or less.

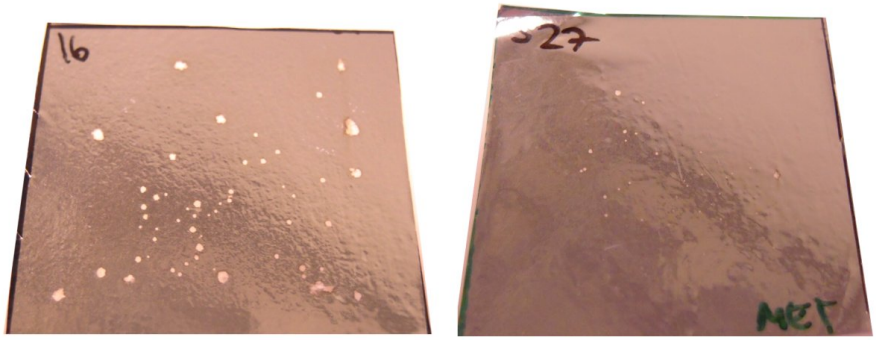

Figure 6.13. Effect of external pressure on the clearing area as seen from the metallized side (left: ~2.0 MPa of pressure, right: ~3.5 MPa of pressure).

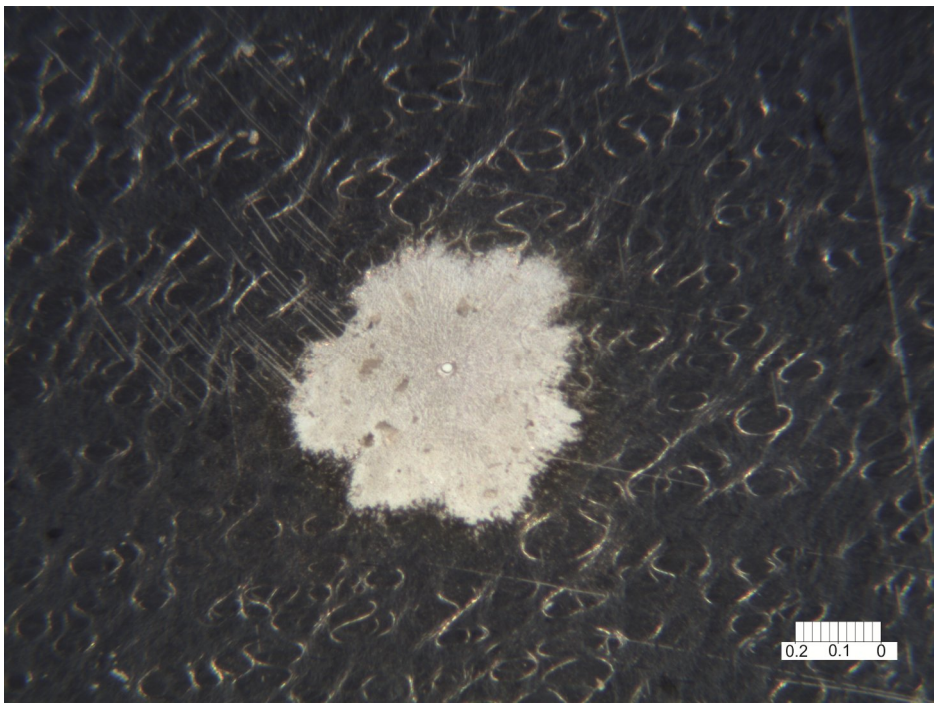

Figure 6.14. A microscope picture of a self-healing at approx. 2.0 MPa of pressure. The scale bar is in millimeters

Although the application of external pressure greatly reduced the clearing size and energy, the self-healing mechanism failed frequently as the voltage was increased. This resulted in a severe puncture through the dielectric, and due to the molten polypropylene, it was often hard to detach the films from each other after the measurement. The permanent breakdowns often took place adjacent to the mask film edge; a microscope picture of such a permanent breakdown site is shown in Figure 6.15.

Lastly, it was interesting to notice that when external pressure was applied, consecutive breakdowns often took place on a small clearing area. This is depicted in Figure 6.16, which clearly shows multiple pinholes on a small clearing area. Especially at higher voltages it was noticed that such a sequential event often lead to a permanent breakdown close to the mask film edges.

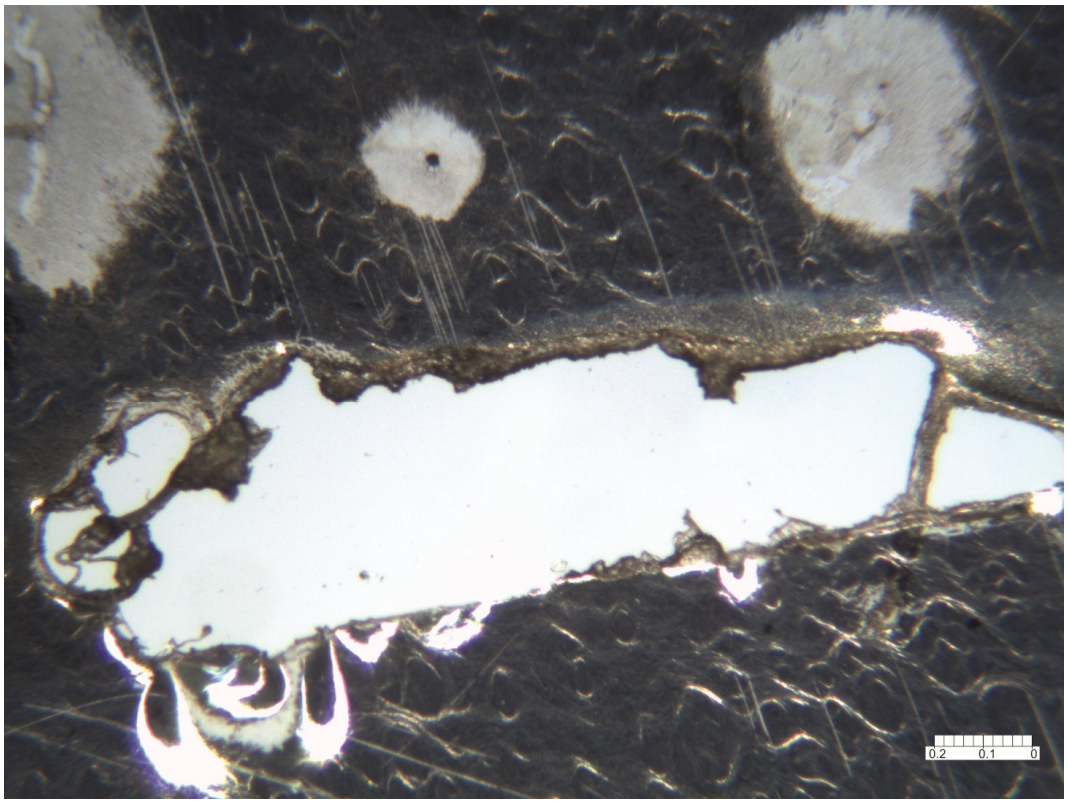

Figure 6.15. Permanent breakdown site adjacent to the mask film edge as seen from the metallized side (approx. 2.0 MPa of external pressure). Scale bar is in millimeters.

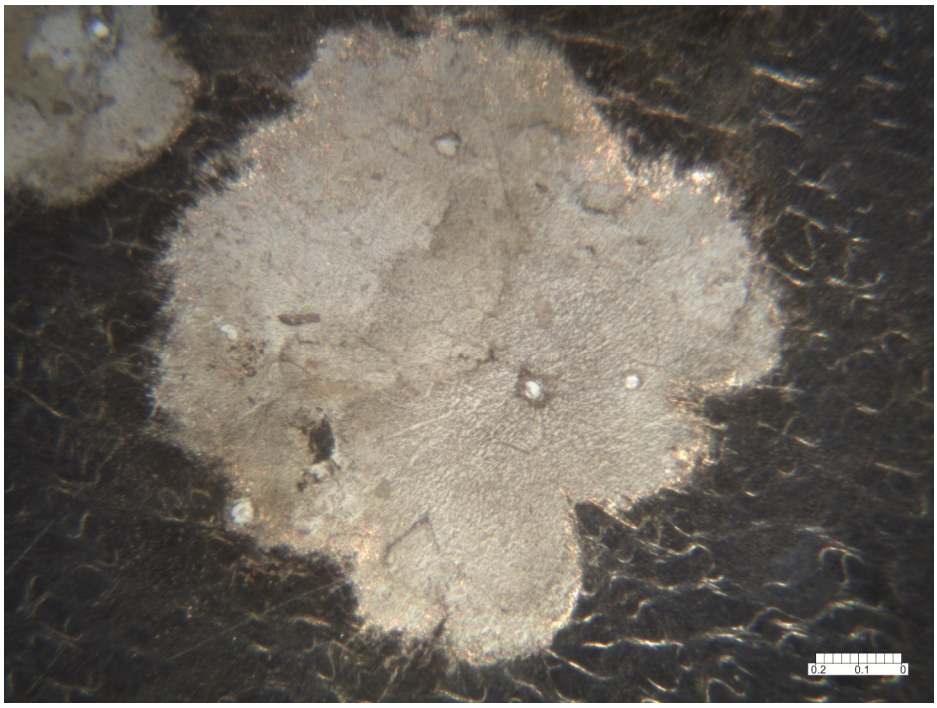

Figure 6.16. Multiple breakdown channels on a small clearing area (approximately 2.0 MPa of external pressure). Scale bar is in millimeters.

Discharge energy analysis

Regarding to the measurement of the current pulses with the oscilloscope during self-healing, it was often challenging to find a suitable measurement range in order to successfully record all the self-healing events without clipping the current signal during larger-energy clearings. The reason for this was that at lower voltages, the current pulses during self-healing were extremely low, but as the voltage was increased, clearing events began to take place more rapidly with peak currents in the range of 30 to 40 A. Therefore, if the measurement range of the oscilloscope was chosen according to low-energy clearings, the higher energy clearings at higher voltages inevitably lead to saturation of the current signal. The reason for the rapid, high-energy clearings was speculated to originate from the electric field distortion due to the windowed mask film and the additional piece of polyimide film. Indeed, it was often noticed that a rapid sequence of clearings and eventually a permanent breakdown occurred adjacent to the window edges of the mask film at higher voltages.

On this account, parts of the current pulse data of samples 11-15 measured with the oscilloscope included saturated current pulses. Thus it was later concluded that only the self-healing data of samples 12 and 13, which did not contain saturated pulses, should be taken into account for the self-healing energy analysis. As these measurements were made with a square-windowed mask film, additional set of measurements were made with circular polyimide mask film with various external pressures. The chosen clamping device bolt-torques were 4.0, 6.0 and 8.0 Nm (corresponding roughly to pressure values

of 2.0, 2.5 and 3.0 MPa). Two film samples were measured with each external pressure value.

The calculated average pulse rise time and pulse duration for each set of samples is presented in Table 6.8. When compared to average pulse rise time and duration of the samples 1-10 with no external pressure (30.7 ns and 341.9 ns, respectively), the results presented in Table 6.8 clearly show that the external pressure greatly reduces the average duration of a self-healing event.

Table 6.8. Pulse time properties of measured samples with external pressure.

	Samples 12 & 13	Samples 17 & 18	Samples 19 & 20	Samples 21 & 22
Window type	Square	Circular	Circular	Circular
Bolt-torque (Nm)	4.0	4.0	6.0	8.0
Average pulse rise time (ns)	9.15	14.97	11.99	14.23
Average pulse duration (ns)	111.71	113.13	90.69	90.15

The discharge energy data of the aforementioned measurements is presented in Table 6.9. It can be noticed that for samples 17-22 (with circular-windowed mask film), the amount of recorded self-healing events and the peak currents were in fact higher than those of samples 12-13 (mask film with square window). However, this should be interpreted as inferiority of square-windowed mask film in terms of electric field distortion; the self-healing of the samples measured with a circular-windowed mask film was clearly more effective in comparison to samples 12-13, which suffered a permanent breakdown after about 15 clearing events.

Table 6.9. Self-healing analysis of film samples with various external pressure values (pressure ranging from 2.0-3.5 MPa).

Sample number	Window type	Bolt-torque (Nm)	Number of self-healing events recorded	Avg. peak current (A)	Max. peak current (A)	Avg. clearing energy (mJ)
12	Square	4.0	15	10.53	22.47	13.4
13	Square	4.0	14	6.40	15.82	6.1
		Average:	*15*	*8.46*	*19.14*	*9.75*
17	Circular	4.0	111	11.71	31.96	12.2
18	Circular	4.0	89	8.63	24.68	11.1
		Average:	*100*	*10.17*	*28.32*	*11.68*
19	Circular	6.0	61	11.95	35.44	14.6
20	Circular	6.0	60	9.88	23.42	11.1
		Average:	*61*	*10.91*	*29.43*	*12.82*
21	Circular	8.0	122	8.28	22.15	8.1
22	Circular	8.0	103	16.00	40.19	13.7
		Average:	*113*	*12.14*	*31.17*	*10.88*

In conclusion to self-healing analysis, a comparison between the calculated average discharge energies with and without external pressure and the standard deviation is shown in Figure 6.17. It is obvious that the application of external pressure greatly reduced the average discharge energy. However, self-healing energy analysis also suggests that a more suitable way for application of external pressure is needed for future studies. It is also clear that a constant voltage stress should be used instead of voltage increase test in order to better examine the self-healing mechanism at specific conditions.

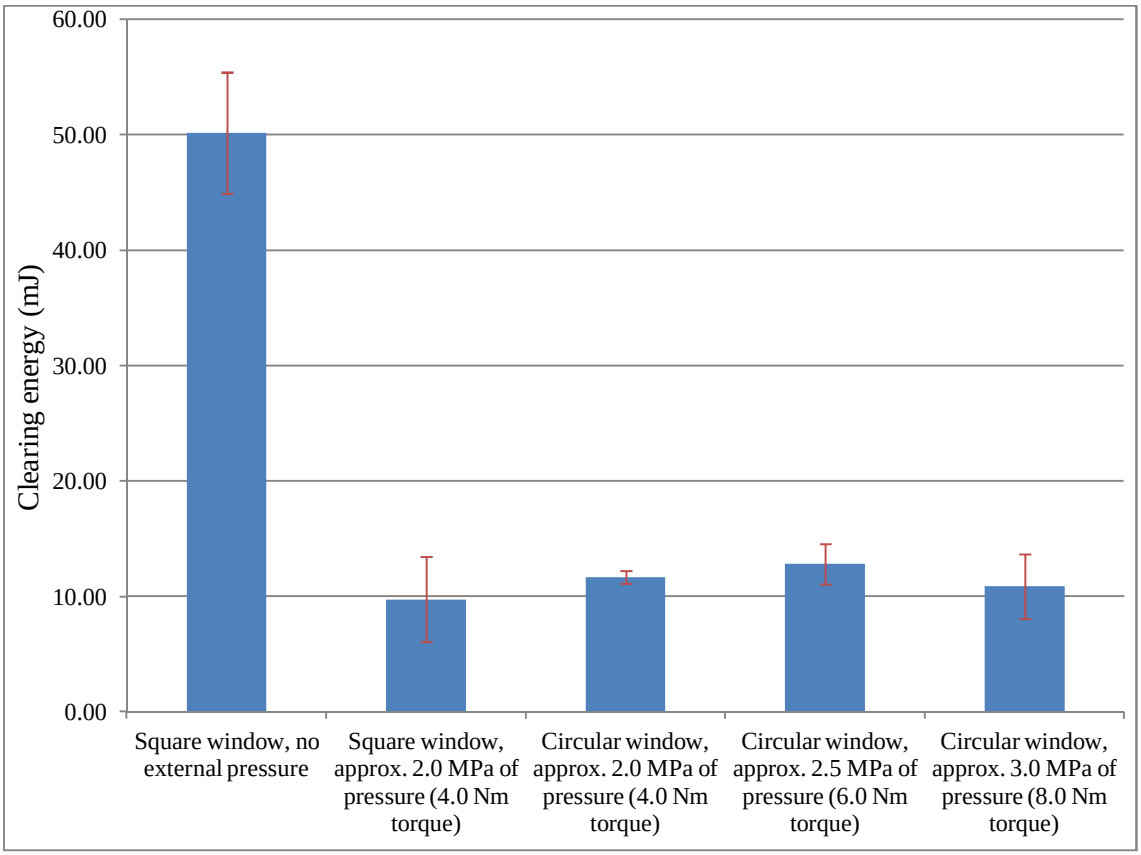

Figure 6.17. Comparison of the calculated average discharge energies with various externally applied pressure (with standard deviation).

6.3 Future work

The Weibull analysis and the discharge energy analysis presented in the previous sub-chapters suggest that the measurement system used in this thesis offers a practical way for making electrical measurements for metallized dielectric film samples with no externally applied pressure. The film arrangement consisting of a windowed mask film enables easy measurement of small sample areas. Therefore, within the NANOPOWER –project, electrical tests for metallized polypropylene nanocomposite film samples at zero external pressure may be performed in the future based on the measurement system of this thesis. Regarding to application of polypropylene nanocomposites in metallized film capacitors, it is essential to examine the performance of metallized nanocomposite films in comparison to reference films in terms of dielectric strength and self-healing capability.

However, the results obtained from the measurements with externally applied pressure suggest that an alternative test capacitor structure should be developed in the future in order to properly examine the pressure dependency of dielectric strength and self-healing capability of metallized polypropylene nanocomposite films. Although the application of pressure had a significant effect on self-healing, the main cause for the problems with dielectric strength measurements seemed to be the local electric field distortion caused by the windowed mask film and the additional piece of polyimide film used for focusing the external pressure on the effective area of the test capacitor. However, the electric field distribution should be modelled with e.g. FEM-modelling in order to confirm this.

One possible solution could be to use a specific metallization pattern for the sample film; if a free margin was left on each side of the sample film, as shown in Figure 6.18, the need for a windowed mask film would be eliminated. Thus, the external pressure would distribute more evenly on the effective area of the test capacitor and the local distortion of the electric field due to a windowed mask film would be prevented. However, it should be studied whether such a metallization pattern itself would induce problems with the electric field distribution, especially at the edges of the metallization. Lastly, constant metallization thickness should be used for the test films.

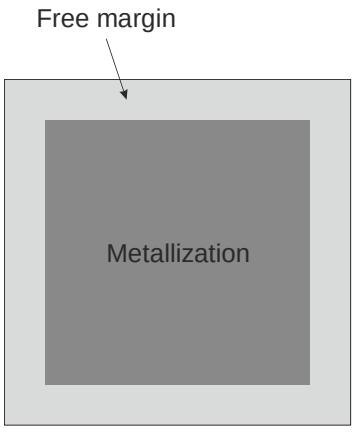

Figure 6.18. Possible metallization pattern for future studies.

In addition to the metallization pattern, softer and smoother material (e.g. rubber) should be used between the film arrangement and the Bakelite plates in order to get smoother contact interfaces and a more even pressure distribution. Lastly, a more precise method for determining the pressure exerted on the dielectric may be needed; although the Prescale film offers a practical way for examining the achieved pressure distribution, the actual amount of pressure may only be approximated.

Regarding to the measurement procedures, independent tests should be made for dielectric strength studies and for self-healing capability studies in the future. The voltage ramp test used in this thesis is a very good test method for determining the dielectric strength of the test film. However, as the discharge energy during self-healing is proportional to the voltage level (see Equation (4-5)), the discharge energies obtained with voltage ramp measurements represent the whole range from low- to high-energy clearings. Therefore, the self-healing mechanism and its pressure dependency should be examined with constant voltage stress in order to get comparable results between different dielectric materials.

Lastly, the dependency of discharge energy on the thickness of the dielectric film and the metallization resistivity should be determined. In case of pre-stage nanocomposite films, the variation in the local film thickness may be considerable and thus, the obtained discharge energy results should be transformed to an equivalent standard thickness for further analysis and comparison.

Apart from dielectric strength and self-healing capability, the other possible future research subjects for the nanocomposite candidate materials are e.g. long-term aging and corrosion studies. Long-term voltage stress tests should be made in various environmental conditions in order to examine the loss of capacitance over time (due to self-healing) and to determine if the corrosion properties of the polypropylene nanocomposites differ from those of plain polypropylene.

In addition to the aforementioned properties, the space charge properties should be studied as well. In this thesis the role of space charge accumulation and its effects on the studied properties remained unclear, although as the measurements were short-term by nature, it was speculated that there was not enough time for a considerable amount of space charge to build up. Therefore, especially in case of nanocomposite dielectrics, it would be extremely interesting to conduct long-term voltage stress tests at a constant voltage level in order to examine the effect of space charge on the electrical properties of the material. As discussed in Chapter 3, nanocomposite dielectrics may have unique mechanisms (e.g. the QDC-mechanism) which equalize the space charge profile and thus, reduce the local electric field distortion due to space charge accumulation.

7 SUMMARY

The purpose of this thesis was to study the application of polypropylene nanocomposites in metallized film capacitors under DC voltage. The research subject was approached by first conducting an extensive literature research on various topics related to polymers, polymer nanocomposites and metallized film capacitors. At first, chemical, structural and electrical properties of polymers were studied with the focus on polypropylene in order to serve as a basis for further discussion about dielectric polymer nanocomposites. Thereafter, the structure and the operation of metallized film capacitors were studied in depth. Lastly, various failure mechanisms specific for metallized film capacitors were discussed. The main objective of the literature research was to form an overall picture of the research subject and to serve as a basis for the empirical part of this thesis and for future research.

In the empirical part of this thesis, the main objective was to plan, construct and test a measurement system which could be used in the future for conducting various DC tests for metallized polypropylene nanocomposite film samples in conditions closely resembling those of a cylindrically wound capacitor element. A test capacitor structure with a specific film arrangement was used. The film arrangement comprised of a windowed polyimide mask film which enabled easy measurement of small sample areas. In addition, the effect of external pressure on the electrical properties of the film was taken under consideration by exerting compressive force on the test capacitor structure by using a custom-built bolt-adjustable clamping device. Pressure sensitive film (Fujifilm Prescale) was used to examine the pressure distribution and to approximate the pressure on the effective area of the test capacitor. The tests were conducted for industrial scale metallized polypropylene film samples with linearly thickening zinc metallization (Tervakoski film PZY).

The studied electrical properties were dielectric strength, maximum permissible electric field stress and self-healing capability of the film. These properties were tested by conducting a short-term voltage ramp test for multiple film samples with and without externally applied pressure. The dielectric strength was determined by exploiting the self-healing mechanism of metallized dielectric film. After the tests, the breakdown results were fitted in Weibull-distribution. The maximum permissible electric field stress was estimated from the Weibull-distribution as the electric field stress corresponding to 1% failure probability. The self-healing capability of the test film was examined by determining the average energy discharged during self-healing. The charging current and the test capacitor voltage during each registered clearing event were recorded and the average discharge energy was calculated based on the

measurement data. Lastly, the clearing spots on the film samples were examined visually and with a microscope.

The obtained results suggest that the measurement system offers a practical way for performing various electrical tests on metallized dielectric film samples with no externally applied pressure. The breakdown values obtained with zero external pressure (N=137) fitted very well in the Weibull-distribution and the corresponding scale parameter was in good agreement with the values often cited in the literature. In addition, for all the samples except for one, the breakdown mechanism was effective even up to the limiting value of the voltage ramp.

On the other hand, the application of external pressure with the bolt-adjustable clamping device yielded unexpected results as the dielectric strength of the test film was impaired considerably. The problem was assumed to originate from the test capacitor structure itself – the main cause for the problems with dielectric strength was assumed to be the local electric field distortion caused by the windowed mask film and the additional piece of polyimide film which was used for focusing the external pressure on the effective area of the test capacitor. This lead to clearings at relatively low voltage levels and as the voltage was increased enough, the self-healing mechanism often failed which lead to a permanent breakdown through the dielectric. This was presumably due to the local electric field distortion close to the mask film edges and not because of the properties of the polypropylene film. Thus, after various tests it was concluded that the film arrangement used in the test capacitor was not very suitable for examining the effect of external pressure on the breakdown strength of metallized dielectric film.

However, the application of external pressure had a considerable effect on the self-healing capability of the metallized polypropylene film. With externally applied pressure (ranging from approximately 2.0 to 3.0 MPa), the average discharge energy, current pulse duration and clearing spot area reduced dramatically. A rather obvious physical explanation for the observations is that the external pressure hindered the expansion of the hot plasma between the film layers during self-healing. Therefore, more heat concentrated on a smaller area and thus the energy required for the metallization to vaporize was smaller in comparison to self-healing with zero inter-layer pressure. The effect of external pressure on self-healing was also verified by visual and microscopic examination of the films; the average clearing spot size reduced dramatically, from approximately 5-8 mm^2 (zero inter-layer pressure) to less than 0.5 mm^2 (approximately 3.0 MPa of pressure). All the observations regarding to self-healing capability and its pressure dependency were coherent with the references cited in the theoretical part of this thesis.

Based on the results obtained, proposals for future work were given. The measurement system may be used for conducting electrical tests for metallized polypropylene nanocomposite films in the future. However, an alternative test capacitor structure has to be developed in order to enable better examination of the pressure dependency of the dielectric strength of the test film. It was also concluded that separate tests have to be conducted for dielectric strength and self-healing capability studies.

Finally, other possible research subjects such as long-term aging studies in various environmental conditions with constant voltage stress and space charge accumulation studies of the nanocomposite films were discussed.

REFERENCES

[1] M. Aro, J. Elovaara, M. Karttunen, K. Nousiainen, and V. Palva, *Suurjännitetekniikka*, 2nd ed. Helsinki, Finland: Otatieto, 1996.

[2] J. Keith Nelson, *Dielectric Polymer Nanocomposites*.: Springer US, 2010.

[3] Tampere University of Technology, Technical Research Centre of Finland (VTT), and University of Jyväskylä, "Novel polymer nanocomposites for power capacitors (NANOPOWER) - Scheme for a research project," Tampere, 2010.

[4] M Takala, "Electrical Insulation Materials towards Nanodielectrics," Department of Electrical Energy Engineering, Tampere University of Technology, Tampere, PhD Thesis 2010.

[5] T. Tanaka, G.C. Montanari, and R. Mulhaupt, "Polymer nanocomposites as dielectrics and electrical insulation-perspectives for processing technologies, material characterization and future applications," *IEEE Transactions on Dielectrics and Electrical Insulation*, vol. 11, no. 5, pp. 763-784, 2004.

[6] C.W. Reed and S.W. Cichanowskil, "The fundamentals of aging in HV polymer-film capacitors," vol. 1, no. 5, pp. 904-922, 1994.

[7] W.J. Sarjeant, J. Zirnheld, and F.W. MacDougall, "Capacitors," vol. 26, no. 5, pp. pp.1368-1392, 1998.

[8] W.J. Sarjeant, "Capacitor fundamentals," in *Proceedings of the 19th Electrical Electronics Insulation Conference - '89 EEIC/ICWA Exposition*, Chicago, 1989, pp. 1-51.

[9] R. O. Ebewele, *Polymer Science and Technology*, 1st ed. Florida: CRC Press, 2000.

[10] J. Seppälä, *Polymeeriteknologian perusteet*, 5th ed. Helsinki, Finland: Otatieto, 2005.

[11] L. H. Sperling, *Introduction to Physical Polymer Science*, 4th ed. Hoboken, USA: Wiley, 2005.

[12] L. A. Dissado and J. C. Fothergill, *Electrical degradation and breakdown in polymers*. United Kingdom: Peter Peregrinus Ltd., 1992.

[13] D. W. Kim and K. Yoshino, "Morphological characteristics and electrical conduction in syndiotactic polypropylene," *Journal of Physics D: Applied Physics*, vol. 33, pp. 464-471, 2000.

[14] G. G. Raju, *Dielectrics in Electric Fields*. New York: Marcel Dekker Ltd, 2003.

[15] T. Blythe and D. Bloor, *Electrical properties of polymers*, 2nd ed. New York: Cambridge University Press, 2005.

[16] J. R. Reitz, F. J. Milford, and R. W. Christy, *Foundations of Electromagnetic Theory*, 4th ed. USA: Addison-Wesley, 1992.

[17] H. Ranta, "Long-term electrical properties of polypropylene nanocomposites for high voltage capacitor applications," Department of Electrical Energy Engineering, Tampere University of Technology, Tampere, Master of Science Thesis 2008.

[18] S. Holé, "Recent developments in the pressure wave propagation method," *IEEE Electrical Insulation Magazine,* vol. 25, no. 3, pp. 7-20, 2009.

[19] T. Mizutani, "Space charge measurement techniques and space charge in polyethylene ," *IEEE Transactions on Dielectrics and Electrical Insulation,* vol. 1, no. 5, pp. 923-933, 1994.

[20] H. G. Karian, *Handbook of Polypropylene and Polypropylene Composites*. New York, USA: Marcel Dekker, 1999.

[21] G. Picci and M. Rabuffi, "Status quo and future prospects for metallized polypropylene energy storage capacitors," in *Pulsed Power Plasma Science*, vol. 1, 2001, pp. 417-420.

[22] Borealis AG corporation web site, accessed on August 2011. [Online]. http://www.borealisgroup.com/

[23] D.G. Shaw, S.W. Cichanowski, and A. Yializis, "A Changing Capacitor Technology - Failure Mechanisms and Design Innovations," *IEEE Transactions on Electrical Insulation,* vol. EI-16, no. 5, 1981.

[24] E. Abdel-Bary, *Handbook of Plastic Films*. Shrewsbury, UK: Smithers Rapra, 2003.

[25] T.J. Lewis, "Nanometric dielectrics," *IEEE Transactions on Dielectrics and Electrical Insulation,* vol. 1, no. 5, pp. 812-825, 1994.

[26] C. Green and A. Vaughan, "Nanodielectrics - How Much Do We Really Understand," *IEEE Electrical Insulation Magazine,* vol. 24, no. 4, pp. 6-16, 2008.

[27] J. K. Nelson, "The Development, Properties and Future of Dielectric Nanocomposites - Invited lecture," in *Nordic Insulation Symposium - NORD-IS 11*, 2011.

[28] L. Jiongxin, "High Dielectric Constant Polymer Nanocomposites for Embedded Capacitor Applications," School of Materials Science and Engineering, Georgia Institute of Technology, Atlanta, PhD Thesis 2008.

[29] R.C. Smith, C. Liang, M. Landry, J.K. Nelson, and L.S. Schadler, "The mechanisms leading to the useful electrical properties of polymer nanodielectrics," *IEEE Transactions on Dielectrics and Electrical Insulation,* vol. 15, no. 1, pp. 187-196, 2008.

[30] T. Tanaka, M. Kozako, N. Fuse, and Y. Ohki, "Proposal of a multi-core model for polymer nanocomposite dielectrics," *IEEE Transactions on Dielectrics and Electrical Insulation*, vol. 12, no. 4, pp. 669-681, 2005.

[31] T. Tanaka, "Dielectric nanocomposites with insulating properties," *IEEE Transactions on Dielectrics and Electrical Insulation*, vol. 12, no. 5, pp. 914-928 , 2005.

[32] M. Takala et al., "Dielectric properties and partial discharge endurance of polypropylene-silica nanocomposite," *IEEE Transactions on Dielectrics and Electrical Insulation*, vol. 17, no. 4, pp. 1259-1267, 2010.

[33] M. Danikas and T. Tanaka, "Nanocomposites - A review of electrical treeing and breakdown," *IEEE Electrical Insulation Magazine*, vol. 25, no. 4, pp. 19-25, 2009.

[34] H. D. Young and R. Freedman, *University Physics with Modern Physics*, 11th ed.: Addison Wesley, 2003.

[35] General Atomics Electronic Systems, Inc. , "Capacitor Engineering Bulletins," San Diego, Cited on July 2011, available at http://www.ga-esi.com/support/ep/tech-pubs.php.

[36] T. Rinne, "Metalloitujen ohutkalvokondensaattoreiden ominaisuudet tasajännitteellä," Department of Electrical Energy Engineering, Tampere university of technology, Tampere, Master of Science Thesis 2011.

[37] S.A. Boggs, J. Ho, and T.R. Jow, "Overview of laminar dielectric capacitors," vol. 26, no. 2, pp. 7-13, 2010.

[38] Tervakoski Film, Corporation web site. Metallized film product profiles. Accessed on August 2011. [Online]. http://www.tervakoskifilm.com/

[39] C. Guillermin and J. M. Lupin, "Partial discharges measurements on dry metallized film capacitors," in *Proceedings of the 22nd Nordic Insulation Symposium*, Tampere, 2011.

[40] B. Drugge, M. Carlen, S. Laihonen, and L. Spronck, "Cut and dried! - A new dry capacitor for high-voltage DC applications," *ABB Review*, 1/2003.

[41] Q. Xiaoguang and S. Boggs, "Analysis of the effects of end connection quality on the dielectric loss of metallized film capacitors," *IEEE Transactions on Dielectrics and Electrical Insulation*, vol. 11, no. 6, pp. 990-994, 2004.

[42] EPCOS AG , "General technical information," in *Film Capacitors*, 0409th ed.: EPCOS AG, 2009, p. 42.

[43] EPCOS AG , "MKV Power Electronic Capacitors for Heavy Duty Applications - Product profile," 2008.

[44] J. Kammermaier, "Physical and chemical conditions for self-healing in metallized capacitors," in *Proceedings of the Symposium on High-energy-density Capacitors and Dielectric Materials*, Washington, 1981, p. 78.

[45] H. Heywang, "Physikalische und chemische Vorgänge in selbstheilenden Kunststoff-Kondensatoren," *Colloid & Polymer Science*, vol. 254, no. 2, pp. 138-147, 1976.

[46] J. H. Tortai, A. Denat, and N. Bonifaci, "Self-healing of capacitors with metallized film technology: experimental observations and theoretical model," *Journal of Electrostatics*, vol. 53, no. 2, pp. 159-169, 2001.

[47] B. Peng et al., "Calculation and measurement of metalized film capacitor's inner pressure and its influence on self-healing characteristics," *IEEE Transactions on Dielectrics and Electrical Insulation*, vol. 17, no. 5, pp. 1612-1618, 2010.

[48] W.J. Sarjeant, I.W. Clelland, and R.A. Price, "Capacitive components for power electronics," *Proceedings of the IEEE*, vol. 89, no. 6, pp. 846-855, 2001.

[49] R. W. Brown, "Electrical and Thermal Modelling of Low Power Metallised Polypropylene Capacitors," RMIT University, Melbourne, PhD Thesis 2007.

[50] C.A. Nucci, S. Pirani, and M. Rinaldi, "Electrode-end contact degradation of metallized polypropylene capacitors in power applications," in *Proceedings of the 3rd International Conference on Properties and Applications of Dielectric Materials*, 1991 , pp. 466-469.

[51] S. Qin and S.A. Boggs, "Limits to the performance and design of high voltage metalized film capacitors," *IEEE Transactions on Dielectrics and Electrical Insulation*, vol. 17, no. 4, pp. 1298-1306, 2010.

[52] J.B. Ennis, J. Rauch, X.H. Yang, and J. Atkins, "Comparison of film capacitor designs for a high power density application," in *IEEE International Power Modulator and High Voltage Conference (IPMHVC)*, 2010, pp. 225-228.

[53] WIMA Corporation web site. "Technical information", accessed on August 2011. [Online]. http://www.wima.de/en_index.php

[54] IEC (International Electrotechnical Commission) and IEEE (Institute of Electrical and Electronics Engineers), "Guide for the statistical analysis of electrical insulation breakdown data," IEC 62539/ IEEE 930 standard 2007.

[55] S. Tandon, "Modeling of stresses in cylindrically wound capacitors: Characterization and the influence of stress on dielectric breakdown of polymeric film," University of Massachusetts Amherst, Massachusetts, PhD Thesis 1997.

[56] J. Ho and S. Boggs, "Effect of UV treatment on the dielectric strength of BOPP capacitor film," in *Conference Record of the IEEE International Symposium on Electrical Insulation*, 2006 , pp. 314-317.

[57] D. Xin, L. Fuchang, L. Jin, Y. Zonggan, and W. Nanyan, "Influence factors for the self-healing of metallized polypropylene capacitors," in *Annual Conference Report on Electrical Insulation and Dielectric Phenomena*, 2000, pp. 461-465.

[58] P.-O. Sassoulas, B. Gosse, and J.-P. Gosse, "Self-healing breakdown of metallized polypropylene," in *Proceedings of the IEEE 7th International Conference on Solid Dielectrics*, 2001, pp. 275-278.

[59] P. J. Duncan, N. Williams, and P. S. Dodds, "Forces in Cylindrical Metallized Film Audio Capacitors," in *Audio Engineering Society Convention 126*, 2009, p. 11.

[60] Fujifilm Corporation. (2011, September) Fujifilm Prescale product specification. [Online]. http://www.fujifilm.com/products/prescale/prescalefilm/

[61] Wikipedia. "Sheet resistance" - a wikipedia article, accessed on July 2011. [Online]. http://en.wikipedia.org/wiki/Sheet_resistance

[62] D. G. Shaw, A Changing Capacitor Technology - Video recording of DEIS conference presentation, 1983,
Video available at http://ewh.ieee.org/soc/deis/Videos/Video13.html.

APPENIDX A – PRESCALE FILM PRESSURE CHART

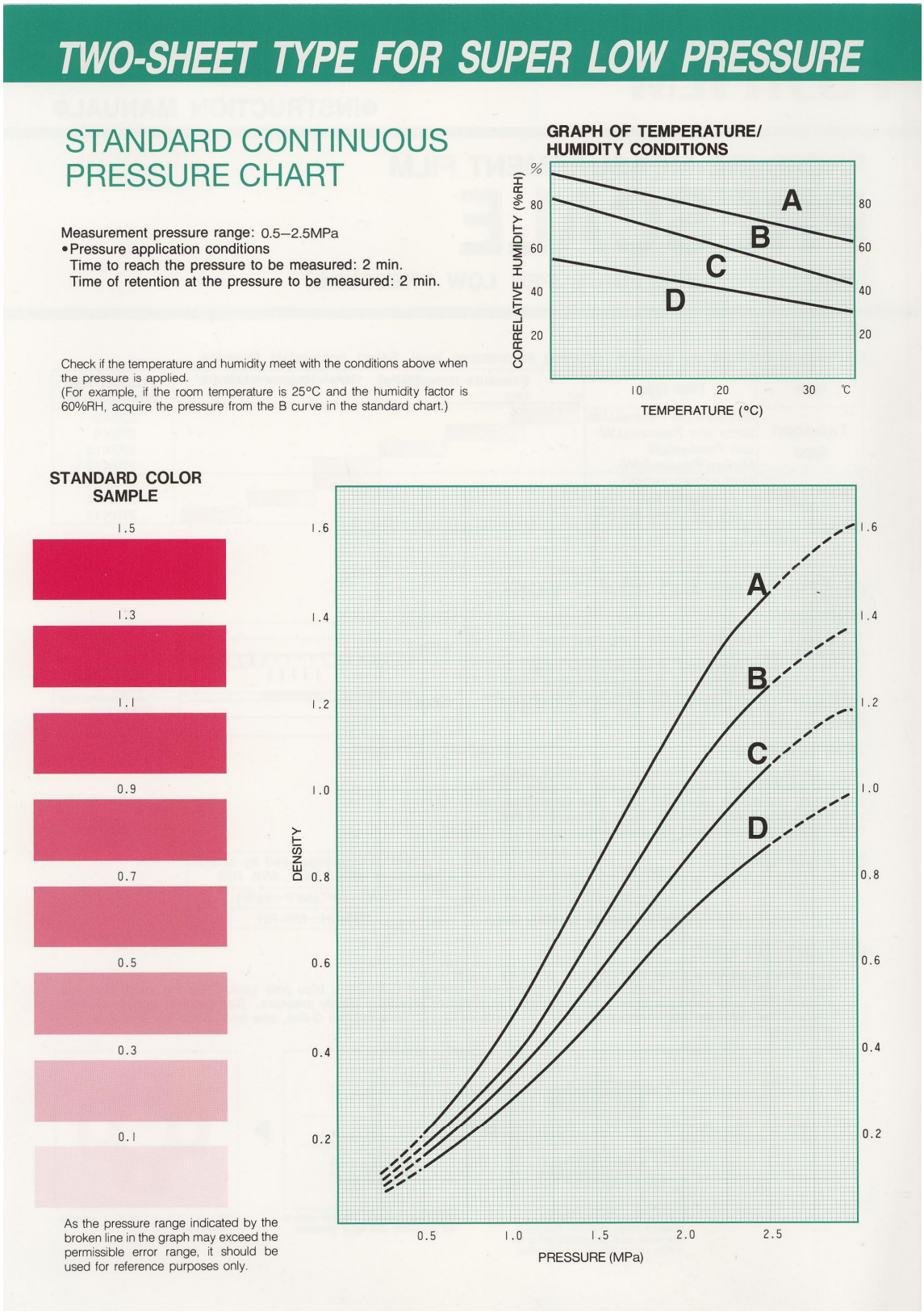

Figure A.1. Pressure chart for Fujifilm Prescale pressure sensitive film. [60]